經濟部

經濟部標準檢驗局 98 年度科專計畫

計畫名稱：太陽光電模組加速老化因子之研究

太陽光電模組加速老化因子之研究計畫

期末報告

執行期間：98 年 5 月 13 日起 至 98 年 11 月 30 日 止

主辦單位：經濟部標準檢驗局

執行單位：財團法人成大研究發展基金會

中華民國九十八年十一月

經濟部標準檢驗局98年度委辦計畫期末報告

審查意見回覆表

計畫名稱：太陽光電模組加速老化因子之研究
執行單位：財團法人成大研究發展基金會
執行期間：98 年 5 月 13 日起至 98 年 11月 30 日止

委員	審查意見	意見回覆
A 委員	1.本委辦計劃乃針對太陽光電模組加速老化因子之研究其中老化因子包含以下數項: (1)溫度冷熱變化、(2)材料介面間鋁化合物生成、(3)高溫、照度及(4)紫外線等。 2.本計畫針對每一因子對於太陽光電模組加速老化之影響，可稱詳盡。唯考慮其結果之實用性與因子間互相作用，茲有以下意見： ● 建議多蒐集本土的數據(文獻多引用外國的數據) ● 應標示因子間交互作用的影響 ● 因子數值與「加速老化」關聯 除以上建議外，本計畫能在短短不到6個月時間完成諸多分析，誠屬不易	1. 由於本國過去欠缺加速老化完整實驗數據與報告，由國外文獻可找到較多針對太陽能模組老化原因之研究探討，故本研究報告中以參考國外文獻為主，往後若國內建構起相關加速老化實驗設備，則未來可納入國內研究文獻報告。 2. 已增加第6.8節(期末報告第51頁)「太陽能模組老化因子間之交互作用」探究之影響。 3. 本研究「太陽光電模組實驗設計分析研究報告」及「太陽光電模組加速試驗分析研究報告」已針對溫度、濕氣與紫外線等因子強度越高，造成模組老化速度愈加快，進行討論。至於加速老化測試條件與實際使用壽命之間之關聯性，尚需未來建構加速老化測試設備試驗後與實際長時間戶外實際運轉試驗，所得兩結果相互比較分析，方可得較準確之結論。

經濟部標準檢驗局98年度委辦計畫期末報告

審查意見回覆表

計畫名稱：太陽光電模組加速老化因子之研究
執行單位：財團法人成大研究發展基金會

執行期間：98 年 5 月 13 日起至 98 年 11月 30 日止

B 委員	1.研究重點為結晶矽型和薄膜太陽能膜組之加速老化因子。並歸納出初始短路電流下降、串聯電阻增加、以及太陽模組變色等老化現象表現出來。 2.探討變因包含冷熱循環、水氣入侵、邊框材料變質、鹽度與溼度、紫外線等影響參數。 3.各項所提結論論點，可否轉化成為檢測標準、檢測方法或是可得致老化因子的加速檢測模式 4.需求規範書中所列兩主項工作內容(一)由實驗設計找出各實驗因子的影響(二)加速老化因子研析，依加強明顯影響因子，分析老化程度，均已執行，並得致定性結論。但實驗設計手法部份已變更未執行。 5.可否有進一步定量結果，供發展有效之加速驗證技術。 6.二項工作內容均已有部分執行，但需求規範之各項細節仍未完全呈現在報告中。	3. 所提結論可作為檢測依據，若需制定確切檢測參數，尚需以太陽能模組實際進行加速老化試驗與長時間戶外運轉測試，並兩相比較結果方可得之。 4. 礙於國內尚無加速老化試驗設備，並囿於計畫執行時間僅約六個月以及經費限制，故實際測試部分經計畫期初說明會與期中會議報告結論，改以蒐集分析現有文獻方式呈現，並已於期末報告第5頁計畫目標一節加以說明。 5. 相關說明謹列於「太陽光電模組加速試驗分析研究報告」第5-34頁。 6. 針對報告內容與需求規範部分細節未完全呈現之原因，乃由於計畫實驗設計手法部份有前述變更，故實驗設計與試驗結果部份，以歸納研析現有文獻方式，並分別詳述於「太陽光電模組實驗設計分析研究報告」及「太陽光電模組加速試驗分析研究報告」中，而各因子間交互作用則另於第6.8節(第51頁)探討。

經濟部標準檢驗局98年度委辦計畫期末報告

審查意見回覆表

計畫名稱：太陽光電模組加速老化因子之研究
執行單位：財團法人成大研究發展基金會

執行期間：98 年 5 月 13 日起至 98 年 11 月 30 日止

C 委員	依需求規範書審核期末成果報告，提出以下幾點意見 1. 需求規範書要求須完成三份報告:(1)太陽光電模組實驗設計分析研究報告、(2)太陽光電模組加速試驗分析研究報告、(3)期末報告。但受託單位僅提供第(3)，未見(1)與(2)報告。 2. 需求規範書第三（一）項，有關實驗設計內容中，提到「....進而找出最佳之設計參數」，在報告中未見此結果之呈現。 3. 規範書要求「本計畫擬透過實驗設計之手法，分析影響太陽能光電模組老化之因子....」。但期末報告的計畫目標及說明(P5)卻陳述「...實驗測試及記錄檢測數據礙於國內設備、經費與時間限制，得於未來國內相關設備設置齊全後，參考本計畫成果另案實施辦理」。兩者存有明顯差異，請補充說明其原因。	1. 已敬附上(1)與(2)報告。 2. 實驗設計參數可參考現有文獻中對太陽能模組加速老化測試之設計，結果已於「太陽光電模組實驗設計分析研究報告」第3-19頁中詳述。 3. 計畫執行後，發現國內尚無建置加速老化試驗設備，現有之部分設備尺寸與規格，無法執行相關老化試驗，且囿於計畫執行時間僅約六個月以及經費限制，無法於短時間內完成加速老化試驗設備之建置，且若擬與實際老化測試結果對比，由現有文獻顯示，需至少數年至十餘年時間加以測試比對，因此經計畫期初說明會與期中會議報告討論結論，改以蒐集分析現有文獻方式呈現，此一補充說明已敘述於報告第5頁中。

目錄

壹、 計畫緣起 1

貳、 計畫目標及說明 5

參、 研究方法、步驟及流程 6

肆、 人力配置 7

伍、 經費配置 9

陸、 執行成果及效益 10

6.1 TCO 腐蝕原因及其對模組的影響 10
6.1.1 偏壓大小與 TCO 腐蝕現象的關係 13
6.1.2 溫度、濕度與金屬框架對 TCO 腐蝕的影響 16

6.2 濕度與氧氣對薄膜太陽能電池模組的影響 17

6.3 冷熱溫度循環、季節變化之影響 19

6.4 材料介面間鋁氧化合物生成的影響 25

6.5 高濕、鹽度環境之影響 31

6.6 紫外線之影響.....35

6.7 模組效能下降與失效常見原因探討 44
6.7.1 初始短路電流下降.....44
6.7.2 串聯電阻的增加.....46
6.7.3 太陽能模組的變色.....48

6.8 太陽能模組老化因子間之交互作用 51
6.8.1 Na^+離子與環境溫度交互影響.....51
6.8.2 Na^+離子與水氣交互影響.....52
6.8.3 溼度、溫度與含氧量之交互影響.....52
6.8.4 水氣後與鋁氧化合物 Al_2O_3 之交互影響.....52

柒、 各月份工作要項 53

捌、 結論與建議 54
參考文獻.....57
附件 59

壹、 計畫緣起

過去數十年來全球經濟快速成長，耗能急遽增加，造成全球氣候異常變遷，因此不分國界的學者開始積極參與再生能源之研究。太陽能發電具備潔淨、無噪音等優點，且太陽的能源蘊藏量豐沛，故亦令其成為最受矚目的再生能源之一。

民國 98 年全國能源會議中，針對我國未來能源產業發展進行討論，結論將新興產業「綠色能源產業旭升方案」分為「能源光電雙雄」和具潛力產業「能源風火輪」兩波推動，並將大型綠能投資計畫，列入國發基金之優先重點投資項目。其中第一波「能源光電雙雄」，已具良好的產業基礎，發展太陽光電和 LED 照明的能量；第二波「能源風火輪」，則推動技術發展處於研發階段的風力發電、生質燃料、氫能與燃料電池、能源資通訊、電動車輛。

圖 1 所示為我國太陽光電產業產值趨勢，據統計 2008 年台灣太陽光電產值規模為新台幣 1011 億元，與 2006 年(535 億元)比較，幾乎成長了 100%。然而西班牙的補助措施提早於 2008 年 9 月停止，補助措施亦已修正為每年 500MW，頓時少了 2,000MW 的市場容量，故 2009 年模組市場轉為平淡，僅有微幅成長。

圖 2 與圖 3 所示分別為我國矽晶型與薄膜型太陽能模組的產能及成長率狀況圖，圖 4 與圖 5 則分別為其產值及成長率圖，由圖可知 2009 年太陽能模組市場已略有供過於求的現象，因此廠商面臨產業需求的環境下，應建立適用標準和檢測能力，提升產品品質，尚能增加市場競爭力。

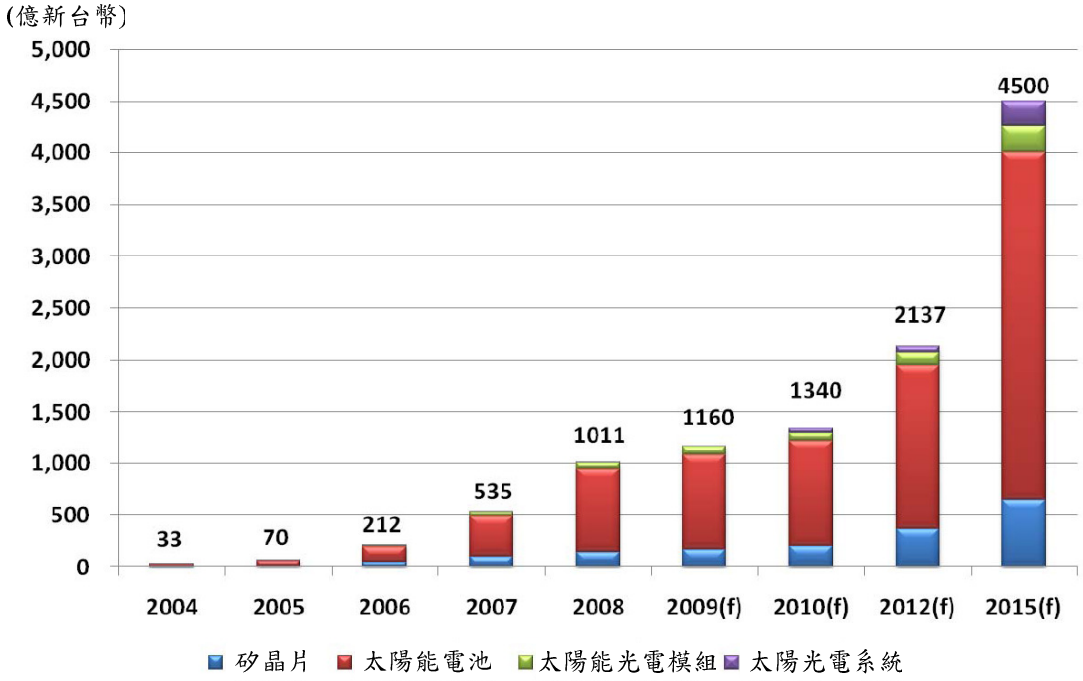

資料來源：工研院太陽光電科技中心(2009/06)

圖1　我國太陽光電產業產值趨勢

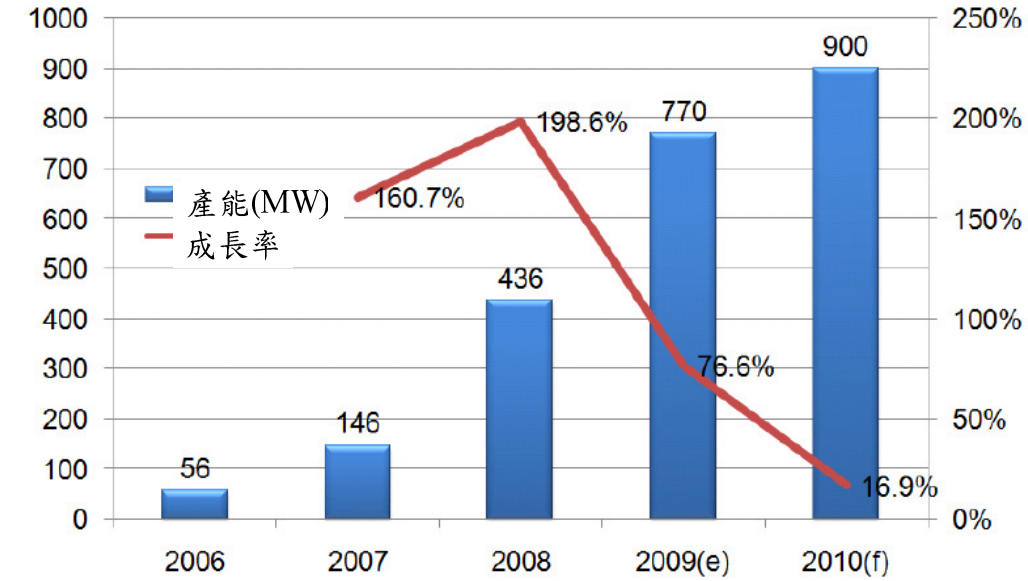

資料來源:工研院IEK (2009/04)

圖2　我國矽晶型太陽能模組的產能及成長率狀況圖

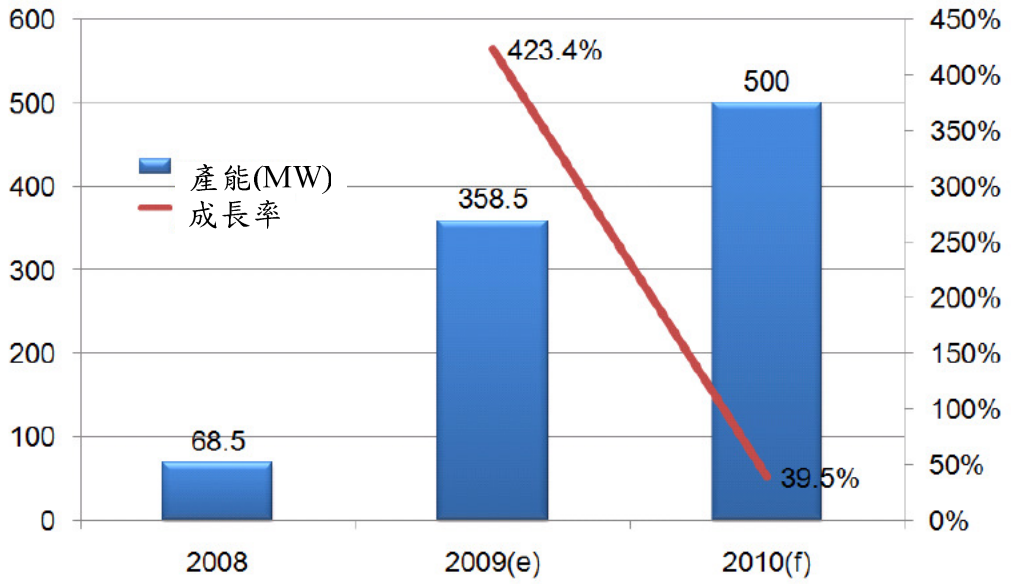

資料來源:工研院IEK (2009/04)

圖3　我國薄膜型太陽能模組的產能及成長率狀況圖

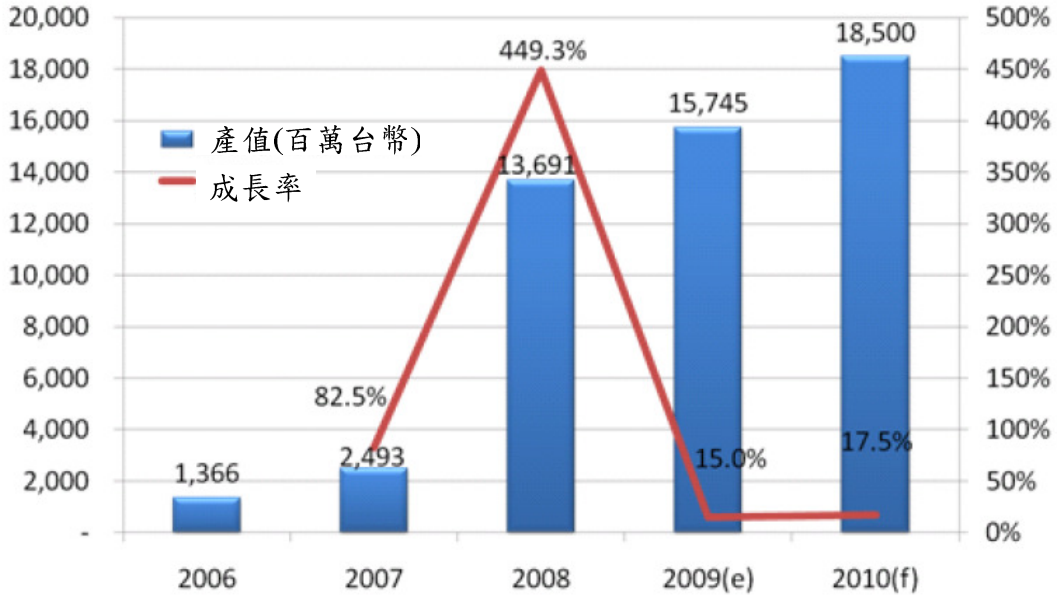

資料來源:工研院IEK (2009/04)

圖4　我國矽晶型太陽能模組的產值及成長率圖

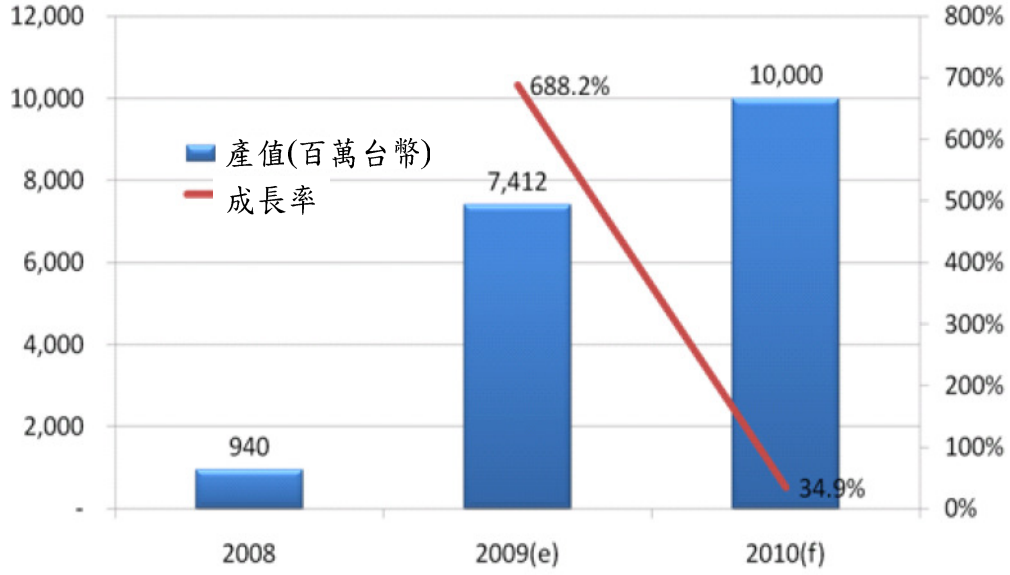

資料來源:工研院IEK (2009/04)

圖5　我國薄膜型太陽能模組的產值及成長率圖

註：加底線為量產廠商，其餘為尚未量產廠商

2005廠商數	0家	2家	8家	5家	25家
2006廠商數	0家	2家	13家	8家	27家
2007廠商數	2家	7家	24家	14家	29家
2008廠商數	8家	10家	28家	18家	36家
2009廠商數	7家	10家	28家	19家	37家

資料來源：工研院IEK整理(2009/07)

圖6　我國太陽光電產業版圖

貳、 計畫目標及說明

太陽光電產業鏈由最上游的原料、太陽能晶片製作、太陽能電池、太陽能模組與系統建置所構成，目前我國國內太陽光電產業鏈的廠商分布如圖 6 所示。其中對模組廠商來說，國內太陽光電受限於產品必須送至國外進行驗證，使得國內產品獲得驗證時間加長，間接阻礙了國內太陽光電模組產品拓展海外市場的機會。

太陽光電模組送至國外驗證不僅成本高、時程長，且驗證結果難以用來協助廠商改良製程，不僅形為國內產品取得驗證時間過長，且對模組經加速老化測試後，對造成性能與可靠度失效原因往往未能掌握。因此之故，本計畫乃以模組加速老化因子之研究，透過掌握性能與可靠度失效原因，期使產品研發時程縮短，取得市場先機，並促使國內太陽光電產業與全球國際市場接軌。

本計畫工作重點方面，在計畫執行後發現國內尚無建置加速老化試驗設備，現有之部分設備尺寸與規格，無法執行相關老化試驗，且囿於計畫執行時間僅約六個月以及經費限制，無法於短時間內完成加速老化試驗設備之建置，且若擬與實際老化測試結果對比，由現有文獻顯示，需至少數年至十餘年時間加以測試比對，因此經計畫期初說明會與期中會議報告討論結論，確定於蒐集與整理有關太陽光電模組加速老化因子文獻，並加研究分析與檢討，以提供標檢局未來制訂太陽光電模組加速老化相關驗證與驗證結果解釋分析之參考。實驗測試及檢測數據記錄分析方法可於未來國內相關測試設備建置後，參考本計畫成果另案實施辦理。

參、 研究方法、步驟及流程

圖 7 所示為本計畫架構樹狀圖，主要目的為研析可能造成太陽能電池模組加速老化或效能劣化的因子，首先探討太陽能電池模組製作流程，並分析模組所使用的各種材料，以探究這些材料劣化的因素，是否與其製作流程或系統安裝步驟有關，最後利用現有模組效能檢測方法及參考國際模組檢測規範，探討太陽能電池模組效能劣化情形與其加速老化因子之間的關聯性。

本計畫主要進行蒐集與匯整國內外學術研究中對太陽能光電模組加速老化因子(如溫度循環、溼度、鹽度、日照與紫外線等)相關文獻，並加以研析與檢討結果，以提供標檢局未來制訂太陽光電模組加速老化相關驗證與驗證結果解釋分析之參考。

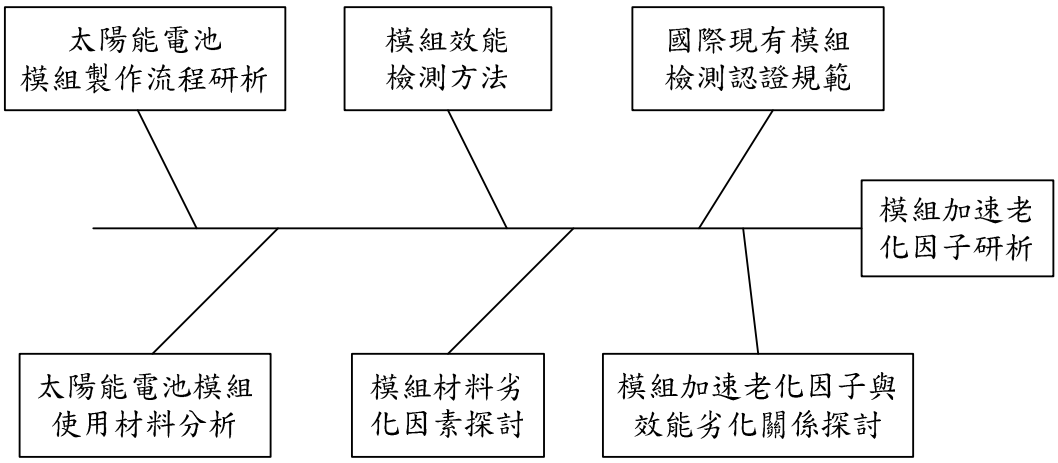

圖7　計畫架構樹狀圖

肆、 人力配置

姓名	計畫職稱	投入人月數及工作重點	學、經歷及專長	
楊宏澤	主持人	整體規劃設計分析、架構建立與進度掌握並負責執行研究、理論指導、工作協調	學歷	1984/09 ~ 1989/01 國立清華大學電機研究所博士 1982/09 ~ 1984/06 國立成功大學電機研究所碩士 1978/09 ~ 1982/06 國立成功大學電機工程學系學士
			經歷	現職： 2008/08 ~國立成功大學電機工程學系教授兼電機工廠主任 經歷： 2007/07 ~2008/08 國立成功大學電機工程學系教授 2004/08 ~2007/07 蔚華科技公司(中原大學借調）總經理室副總經理暨技術長 2000/08 ~2007/07 私立中原大學電機工程學系教授 1995/10 ~2000/07 私立中原大學電機工程學系副教授 1993/01 ~1995/10 中山科學研究院第三研究所技監 1989/05 ~1992/12 中山科學研究院第三研究院技正 1990/08 ~1996/07 國立成功大學電機所兼任副教授
			專長	太陽能與風力發電系統、分散式能源併聯系統、電力系統運轉與規劃、配電系統自動化
楊明長	協同主持人	研究分析、理論指導及管理協調	學歷	1984/08 ~ 1990/07 Case Western Reserve University Chemical Engineering 博士 1981/08 ~ 1984/05 Case Western Reserve University Chemical Engineering 碩士 1976/09 ~ 1980/06 國立成功大學化學工程學系學士
			經歷	現職： 2004/8~ 國立成功大學化學工程學系教授 經歷： 2005/08 ~ 2008/07 國立成功大學化工工廠主任 1991/08 ~ 2004/07 國立成功大學化學工程學系副教授 1990/08 ~ 1991/06 University of Utah Cold Fusion Institute Post Doctorate
			專長	化學工程、電化學技術、燃料電池、化學感測器、電解沉積
廖建棠	研究員	1. 研讀相關文獻及資料 2. 分析各類太陽能電池特性及其老化因子 3. 實驗設計規劃 4. 協助進行實驗測試 5. 分析檢測數據 6. 撰寫期中、末報告	學歷	2009/09~ 國立成功大學電機所博士班 2007/09~2009/06 國立成功大學電機所碩士 2003/09~2007/06 國立勤益科技大學電機工程系學士
			經歷	
			專長	太陽能追日控制系統

姓名	計畫職稱	投入人月數及工作重點	學、經歷及專長	
陳宇範	研究員	1. 研讀太陽能電池模組相關文獻 2. 進行實驗測試 3. 紀錄檢測數據 4. 整理實驗結果 5. 撰寫期中、末報告。	學歷	2008/09~國立成功大學電機工程學系碩士班 2004/09~2008/06 國立高雄應用科技大學電機工程系學士
			經歷	
			專長	再生能源電能轉換系統

伍、 經費配置

財團法人成大研究發展基金會

太陽光電模組加速老化因子之研究計畫

經費支出表(期末報告)

執行期間：98 年 5 月 6 日 至 98 年 11 月 30 日

項目 / 會計科目		預算數(執行數)				備註
		主管機關預算(委託、補助)	自籌款	合計		
				金額(元)	占總經費%	
一、經常支出						
1.人事費(直接薪資)		224,000 (224,000)	0	224,000 (224,000)	25.17% (25.17%)	
2.業務費(其他直接費用-人事、業務)		431,700 (431,700)	0	431,700 (431,700)	48.5% (48.5%)	
3. 委辦作業費用		100,000 (0)	0	100,000 (0)	11.24% (0.0%)	
4.管理費(含公費)		134,300 (116,528)	0	134,300 (116,528)	15.09% (7.54%)	
5.營業稅		0	0	0	0.0%	
小計		890,000 (772,228)	0	890,000 (772,228)	100.0% (81.22%)	
二、資本支出						
小計		0	0	0	0	
合計	金額	890,000 (772,228)	0	890,000 (772,228)	100.0% (81.22%)	
	占總經費%	100.0% (86.77%)	0.0%	100.0% (86.77%)		

製表：　　主辦會計：　　計畫主持人：　　機關主管：

陸、 執行成果及效益

本計畫研究重點主要以佔市場大宗之結晶矽型和薄膜太陽能電池模組為。其研究重點包含(1) 研析 TCO 腐蝕原因及其對模組之影響、並歸納可能造成 TCO 腐蝕之各項因子、(2)分析溼氣與氧氣與薄膜太陽能電池模組老化之關聯性、(3)結晶矽型模組經季節變遷之冷熱溫度循環與溼度變化，使模組由邊框開始向內發生剝離現象、(4)探討非晶矽薄膜太陽能電池模組中所產生鋁氧化合物，使太陽能電池、EVA 和玻璃之間剝落而產生間隙，造成水氣的侵入和腐蝕現象、(5)在靠海的高鹽度環境下，太陽能模組表面含較高量的鈉和磷成分，其造成玻璃與模組介面間附著力降低、(6)結晶矽太陽能模組在經過長時間的室外光照下，常因紫外線造成 EVA 變質褐色化的現象，使模組發電量顯著下降之問題。

最後歸納出太陽能電池模組長時間使用曝曬，最常見使輸出功率下降的主要原因，包括初始短路電流下降、串聯電阻的增加、太陽能模組的變色等三種現象，將於以下各節詳加說明。

6.1 TCO 腐蝕原因及其對模組的影響

薄膜型太陽能電池可分成 superstrate 和 substrate 兩種結構，如圖 8 所示。superstrate 結構為在玻璃基板上鍍 TCO 層後，在依序鍍下 p-i-n 三層矽薄膜；而 substrate 結構則為在不透光基板上先鍍下金屬層，再依序鍍下 n-i-p 三層矽薄膜，最後再鍍上 TCO 層。兩種結構因沉積長晶的方向不同而有所差異，其中 superstrate 結構因玻璃基板與 TCO 層直接接觸，造成太陽能模組在運轉時 TCO 的腐蝕老化現象，進而導致模組效率的降低。

由於 TCO 腐蝕老化係薄膜太陽能電池模組劣化重要之影響因子，以下各節乃針對造成 TCO 腐蝕老化的原因，及其對模組的影響作討論，並對各項加速 TCO 腐蝕老化的因素做探討。

TCO(Transparent Conductive Oxide)俗稱透明電極，其具高透光率及導電性，故一般作為薄膜太陽能電池的前端電極，如圖 9 所示。常見的 TCO 以 SnO_2:F 的化合物為其材料，根據許多研究顯示[1-4]，太陽能模組於長時間使用後，常發現 TCO 腐蝕老化的現象，造成太陽能電池的串聯電阻增加，進而降低輸出電流，導致輸出功率下降。或由於 TCO 腐蝕造成太陽能電池發生龜裂現象，使模組本身遭受破壞而損毀，如圖 10、圖 11 所示。

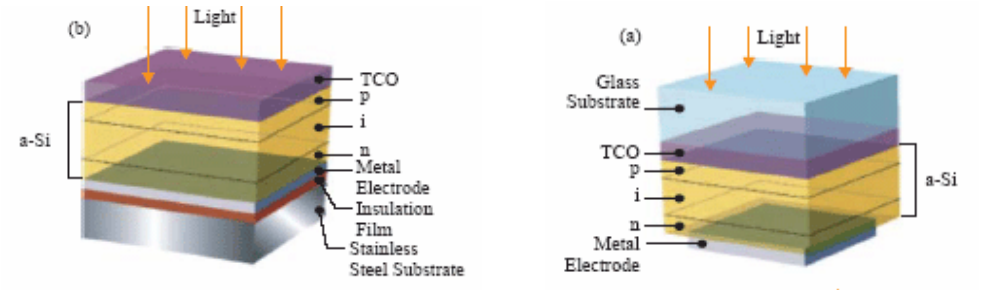

(a) (b)

圖8　(a)Substrate (b) Superstrate 結構示意圖

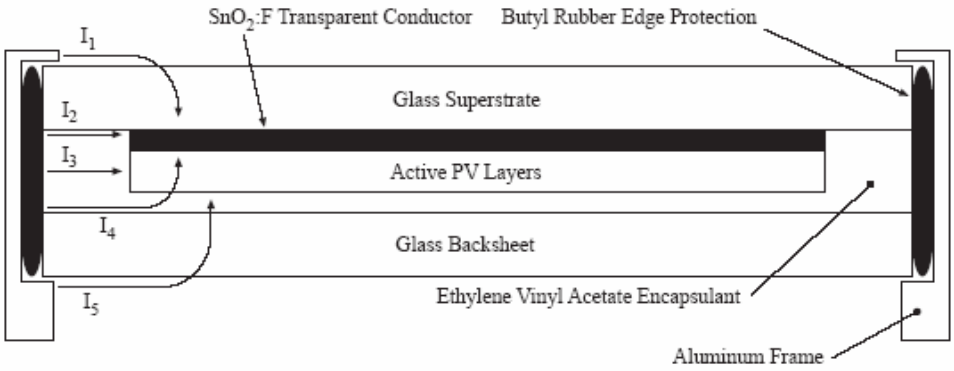

圖9　Superstrate 薄膜太陽能電池剖面圖[3]

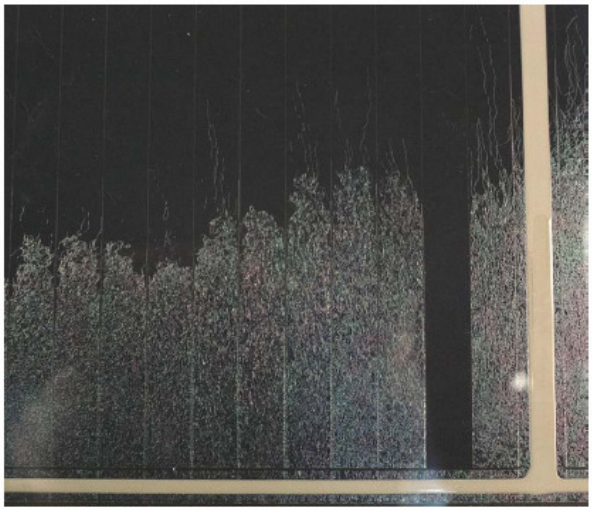

圖10 TCO 腐蝕的龜裂現象[1]

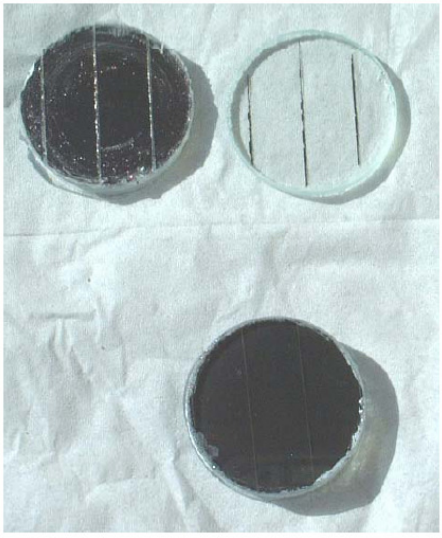

圖11 TCO 腐蝕使前端玻璃與電池剝離[1]

造成 TCO 腐蝕的主要原因為其本身化學反應所致，實際的化學反應目前仍尚未完全被發現，但主要可推測參與化學反應的因子為 $Na^+ + H_2O + SnO_2$:F，使 SnO_2:F 因化學反應變成了 SnO，其中 Na^+離子為來自前端玻璃釋出(soda-lime glass)，而 H_2O 為外在環境的水蒸氣經由模組邊緣滲透進入。

為了證明 Na^+離子在 TCO 腐蝕現象中扮演著重要的角色，

Solarex 太陽能公司進行之實驗[1]，使用兩種不同種類的玻璃在分別兩模組上，一種為常見含鈉的 soda-lime glass，另一種為 borosilicate 玻璃，同時在相同環境、相同偏壓底下測試，結果發現使用 borosilicate 玻璃的模組並未發現如圖 10 之 TCO 腐蝕現象，而含鈉的 soda-lime glass 則呈相反的結果，因此證明了鈉離子為 TCO 腐蝕的主因。

美國國家再生能源實驗室(NREL)對 Na^+離子如何與 TCO 接觸之實驗[1]為在兩個相同的太陽能模組上分別外接+600DC 及 -600DC 的直流偏壓，一端接於模組金屬鋁框上，一端則接於模組輸出短路點上，示意圖如圖 12 所示。結果發現只有在負偏壓的狀況下才會發生 TCO 腐蝕的現象，因此可推測是負偏壓造成的漏電流(leakage current)方向將 Na^+離子導入 TCO 層，唯有在金屬框架的電壓大於電池層的情況下，漏電流才能將玻璃上的納離子帶至 TCO 層與 SnO_2:F 發生化學反應，造成腐蝕現象。

6.1.1 偏壓大小與 TCO 腐蝕現象的關係

本實驗為美國 Florida Solar Energy Center (FSEC)所做的實驗[2,5]，將八個太陽能模組分別偏壓±600V、±300V、±150V 及兩組未偏壓，而-600V 偏壓的模組於 8 個月後產生肉眼可見的 TCO 腐蝕現象，-300V 偏壓的模組於 15 個月後產生腐蝕現象，-150V 偏壓的模組約在 27 個月後，而正偏壓的模組均未發生 TCO 腐蝕現象。實驗實體配置照片如圖 13 所示，其中-600V、-300V、-150V 與無偏壓的損壞面積實體照片分別如圖 14~圖 15 所示，由圖可看出腐蝕的部分皆在模組的邊緣附近發生，因此也可證明水氣透過邊緣滲透進

模組發生化學反應才產生 TCO 腐蝕的現象。

表 1 所示為偏壓測試與模組特性變化關係，由表可知負偏壓越大模組損壞情形越嚴重。

表1　偏壓測試與模組特性對照表[2]

測試條件	最大輸出功率	填充因數(Fill Factor)	串聯電阻
原始	46.6W	64%	15Ω
-150V 偏壓	37W	56%	30Ω
-300V 偏壓	5.6W	20%	382Ω
-600V 偏壓	0.82W	0%	

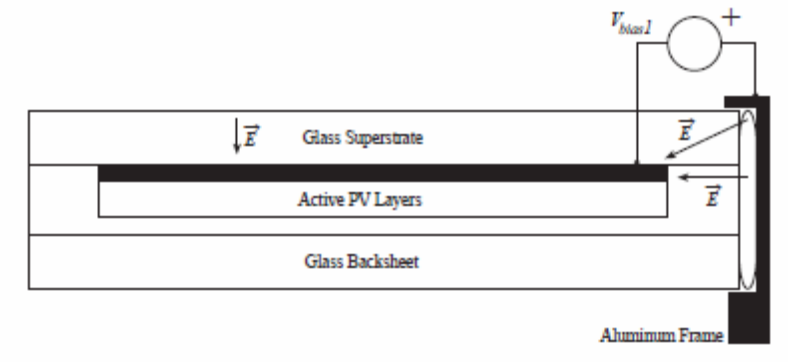

圖12 模組直流偏壓示意圖[3]

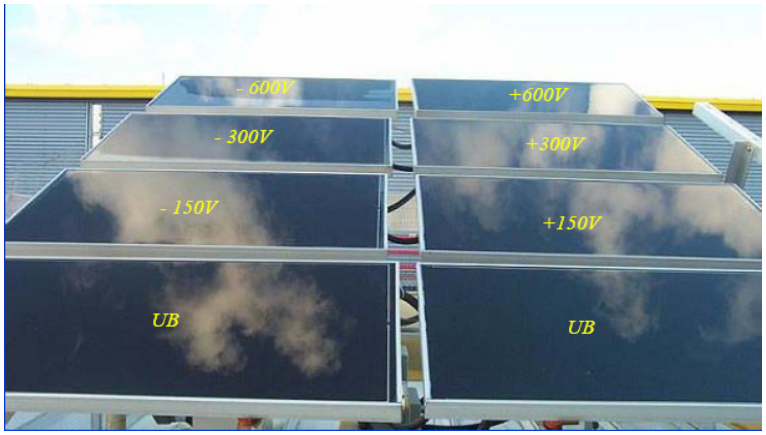

圖13 偏壓大小與 TCO 腐蝕現象關係實驗配置圖[5]

圖14 -600V 偏壓模組 24 個月後的損壞範圍實體照片[5]

圖15 -300V 偏壓模組 30 個月後的損壞範圍實體照片[5]

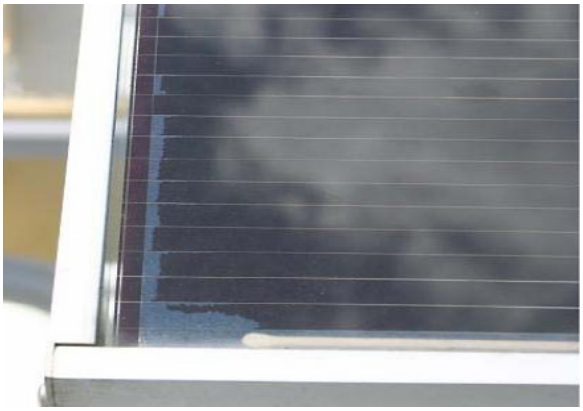

圖16 -150V 偏壓模組 30 個月後的損壞範圍實體照片[5]

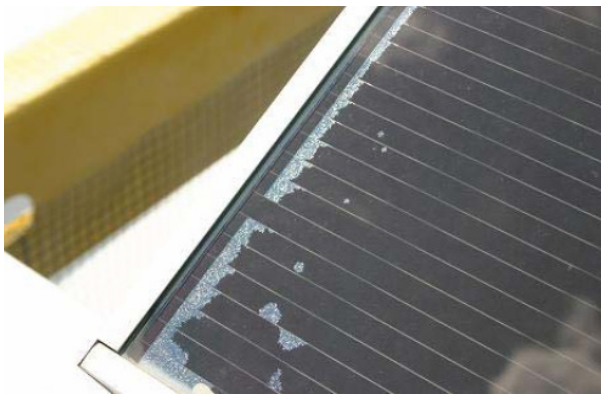

圖17 無偏壓模組 30 個月後的損壞範圍實體照片[5]

6.1.2 溫度、濕度與金屬框架對 TCO 腐蝕的影響

表 2 為各種環境條件下的測試結果[3]，以下分別針對溫度、濕度與金屬框架對 TCO 腐蝕的影響加以探討。

由表 2 第 1、2 及 3 項可知在相同偏壓與相同溼度下，分別放置於溫度 85°C、72°C、60°C 環境下測試。結果溫度越高產生的漏電流 IL 越大，且模組損壞面積亦越大，因此環境溫度提高會加速 TCO 腐蝕，圖 18 所示為在不同溫度條件下模組損壞速率曲線。

水蒸氣對 TCO 腐蝕的影響有兩大因素，第一種是水蒸氣經由邊緣滲透進模組，並與 TCO 作化學反應產生腐蝕現象；第二種是環境的溼度會造成金屬框架和玻璃的導電度增加，進而增加漏電流，增加損壞速率。表 2 中第 1 項與第 10 項測試相對濕度分別為 0%與 85%，可比較得環境溼度較高時 TCO 腐蝕速率越較快。

由表 2 中第 1 項與第 9 項測試可得，將金屬框架移除後漏電流大小明顯下降，裝置金屬框架的模組在相對少的時間內所受的損害面積也較多，因此金屬框架亦是影響漏電流大小的因素之一。

表2　為各種環境條件下的測試結果[3]

	Sample	T/RH (°C,%)	Total Time (h)	I_L (μA)	Total Charge (C)	Damage Area (%)	Damage Rate (mm^2/h)	ΔP_{max} (%)	Comments
1	2020	85/85	230	17→3	4.6	14.8	450	-39.6	a-Si, framed
2	1051	72/85	400	3→2	2.9	10.9	240	-38.6	a-Si, framed
3	100	60/85	1340	3→1	5.6	8.3	67	-52.2	a-Si, framed
4	3006	85/85	510	10→7	18	0	0	-	CdTe, frameless
5	127	72/85	1240	8→5	32	4.3	24	-	CdTe, frame added
6	127	85/85	190	23→12	8.8	1	37	-	CdTe, frame added
7	8221	72/85	1240	0.2→0.05	0.3	0	0	-	a-Si, frame removed, front contacts
8	8171	85/85	1190	2→0.9	4.4	1.4	97	-5.1	a-Si, silicone edge buffer
9	8221	85/85	360	0.2→0.12	0.16	0.08	0.6	-	a-Si, frame removed, front contacts
10	1148	85/0	470	7→0.7	3.1	0.2	2.7	-	a-Si, framed
11	7016	85/0	630	0.02	0.5	0	0	-	a-Si, frame removed, front contacts
12	7016	85/85	170	9→13	6.4	18	800	-	a-Si, frame removed, front contacts

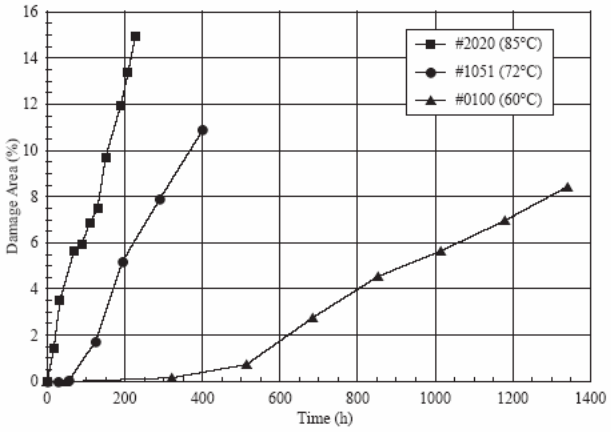

圖18 溫度對損壞面積的速率[3]

6.2 濕度與氧氣對薄膜太陽能電池模組的影響

Shell Solar Industries(SSI)公司自行研發 CIGS-based PV Mini-module 作為實驗用的太陽能電池模組[6]，表 3 為其初始特性參數。實驗中將三個 Mini-module 分別置於下列三種環境:

1. 乾熱(dry heat)測試：環境溫度為85±5℃，將太陽能電池模組置於透明玻璃培養皿中。
2. 溼熱測試(damp heat)：環境溫度為85±5℃，濕度為100%RH，太陽能電池模組置於玻璃瓶中，瓶內裝有阻值為18.8MΩ的去離子水。

3. 浸水測試(water bath)：置於玻璃瓶中，內裝有500mL的去離子水，另外本測試又分為厭氧性和親氧性兩種，分別在瓶內裝氬氣(Ar)和氧氣(O_2)。

結果可發現在乾熱測試中，經過了 1,000 個小時，模組的性能並沒有顯著變化，然而在濕熱測試和浸水測試中，僅經過 168 小時後，模組的最大輸出功率 $P_{max,ave}$ 即自原本的 794.4 mW 減小至 131.6 mW，已低於原本最大輸出功率的 30%以下，如表 4 所示，故可研判出濕度對於太陽能電池模組的老化有明顯的影響。功率下降主因為電流減少，而並非電壓下降，故可推斷為串聯電阻的增加所致。而在厭氧性和好氧性的實驗中，結果顯示裝入氧氣的試驗樣本經過 168 小時候便已失去正常功能，然而裝入氬氣的試驗樣本從 168 小時後輸出功率才開始降低，經過 840 小時後才劣化致與裝入氧氣的試驗樣本一樣，輸出功率低於原本的 30%以下，故可推斷氧氣可增加太陽能電池模組老化的速率。

表3　SSI 所研發 mini-module 的初始特性參數表[6]

Area (cm^2)	36
V_{oc} (V)	4
I_{sc} (mA)	537.6
V_{max} (V)	2.1
I_{max} (mA)	357.3
P_{max} (mW)	794.4
η	10%

表4　各實驗測試項目的模組最大輸出功率[6]

測試類型	時間(hrs)	最大輸出功率
原始未經測試		794.4 mW
乾熱測試	1000	794.4 mW
溼熱測試	168	131.6 mW
浸水測試	168	131.6 mW

6.3 冷熱溫度循環、季節變化之影響

Edge-defined Film-fed growth (EFG)長晶技術製造之太陽能電池，此法可拉出中空的八角形柱體，利用雷射切割就可得到 10 x10 cm^2 的晶片，可節省材料在切割上的損失[7]。文獻[8]中以實驗試驗以 EFG 方式製作的太陽能電池模組之老化現象，實驗中利用以 36 片太陽能電池串並聯而成的太陽能電池模組進行研究，其模組之金屬邊框由鋁製成。表 5 所示為此太陽能電池模組在標準檢測條件(Standard Testing Conditions, STC)下所量測的相關數據。本文藉由該型模組探究類似電池模組結構在冷熱與季節溫度循環下之變化實驗現象。

本實驗前後共進行 34 個月，並且定期進行量測及記錄其相關數據，實驗地點為南非 Nelson Mandela Metropole 大學。由圖 19 可發現此太陽能電池模組老化之情況分布，在圖 19(a)中，可以看到整個太陽能電池模組老化程度分佈，而圖 19(b)、(c)、(d)中，則是分別展示此模組中的部分區塊，由圖 19(b)和(c)，可發現由於每日的溫度循環，剝離的拓展情況隨著距離產生變化，一開始在邊框有些微剝離現象產生，情況慢慢惡化。在圖 19(d)中，可發現剝離的情況沿著匯流排方向成長。而這些剝離的情況所造成的空隙，會使水氣侵入，進而造成太陽能模組介面之間物質上的變化，圖 19(c)中就可明顯看出水氣的侵入，水氣會加速接觸面剝離而導致模組輸出功率下降。

圖 3 為圖 19(b)的部份放大，由圖 20 中虛線即表示水氣侵入的時程分佈，在開始進行戶外曝曬試驗後，剝離的情況便緩慢開始，

並延伸到 Line1(October 2001)，經過一年後，剝離的情況延伸到 Line2(November 2002)，最後隨時間增加惡化至 Line3 (July 2004)。

表5　在 STC 下所量測之電性數據[8]

Performance parameter	Manufacture	Baseline
Maximum power (P_{max})	50W	48.64W
Open circuit voltage (V_{OC})	20.7V	21.11V
Short circuit current (I_{SC})	3.2A	3.10A
Voltage at maximum power (V_{max})	17.0V	21.1V
Current at maximum power (I_{max})	3.0A	3.1A

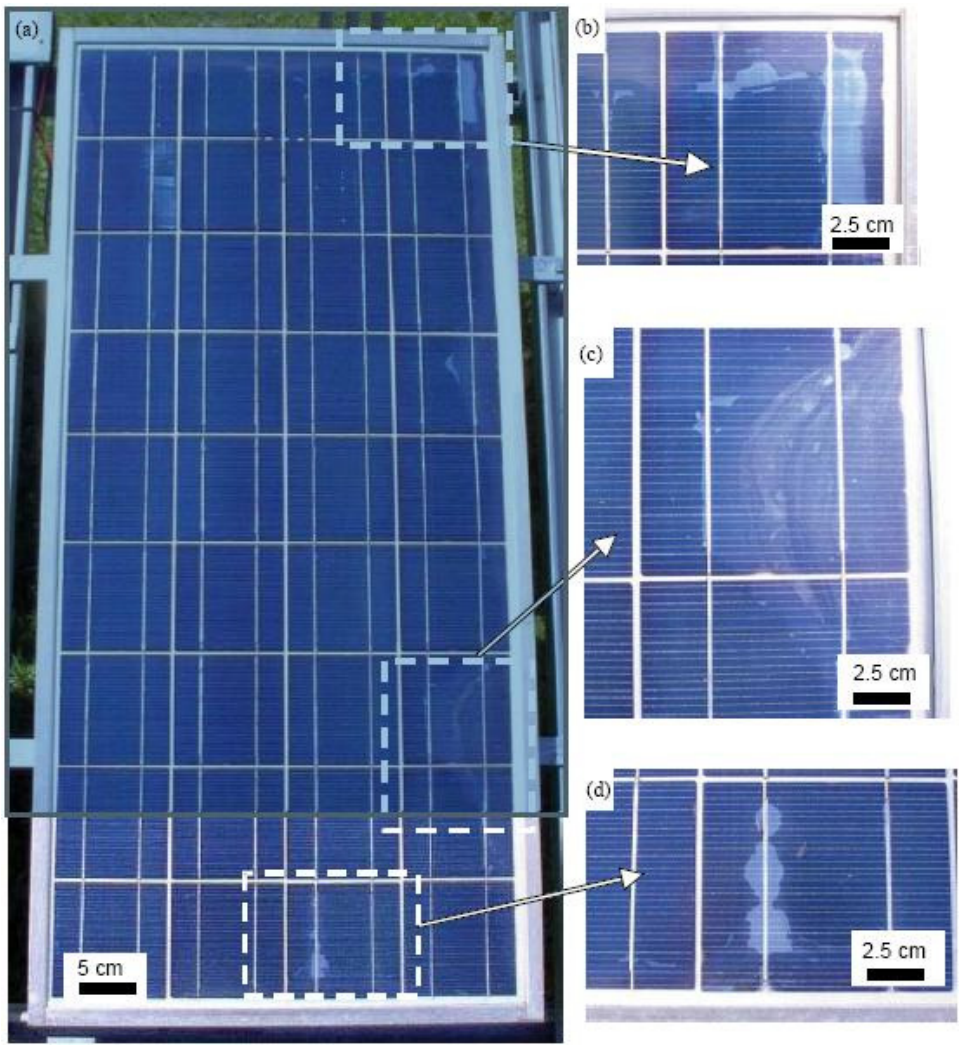

圖19 EFG 模組經過曝曬後劣化圖[8]

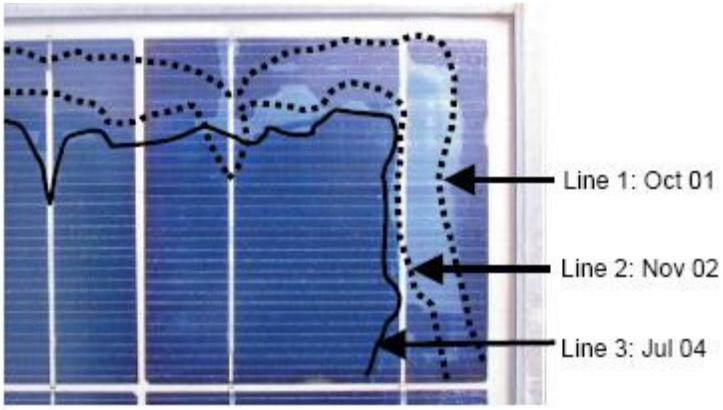

圖20 模組剝離情況時程圖[8]

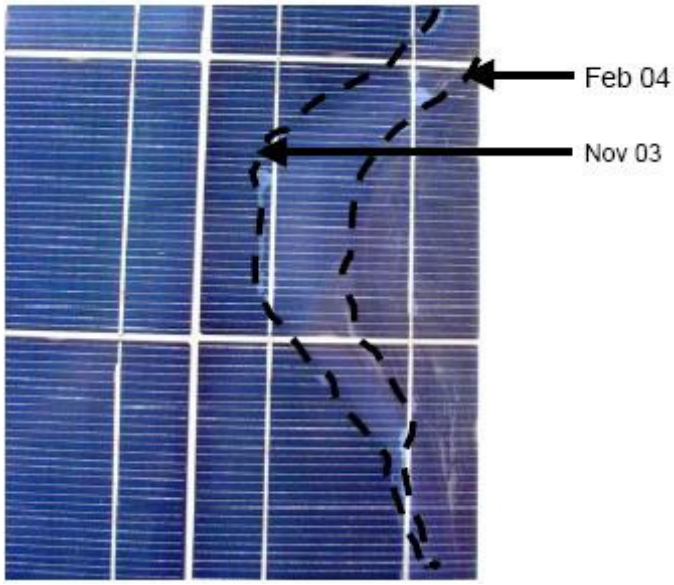

圖21 水氣侵入狀況在不同季節的改變[8]

由圖 21 可發現水氣的侵入也會隨著季節的變化而有所不同，於夏季中(2003 年 12 月到 2004 年的 1 月)，可發現水氣的侵入有退後的跡象，例如圖 21 中在 2004 年 2 月的水氣侵入狀況比起 2003 年 11 月有退後的情況產生。此種水氣侵入退後的現象主要是因氣候狀態變化，當氣候為較炎熱的夏季時，由於蒸發旺盛故已侵入的水氣線會往後退使水氣侵入的情況改善，甚至會使太陽能模組的輸出效率些許回升。

除了觀察太陽能模組外部肉眼可見的變化外，該實驗亦進行實際電性數據的量測，圖 22 中數據為經標準化後的數值，由圖 22 可知，開路電壓(V_{OC})幾乎維持在一個定值，並沒有顯著的變化，但短路電流(I_{SC})在戶外曝曬後開始下降，而輸出最大功率(P_{max})也相對隨之下降，較特殊的部份是在折線中存在短路電流回升的現象，於是輸出功率也跟著提升，此時間恰巧為前述水氣侵入情況退後的時間，因此可以合理的推測此太陽能模組輸出情況之改善與氣候的改變亦有相關。

圖 23 為實驗模組的電流-電壓特性曲線圖，圖中分別為不同時間下所量測出的數據，可發現隨著時間增加，模組之輸出效能逐漸降低。其中短路電流之斜率幾乎維持於一定值，並無顯著變化，表示太陽能電池的並聯電阻在戶外曝曬期間並沒有顯著下降；相對的，開路電壓的斜率卻隨著時間的不同而有所變化，表示太陽能電池之間的串聯電阻逐漸增加。實際電阻值量測的結果顯示，在 2001 年時，串聯電阻為 0.4 歐姆，直到 2004 年時，增加為 0.9 歐姆，由圖 24 中可以由觀察模組匯流排腐蝕現象判斷主要造成串聯電阻上升的原因為匯流排接點間的腐蝕老化所致，如圖 24 所示。。

進一步分析可知模組中各層介面剝落和水氣的侵入都會造成太陽能電池特性不匹配(mismatch)的現象，主要原因為較少的陽光能夠到達發生剝落和水氣侵入處，當有不匹配的情況產生時，會造成該處太陽能電池運作溫度的上升，為了解此現象，該實驗亦量測該太陽能模組表面溫度，如圖 25 所示。

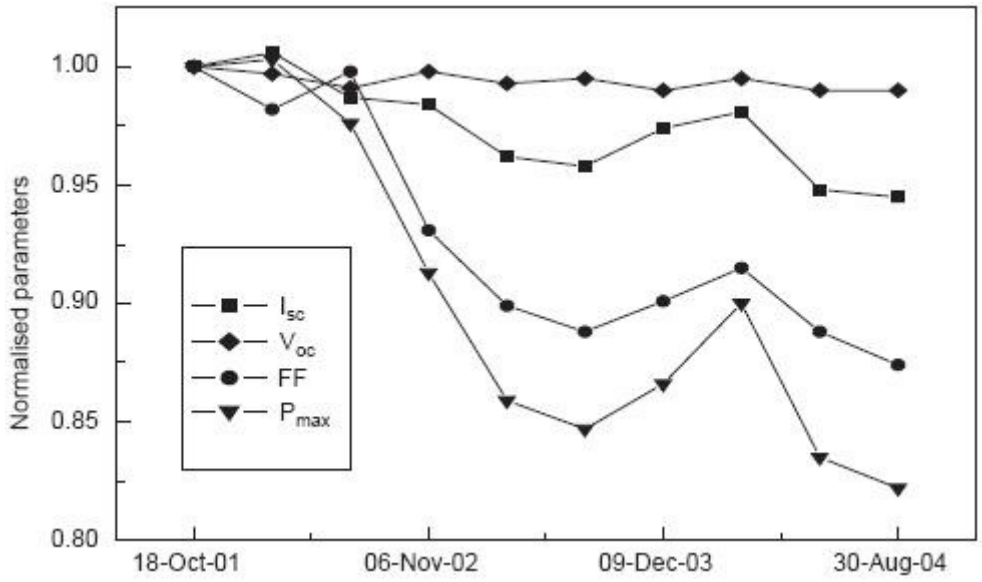

圖22 模組電性參數相對於時間的變化[8]

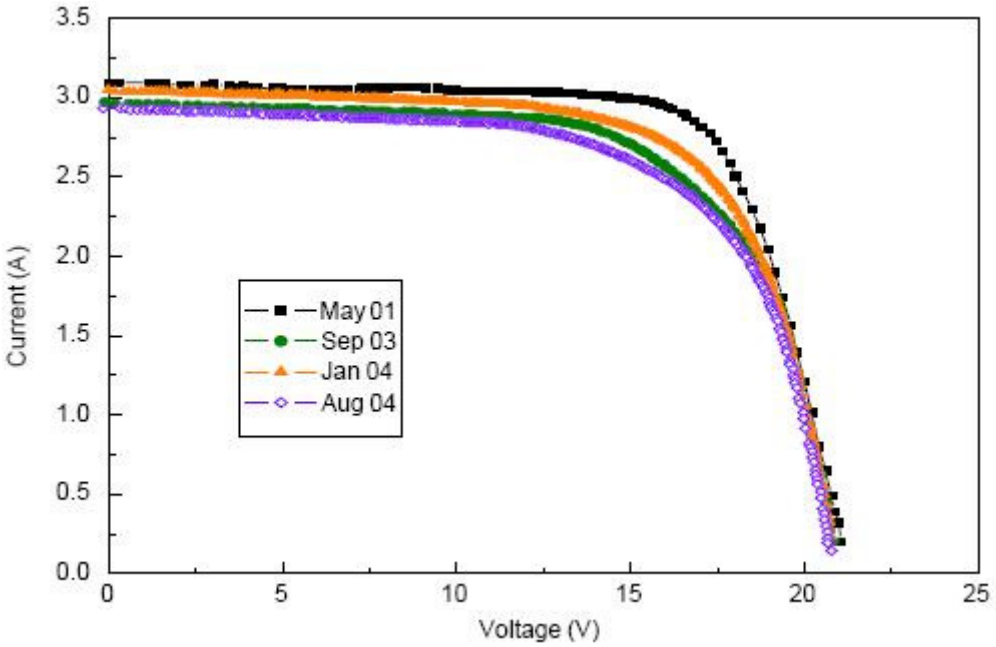

圖23 模組不同時間下的電流-電壓關係圖[8]

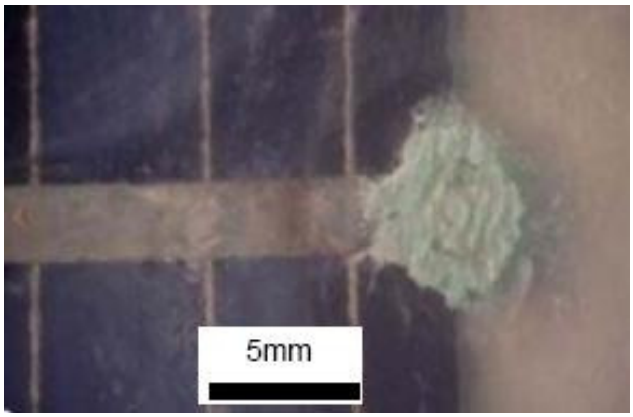

圖24 匯流排接點的腐蝕[8]

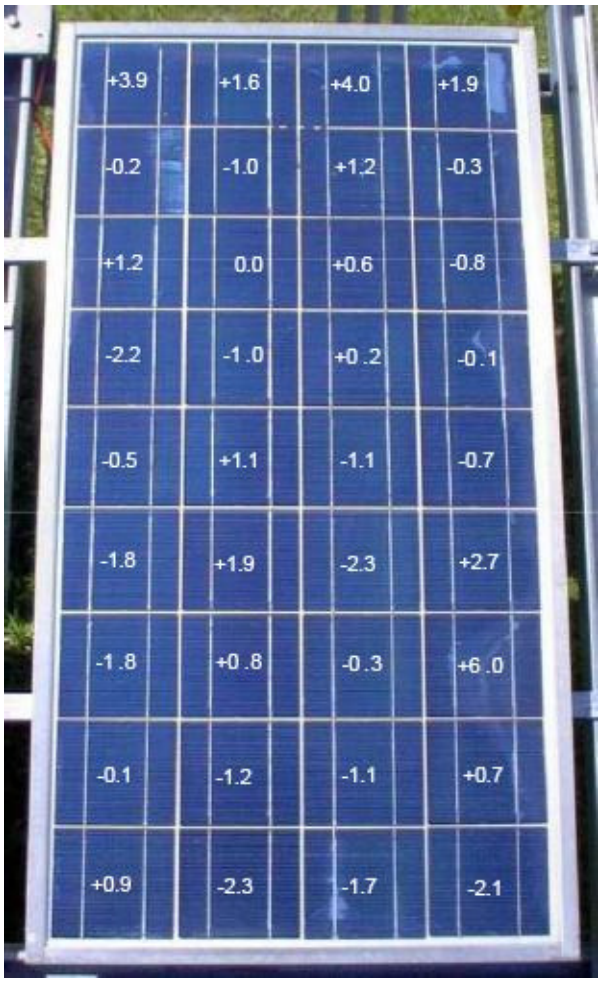

圖25 模組最後曝曬時的溫度與總曝曬運作溫度平均值的差值[8]

由圖 25 可發現，對照圖 19 中被水氣侵入的剝落區域，這些區域的溫度都有顯著提升，該數據是選取在戶外曝曬最後時段的溫度

與總時間溫度平均值(41.1℃)之差值。在顯著的剝落情況區域中，可以發現其溫度的上升較多。

6.4 材料介面間鋁氧化合物生成的影響

該實驗[9]選用非晶矽薄膜太陽能電池模組，p-i-n 結構，額定輸出功率為 14W，但由於 Staebler-Wronski 光劣化效應[10]，會使得其實際輸出功率在首度使用後便先下降約 15%左右。實驗中模組老化情況隨著時間惡化，直到無法輸出有效功率，模組大約有 30%的部份可被觀察到有腐蝕的現象發生。

表 6 所示為此模組輸出最大功率隨時間的變化，可發現其首次開始戶外曝曬實驗後，輸出功率即有下降的情形，經過 80 個日照時數(約 13 天)後，輸出功率則是下降到 5.56W，幾乎為原本的一半。

圖 26 所示為該實驗所使用之太陽能電池架構，中間沒有被滲雜的本質層厚度約為數百 nm，夾在分別約為數十 nm 的 p 型摻雜與 n 型摻雜的非晶矽之間，此兩層非晶矽將會構成一個穿透本質層的電場。

圖 27 為模組之電流-電壓特性曲線圖，由實驗到最後階段所量測之曲線可以得知其輸出效能之退化情形，由表 7 可知，和初始的特性曲線之數據相比較，最大輸出功率值由 12.53W 下降至 2.64，短路電流由 1.13A 下降至 0.28A，而開路電壓降幅相較之下較少，從 24.3V 降至 21.0V。

表6　模組最大輸出功率之量測[9]

Measurement time	Power(W)	Ratio
Initial	12.53	100 %
Prior to outdoor exposure	10.86	86.67 %
After 80 sun-hours	5.56	44.37 %
After 130 sun-hours	5.15	41.1 %
Final, after 3500 sun-hours	2.64	21.07 %

表7　實驗前後模組之特性數據[9]

Time / Parameter	Before	After
P_{max}(W)	12.53	2.64
I_{SC}(A)	1.13	0.28
V_{OC}(V)	24.3	21.0

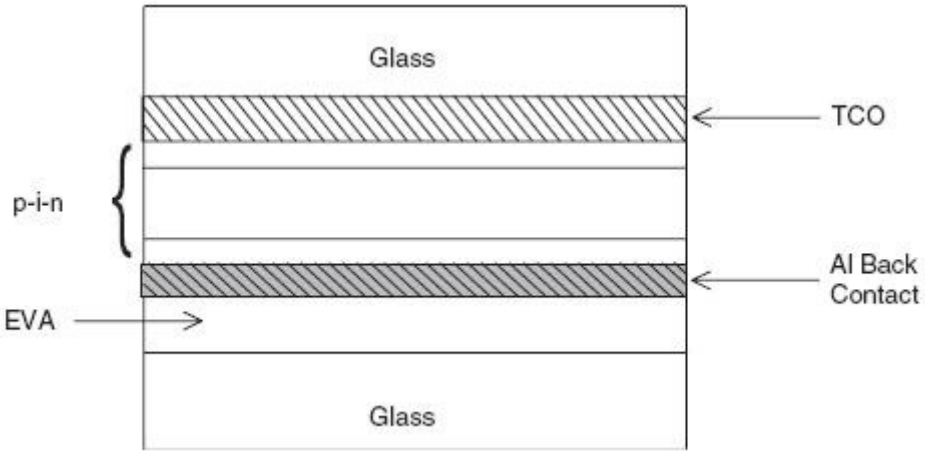

圖26 太陽能電池之組成架構[9]

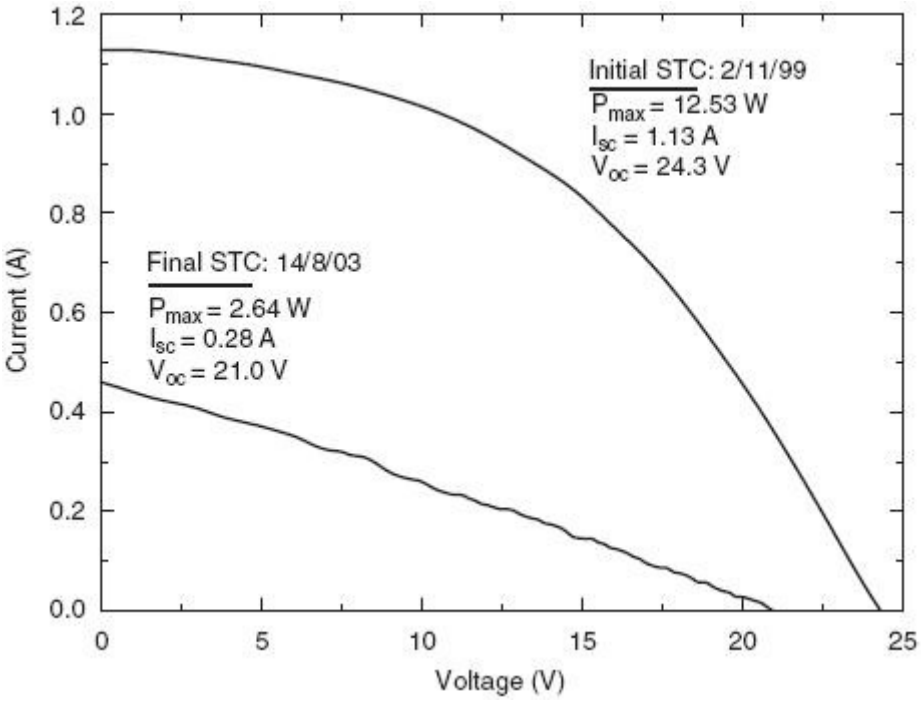

圖27 模組之初始與最終電流-電壓關係曲線圖[9]

由圖 27 中亦可觀察到短路電流之斜率有增加之情形，可推斷為電池間之並聯電組值減少，且可觀察到開路電壓之斜率為減少的情況，即太陽能電池間串聯電阻值之增加，此電阻值之增加主因為在模組中鋁化合物的生成。

將金屬外框拆除後可以見到太陽能電池模組老化的情形，如圖 28 所示，可以清楚看到水氣的侵入以及模組本體上的劣化現象，因為太陽能電池、EVA 和玻璃之間的剝落所造成的間隙，於是造成水氣的侵入和腐蝕。

由圖 29(a)中可看出不同物質介面間的情形，由下到上分別為玻璃、透明導電電極 SO_2、矽、由 EVA 所覆蓋之鋁製背面電極，其中矽/鋁製背面電極/EVA 之間的介面可以看的出來並不平整，此不平整之介面並不會影響彼此間的黏著力，但卻容易造成空間使水氣侵入，圖 29(b)為受到水氣侵入影響後介面之間的變化，明顯的可

以觀察到有大量的鋁氧化物生成，下列式子為此鋁氧化合物生成過程的化學式：

陽極的反應為：

$$Al \rightarrow Ai^{3+} + 3e^{-}\left(E = +1.66eV\right) \tag{1}$$

陰極的反應為：

$$\frac{1}{2}O_2 + H_2O + 2e^{-} \rightarrow 2OH^{-}\left(E^0 = 0.40V\right) \tag{2}$$

由上兩式之生成物可得：

$$Al^{3+} + 3OH^{-} \rightarrow Al(OH^{-})_3 \tag{3}$$

可分解為：

$$2Al(OH)_3 \rightarrow Al_2O_3 + 3H_2O \tag{4}$$

原本化合物 Al_2O_3 之形成可以減緩氧化的情況，然而由於此太陽能電池結構中之鋁製背面電極太薄，易導致整層鋁都被氧化，失去其保護之功能。

隨著戶外曝曬試驗的時間增加，模組水氣侵入與鋁氧化合物生成的情況也隨之擴展，導致更多的水氣侵入，圖 30 可以看出由於水氣侵入所導致的鋁氧化合物生成的情形，此外，由於氣候狀態而產生的溫度變化以及模組內太陽能電池間的不匹配也會導致嚴重的老化情形。

圖28 模組背面之介面剝落與水氣侵入的情形[9]

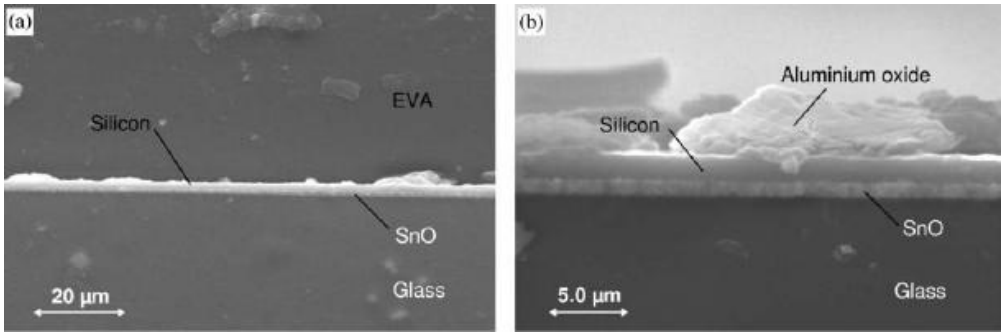

圖29 介面間受影響前後之差別[9]

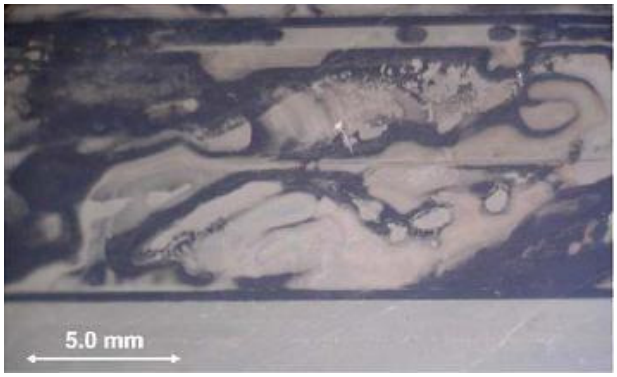

圖30 水氣侵入導致鋁氧化合物生成的情形[9]

該實驗又提到，當水氣侵入與鋁氧化合物生成時，在溫度升高的情況下，在受到此一影響的模組封裝板部份會有氣泡的產生，由圖 31 可以清楚的看到氣泡的形成。

除此之外，由於太陽能模組的表面可能由於氣候狀態會有水珠

形成，如圖 32 所示，水珠在模組表面將會成為類似透鏡的作用，將光線聚焦在模組上，其他光線光線無法照射到水滴內焦點外的範圍，造成遮蔽的現象，而產生熱點(Hot spot)，如圖 33 所示。

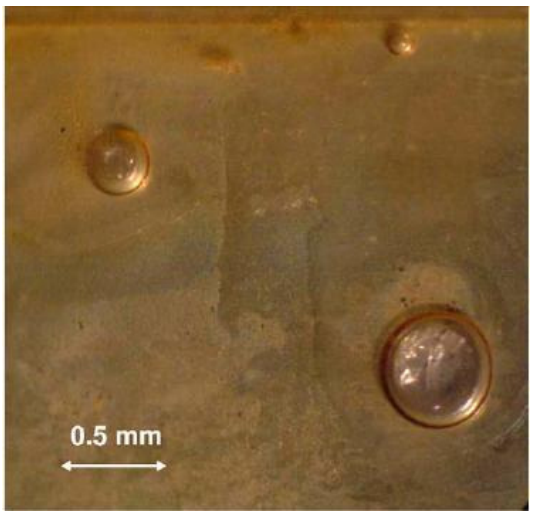

圖31 封裝板介面間的氣泡之形成[9]

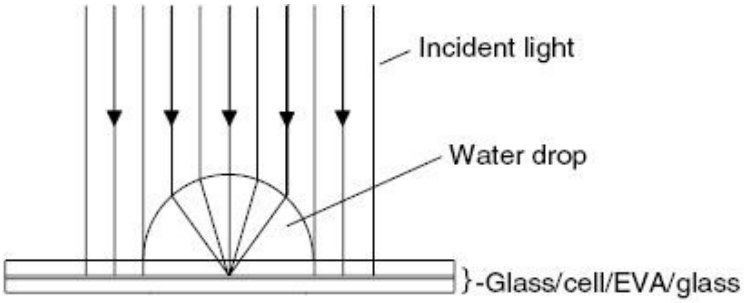

圖32 水珠在模組上產生類似透鏡之效果[9]

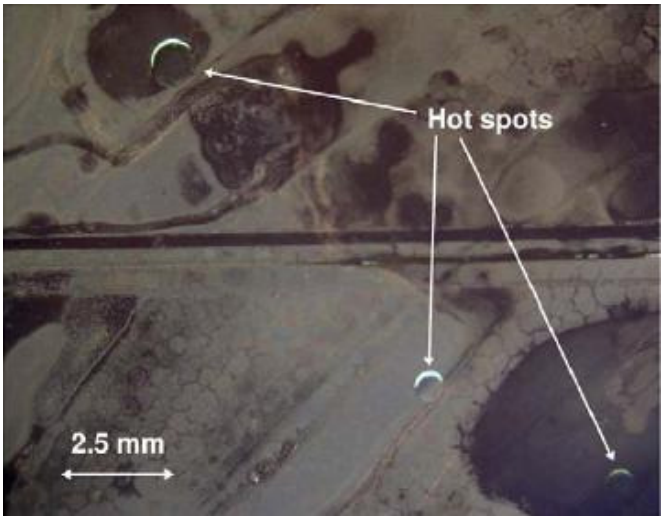

圖33 太陽能電池上熱點之形成[9]

熱點會導致不匹配的情況發生，讓太陽能電池運作溫度升高，且由於水滴類似透鏡的作用產生之焦點會有更高的溫度，可能會使的太陽能電池直接遭受到高溫破壞。

6.5 高濕、鹽度環境之影響

美國佛羅里達太陽能中心(Florida Solar Energy Center)的太陽能電池材料實驗室(PV Materials Laboratory)透過一實驗研究玻璃中鈉含量與模組介面間附著力的相關性[11]。

由於在靠海的高鹽度環境下，太陽能模組表面在經過一段運作時間後總會有較高含量的鈉和磷，據研判表面磷含量主要是由於進行 n 型摻雜所造成，至於表面鈉含量則是導因於沿海氣候的大氣中所含有之鈉，此外，在製造太陽能電池過程中由化學成分助益的擴散作用也是造成鈉與磷含量過高的原因。

由圖 34 可以看出鈉、磷含量與模組介面間附著力的關係圖，當鈉或磷的含量愈多時，附著力愈減弱。故可推論，在製造太陽能電池的過程中有效的監控摻雜的濃度或是雜質的擴散能有效的加以限制，將可延長太陽能電池模組的使用壽命。

在過去，鐵雜質含量在玻璃製造過程中也佔有一定比例，然而由於會讓光線的穿透度降低，且會讓玻璃生成暗綠色的現象，過去石灰岩($CaMg[CO_3]_2$)常被用於製造玻璃，但其含有較多的鐵成分故不適用於低鐵含量製程的玻璃中，當 $CaMg(CO_3)_2$ 成分被降低後，需要用其他物質來補足，於是鈉氧化合物(Na_2O)便被拿來使用，其成分在低鐵含量製成玻璃中大約為 15%以上，由於鈉是較有活性的離子，故需要摻雜 SO_2 來降低鈉之活性。

該實驗共選用五種不同的玻璃作測試，由不同的蘇打灰成分和 SO_2 含量所構成，分別為 Krystal Klear Float、Krystal Klear Float with lower Na_2O、Solite with normal SO_2、Solite with high SO_2 (4 scfh in annealing lehr & 30 psi in the tempering furnace)、Solite with high SO_2 (5 scfh in annealing lehr & 80 psi in the tempering furnace)等五種。

另外實驗用太陽能電池分為四種，分別為有(無)塗上抗反射層(A、N)、有(無)用異丙醇清洗(C、N)，故可以分為 AC、NC、AN、NN。該實驗室進行在濕熱加速測試環境下，環境溫度為 85℃，相對溼度為 85%，進行時間為 1000 小時。

在第一類和第三類型號玻璃中，可以觀察到其玻璃表面粗糙化程度嚴重並且有汙點產生，EVA 和玻璃介面產生之剝落情況清晰可見，且玻璃表面也產生乳白色的斑點，研判為裂化的現象。第四類和第五類則是可看出表面粗操化的程度明顯較少，汙點產生與粉末生成的情況也相對較少，EVA 和玻璃介面則是只有周圍有剝落的情

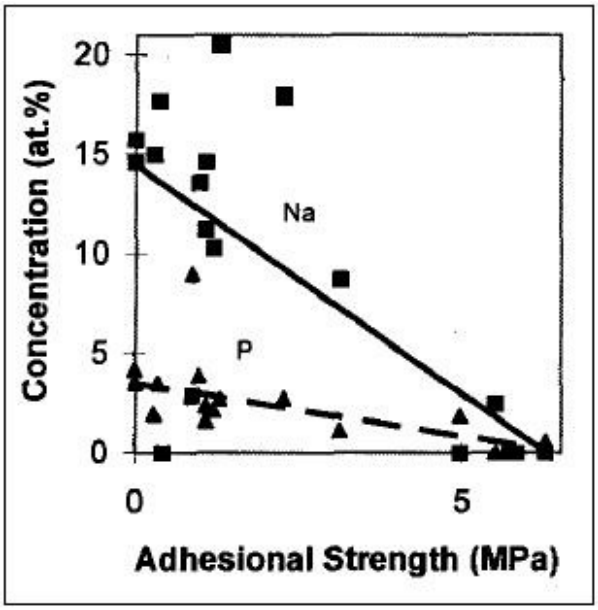

圖34 鈉、磷含量與附著力之相關圖[11]

況，中間部分並沒有此情況產生，且在第五類中因為不同的製造環境所影響，有較少的粉末形成。第二類方面，則沒有粉末生成，且汙點產生的情況是最輕微的，剝落的情形比起其他四類亦最輕微。

由圖 35 可以看到四種不同太陽能電池在第二類玻璃中，經過溼熱測試後不同程度的劣化情況，而圖 36 則是在沒有塗抗反射層且沒有用異丙醇清洗的情況下之太陽能電池，在第一、三、四、五類玻璃中經過測試的情況。如同所預期的，如果太陽能電池有塗上抗反射層，在測試後其呈現的是暗藍色，而沒有塗抗反射層的電池則是呈現單調的暗灰色，此外，也觀察到介面間附著力減弱的情況。在模組中間部份，電池與 EVA 介面之平均附著力，以第一類和第三類為最小，而在模組周圍部分，玻璃和 EVA 介面之平均附著力則是第三類最小，可以發現當增加 SO_2 含量後(即第四類玻璃)，其附著力有明顯的改善，且第二類與第五類的玻璃更是表現出最佳的附著力。

當太陽能模組介面之間產生剝落後，水氣會侵入空隙之間，與鈉或磷產生化學作用，進而使電池間金屬電極產生腐蝕現象，而增加串聯電阻之增加，造成輸出效率降低，故需要加入 SO_2 來抑制這些元素的活性；然而除了增加 SO_2 含量尚需配合適當的製程環境因數，才能達成其效用。

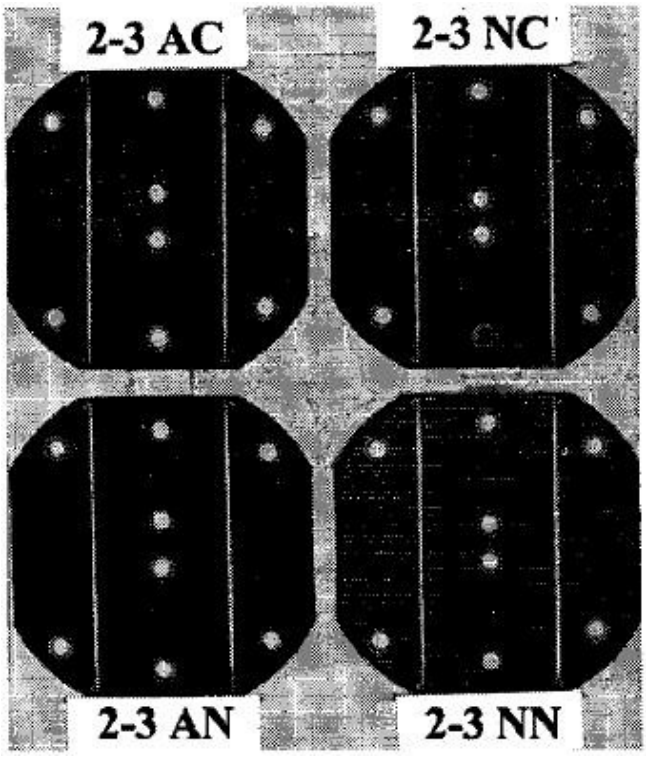

圖35 第二類玻璃中 4 種不同太陽能電池的情形[11]

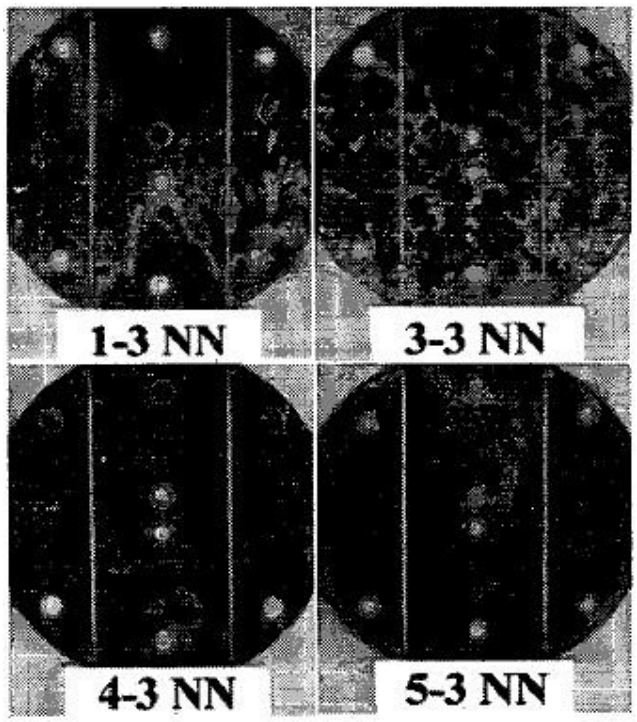

圖36 無塗抹抗反射層且沒有用異丙醇清洗之太陽能電池在四類不同玻璃中的情形[11]

6.6 紫外線之影響

結晶矽太陽能模組在經過長時間的室外光照下，經常會發現用於模組玻璃與電池間的 EVA(ethylene-vinyl acetate)透明黏膠，會有褐色化的變色現象[12]，如圖 37 所示。此一現象會造成模組的遮蔽、光穿透度的降低，進而造成發電效率的下降。許多研究報告曾指出結晶矽太陽能模組會發生 EVA 褐色化的現象，而造成模組效率的大幅降低，然而解釋造成 EVA 褐色化原因之文獻卻相對較少，以下針對造成 EVA 褐色化的因子及如何降低其褐色化的原因有較詳盡的說明介紹[12]。

EVA 是乙烯乙烯酸共聚所組成的化合物。因其同時具有較高的物理強度、高透光度及極佳的絕緣效果，因此經常被太陽能產業所使用，應用作為太陽能電池與玻璃基板間的黏膠。

對於目前工業應用上，EVA 應用在太陽能模組上可分為兩道程序，分別是層壓與固化兩程序。其中層壓時間大約為 8 至 10 分鐘，並處在 120℃的溫度環境；固化程序則依不同的固化劑可分為快速固化(fast-cure)及標準固化(standard-cure)，快速固化大約是 10 至 12 分鐘，並處在 145℃的溫度環境；而標準固化則是約 45 分鐘，並處在 145℃的溫度環境。而經由實驗最後的發現，標準固化比起快速固化有著較顯著的 EVA 褐色化現象。

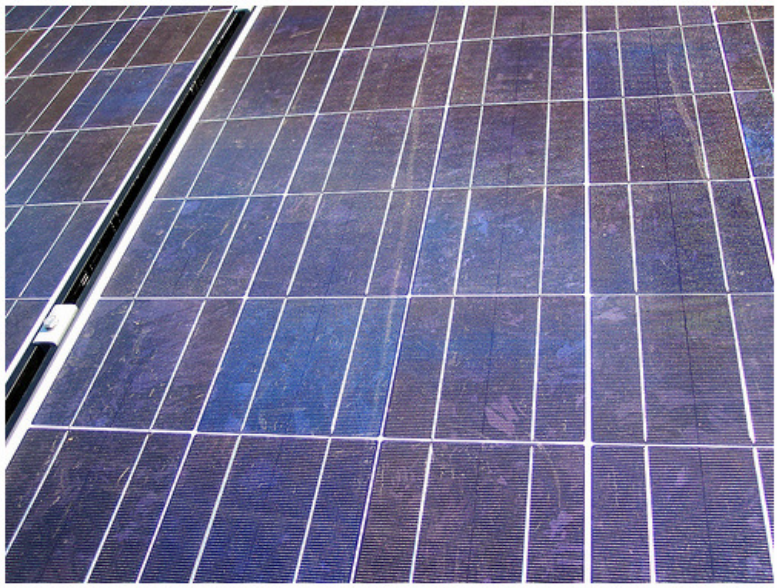

圖37 EVA 褐色化現象[12]

目前市面依快速固化與標準固化兩種，較常用的 EVA 分別為 EVA 15295 與 EVA A9918，其中 EVA 15295 為快速固化時常使用的 EVA，其固化劑使用的是 Lupersol TBEC；而 EVA A9918 為標準固化時常使用的 EVA 產品，其固化劑使用的是 Lupersol 101。兩種固化劑在不同固化時間完成固化後，所剩餘的固化劑濃度如圖 38 所示。

由圖 38 可知快速固化所使用的固化劑 Lupersol TBEC 在經過 10 至 12 分鐘的固化時間後，其所剩餘的固化劑濃度為約 6%；而標準固化所使用的固化劑 Lupersol 101 在經過 45 分鐘的固化時間後，其所剩餘的固化劑濃度約為 42%。而這樣顯著的固化劑剩餘濃度差異，在經過實驗後的分析與觀察，發現較高的固化劑剩餘濃度會產生較高濃度的紫外光激發有機發色團(UV-excitable chromophores)，而所產生的紫外光激發有機發色團因為受紫外線的照射而激發，改變了本身鍵結的形式，而發生變色的現象，因此這

也使得標準固化之 EVA 褐色化速率比快速固化高。

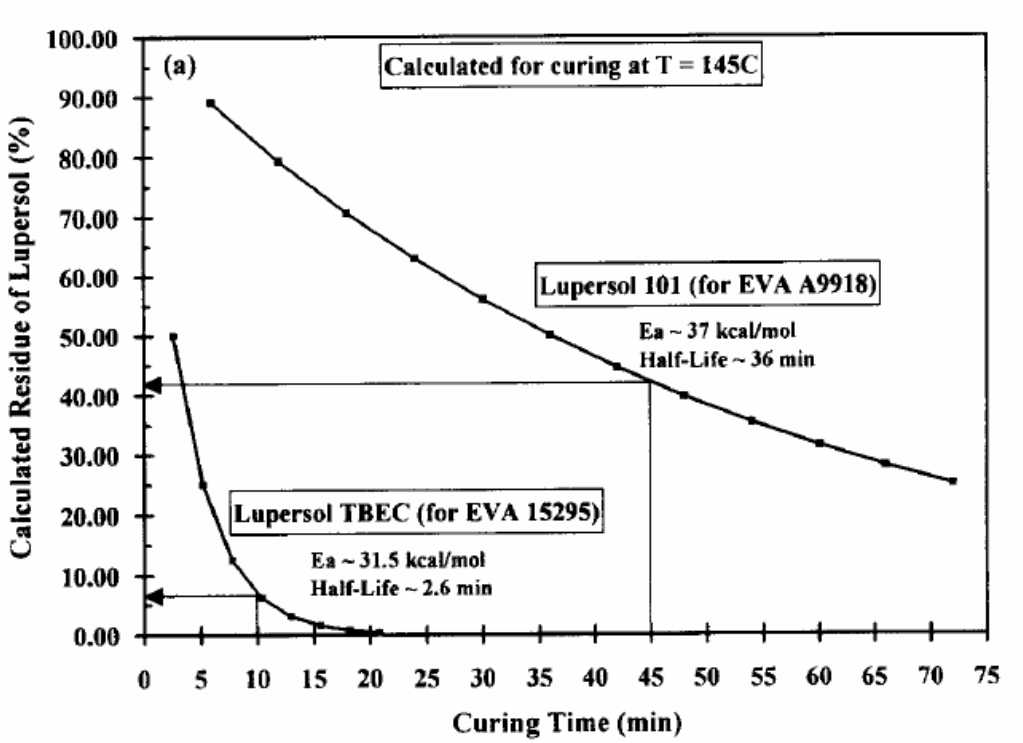

圖38 EVA 固化時間與固化劑剩餘濃度量測圖[12]

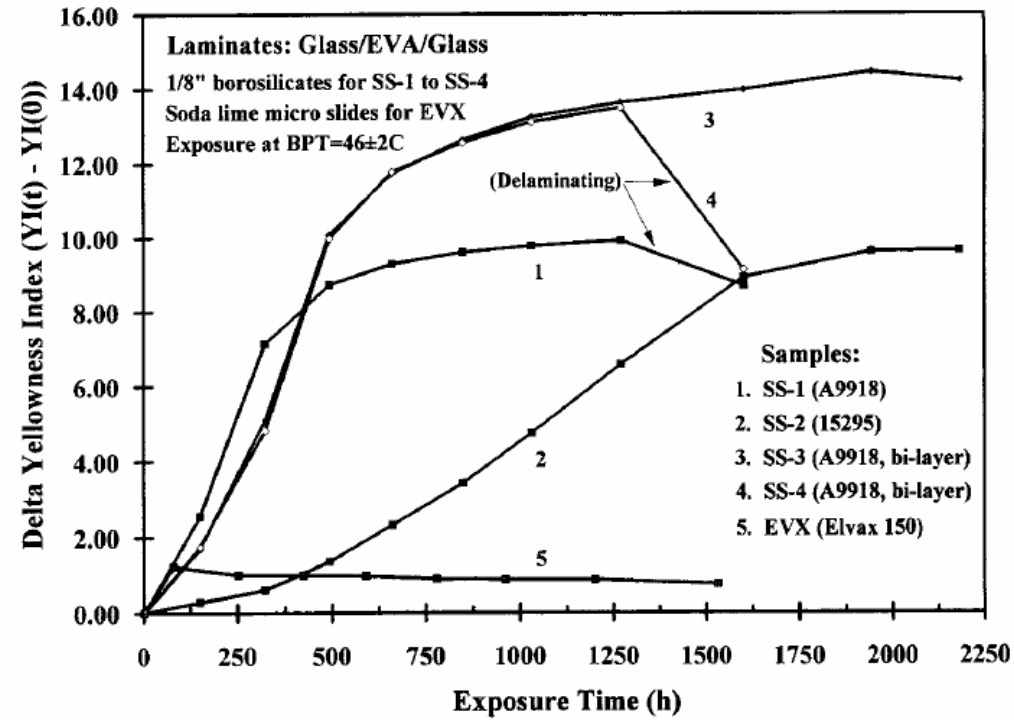

圖39 快速固化與標準固化之 EVA 褐色化速率比較[12]

標準固化與快速固化兩程序之 EVA 褐色化速率如圖 39 所示，其中 SS-1(A9918)為標準固化之 EVA，而 ss-2(15295)為快速固化之 EVA。

然而，在一般的 EVA 製程上，都會混入紫外光吸收體(Cyasorb)來吸收紫外光，以保護紫外光激發有機發色團，避免其被紫外光所激發而變色。有無紫外光吸收體對不同波長大小的光之透光率的比較圖如圖 40 所示，由圖 40 可以看出伴隨著紫外光吸收體可以阻擋紫外光的穿透。儘管如此，根據實驗結果發現，紫外光吸收體會在光照下發生光分解現象，影響氫鍵之鍵結力，同時自由基會因為光化學反應而產生，並破壞紫外光吸收體，使其失去原本隔絕紫外線的效果。

紫外光吸收體光分解的現象如圖 41 所示，圖 41 為紫外光吸收體對不同波長之紫外光的吸收度，吸收度越大表示其吸收體濃度越高，即尚未被分解。圖 41 中亦可看出，吸收度隨著時間在不同的波長波段下都有明顯的降低，其中對 288nm 及 328nm 兩波段原本都有在吸收度上的峰值，但隨著時間其吸收度都有明顯的下降，表示紫外光吸收體光分解的現象發生。

圖 42 與圖 43 分別表示 EVA 經過長時間太陽光照射後其對不同波長大小的光之穿透度變化及穿透度差量的大小變化，由圖 42 與圖 43 皆可看出對於可見光與紅外光波段的光，其穿透率明顯隨著時間增加而降低，其原因是因為隨著 EVA 褐色化的現象發生，對可見光與紅外光造成阻隔效果，降低此波長範圍的光穿透度；而在紫外光波段的光，穿透度卻明顯提升，此乃由於隨著紫外光吸收

體的光分解現象，對於紫外光的吸收度大幅降低，因此造成紫外光的穿透度提升。

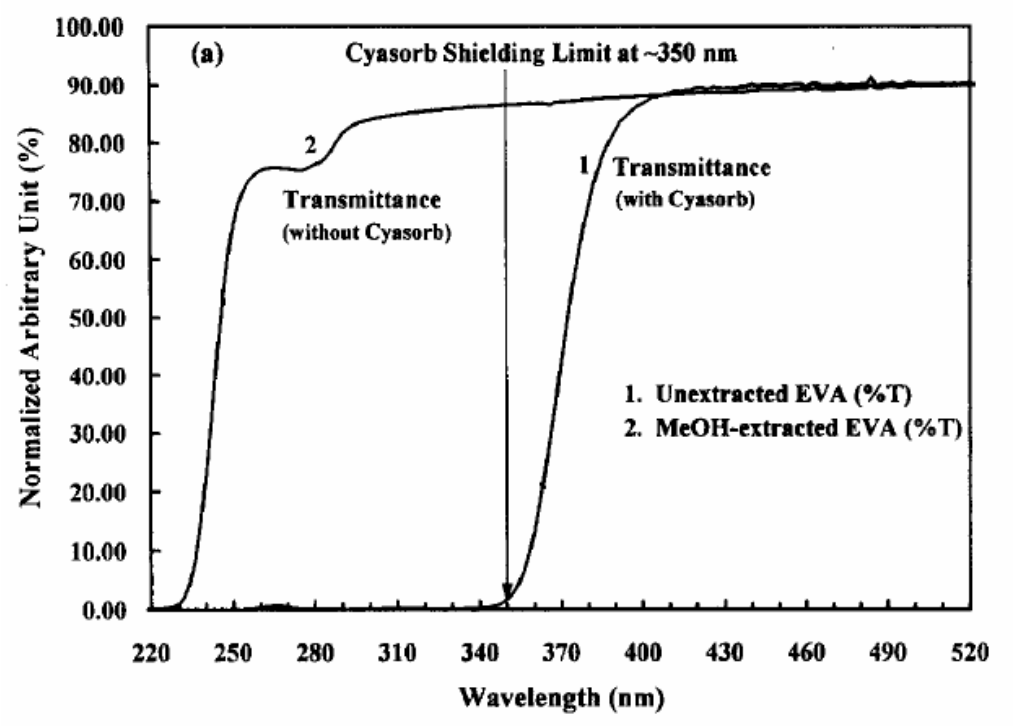

圖40 有無紫外光吸收體對不同波長的光之透光率比較[12]

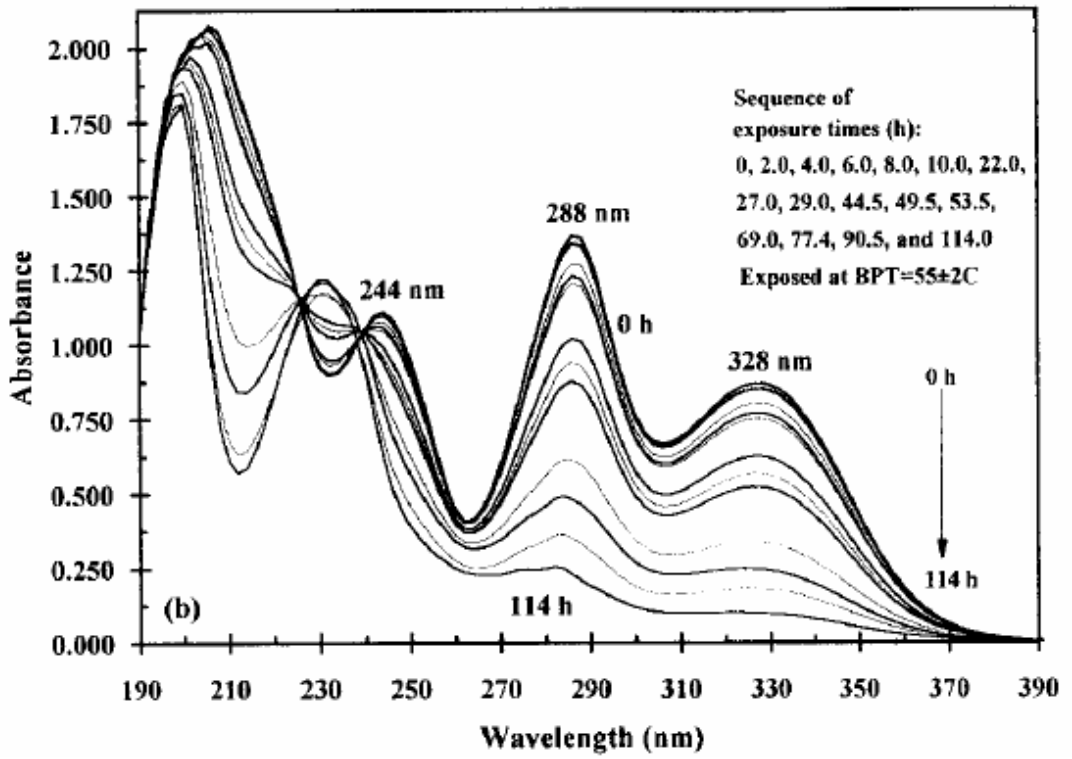

圖41 紫外光吸收體光分解現象[12]

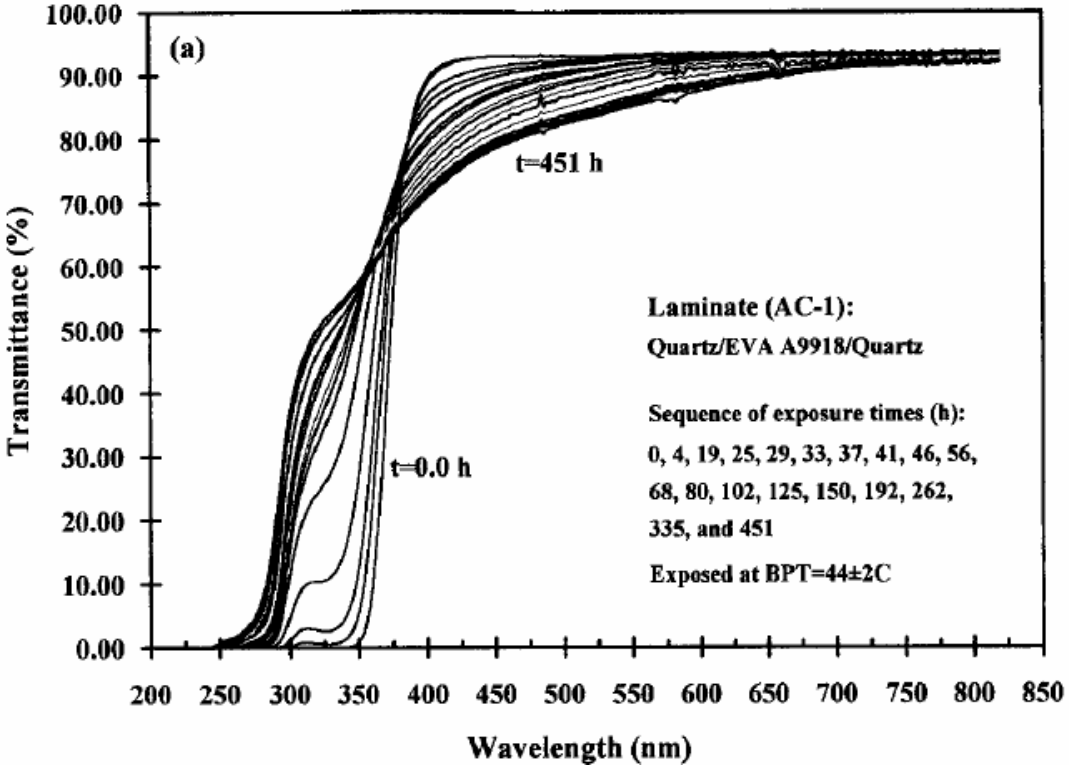

圖42　EVA 隨著時間對不同波長光的穿透度[12]

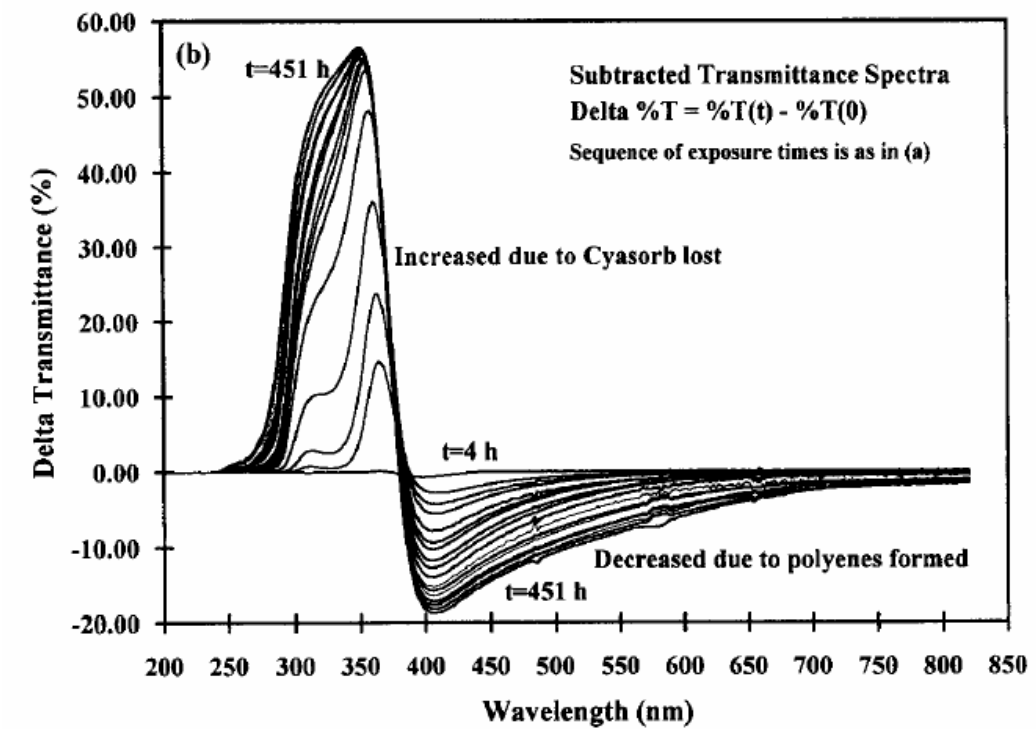

圖43 EVA 隨著時間對不同波長光穿透度的差量大小[12]

以上針對 EVA 褐色化的原因加以說明，並得到在現今工業應用上，標準固化比起快速固化其 EVA 褐色化的速率有明顯快速的結論。另外該篇報告依針對如何減少 EVA 褐色化現象進行實驗及分析，並得到兩個方向來降低 EVA 褐色化現象，分別是穩定紫外光吸收體、濾光玻璃的使用。

先前提到，紫外光吸收體的光分解現象是導致紫外光穿透，進而激發有機發色團使其變色的主因，因此，如何穩定紫外光吸收體使其不發生光分解現象會是降低 EVA 褐色化的方法之一。為了穩定紫外光吸收體，實驗嘗試混和抗氧化劑(Naugard P)及自由基清除劑(Tinuvin 770)於 EVA 中，來中和由光化學反應所產生的自由基，以避免其破壞紫外光吸收體[12]。

圖 44 中縱軸代表紫外光體對 328nm 波段光的正規化吸收度，而橫軸代表放置的時間，R 代表所混合自由基清除劑的單位濃度，K 代表所混合抗氧化劑的單位濃度。由圖 44 可知當未使用抗氧化劑(Naugard P)及自由基清除劑(Tinuvin 770)於 EVA 中時，其紫外光吸收體對 328nm 波段光的吸收度很明顯隨著時間降低，代表紫外光吸收體光分解的現象嚴重；而在同時使用抗氧化劑(Naugard P)及自由基清除劑(Tinuvin 770)於 EVA 中時，我們可以看到其吸收度隨著時間穩定維持在一定值，表示其紫外光吸收體未有明顯的光分解現象，達到了穩定紫外光吸收體的目的。而由圖 44 也可看出單一使用自由基清除劑(Tinuvin 770)比起單一使用抗氧化劑(Naugard P)有較好的穩定效果。

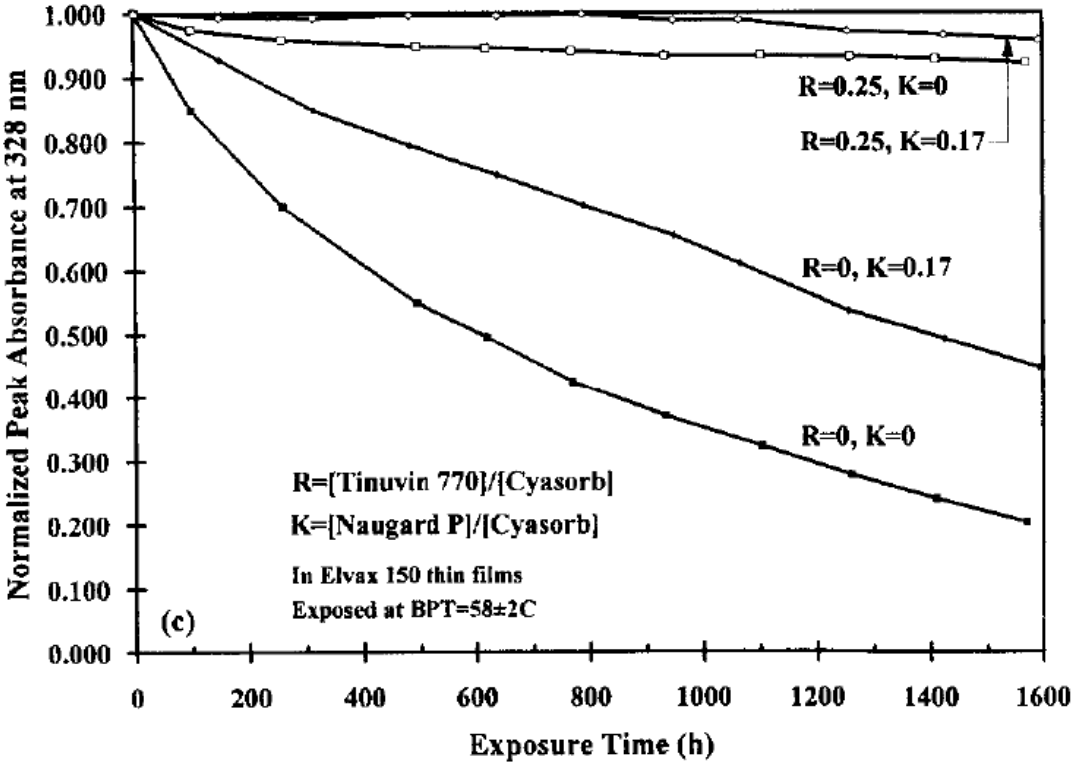

圖44 混合不同穩定劑對紫外光吸收體穩定度比較[12]

另一降低 EVA 褐色化現象的方法是濾光玻璃的使用，藉由玻璃的濾光效果來隔絕紫外光的穿透而造成有機發色團的激發，減少其變色的現象。實驗共使用了四種不同截止波長的濾光玻璃，分別是 270nm、290nm、320nm、340nm 的截止波長，其不同玻璃對不同波長的穿透度如圖 45 所示，由圖 45 可以看出濾光玻璃能對其截止波長以下的波長光有效的進行隔絕的動作，避免截止波長以下的光穿透。

圖 46 為使用不同截止波長濾光玻璃下，隨著時間對 EVA 褐色化變化量的影響，由圖 46 可看出使用越高波長的截止濾光玻璃時可以越減少 EVA 褐色化的現象，因為隨著截止波長選的越大，越多的紫外光可以被隔絕，也使 EVA 褐色化的現象越減小。因此經由實驗結果發現，適當的選擇濾光玻璃的截止光波長，可有效的抑

制 EVA 褐色化的現象。

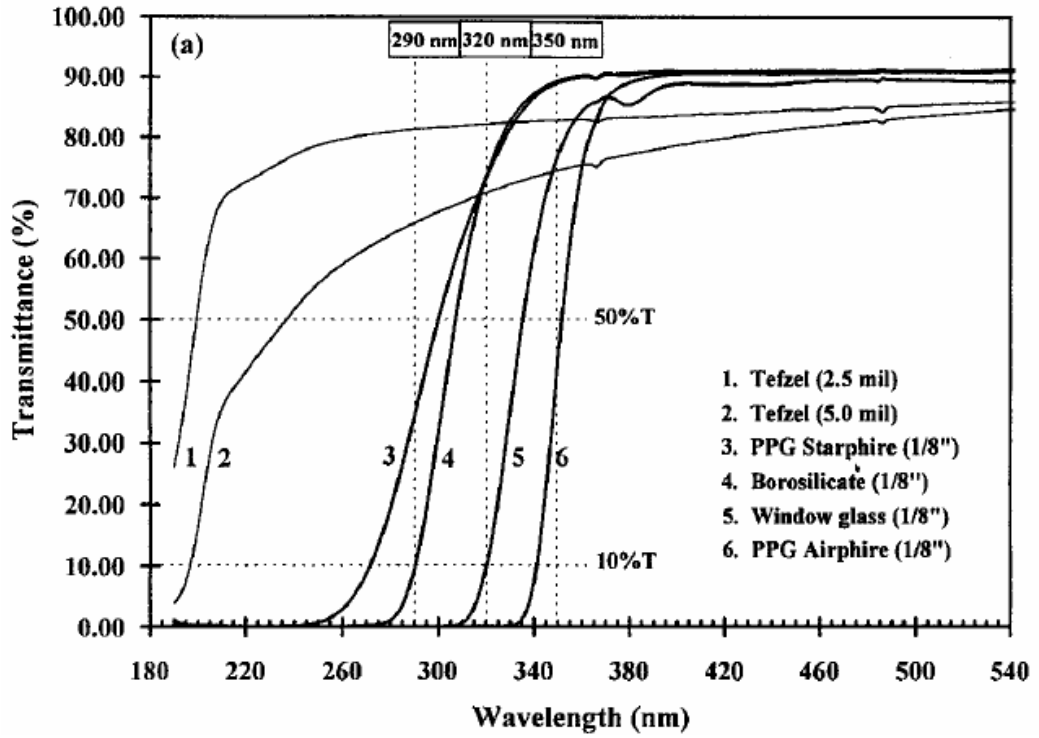

圖45 不同截止波長玻璃對不同波長光的穿透度比較[12]

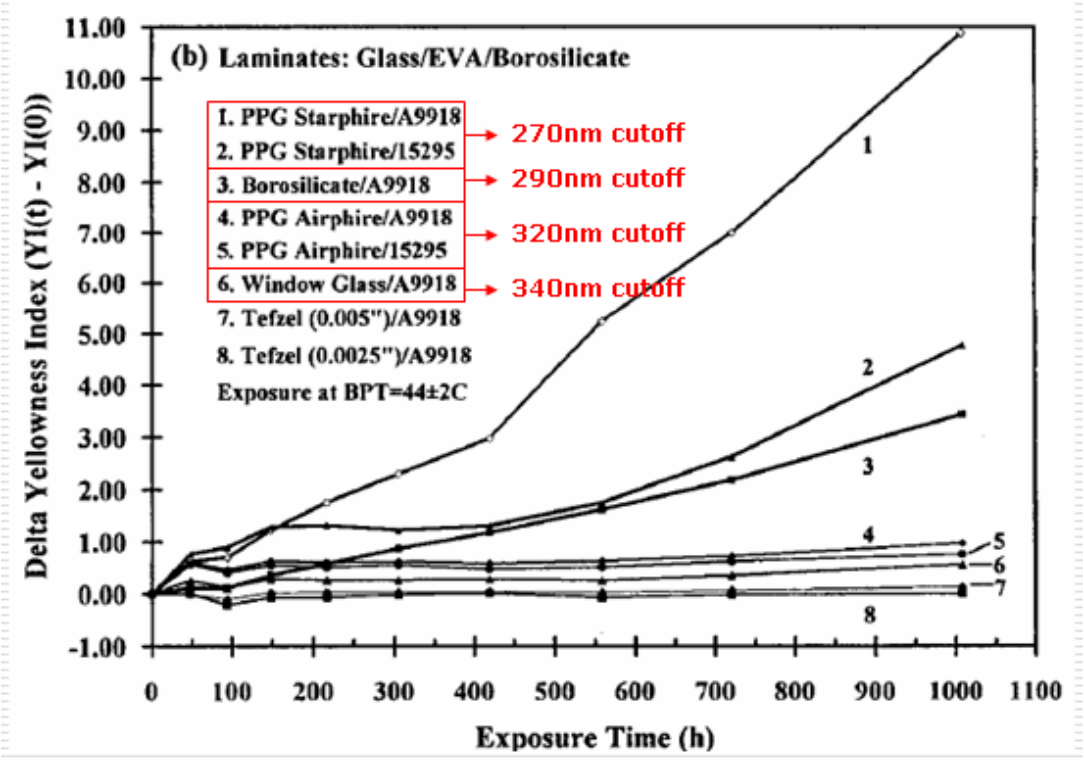

圖46 使用不同濾光玻璃對 EVA 褐色化的影響[12]

6.7 模組效能下降與失效常見原因探討

綜合前述不同製程、材料與環境因素對模組老化的影響，本文續探究因上列因素造成模組長時間曝曬老化的現象。文獻[13]針對結晶矽太陽能電池模組進行長時間的曝曬老化所做的實驗，並比較曝曬於室外與放置於室內的太陽能模組，以觀察老化的因子與現象。其結果共發現了三種主要的劣化現象，分別是初始的短路電流下降、串聯電阻的增加、太陽能模組的變色現象。

實驗總共包含了 26 組結晶矽太陽能模組，分別由三家日本製造商在 1990 年代初期所製造，並在 1991 年至 1993 年分別裝置於日本不同的四個區域，進行長達 10 至 12 年的曝曬實驗。

6.7.1 初始短路電流下降

由實驗結果發現，所有的模組的初始短路電流皆有下降的現象發生，而短路電流下降的現象亦造成輸出功率降低。經由量測可發現這樣的初始短路電流下降大約是以一年 1% 至 5% 的速率，但在大約一年後便趨於穩定不再下降。其量測結果如圖 47 所示。

為了更進一步確定初始短路電流下降之現象是否為太陽能電池在製程技術上的問題所引起，因此另外取用於 2002 年製造的太陽能電池進行實驗，並以 1 kW/m^2 強度的光照射於模組上，以加快其老化速度。實驗結果發現 2002 年所製造的太陽能電池仍然會發生初始短路電流的下降現象，短路電流大致在 300 分鐘內以 3% 的比率降低，而後並趨於穩定，其數據量測結果如圖 48 所示。

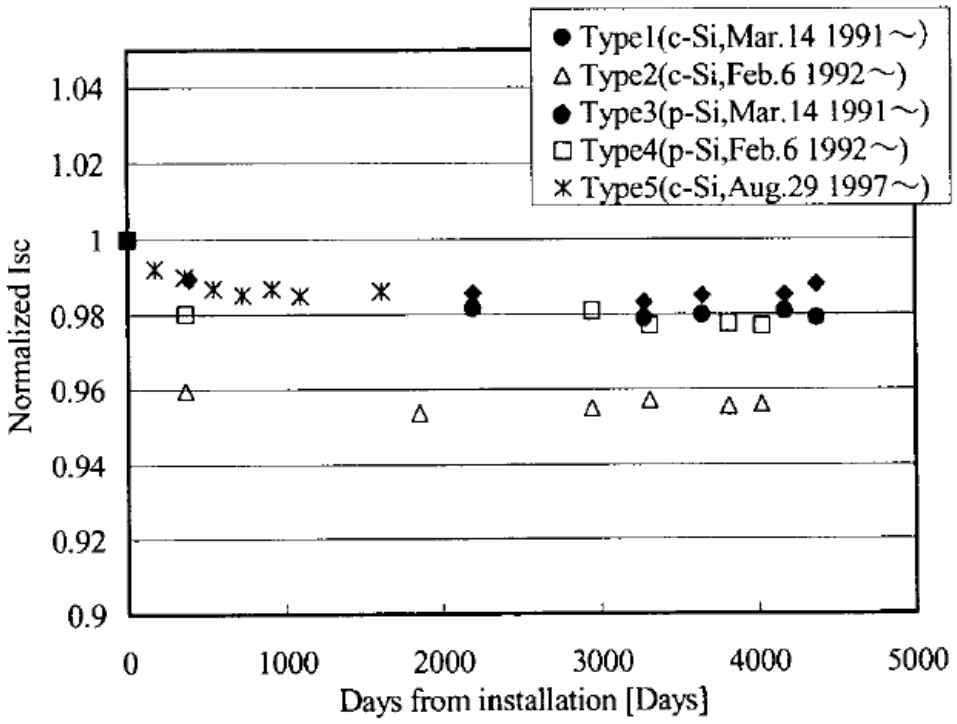

圖47 初始短路電流下降量測圖[13]

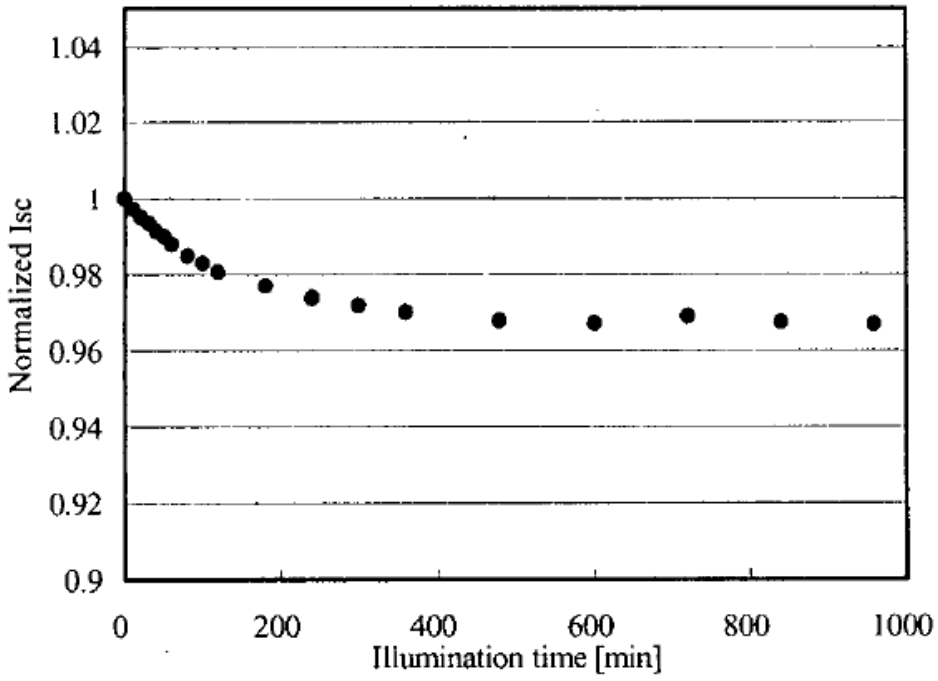

圖48 初始電流下降量測圖(1 kW/m^2 加強光) [13]

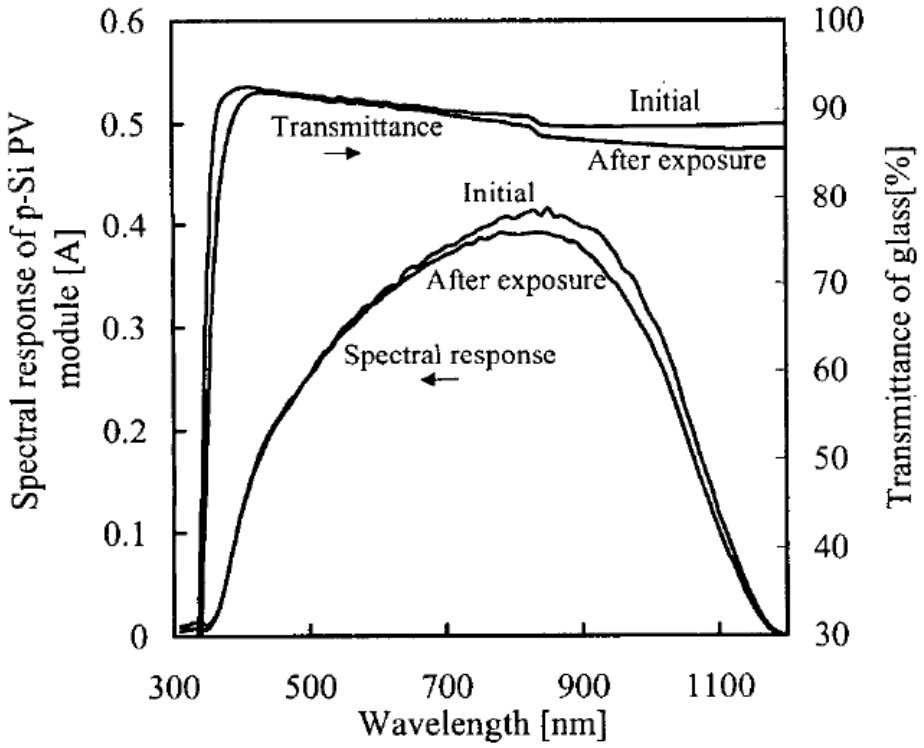

圖49 曝曬前與後的玻璃光學特性變化[13]

為了更進一步找出初始電流下降的原因，作者[13]分別對太陽能電池本身與 Glass/EVA/Glass 兩部份分開進行加強光照射實驗，在經過 300 分鐘後，太陽能電池並未發現先前短路電流的下降，而在 Glass/EVA/Glass 這部份則發現了透光率的降低，因此可推測初始短路電流下降的問題為因光照使玻璃的光學特性發生變化，導致玻璃在紅光與紅外光的透光率降低(如圖 49)，造成短路電流的降低，進而影響太陽能模組發電效率，但此一現象經過某段時間後便會趨近穩定，故並不影響長時間的可靠度。

6.7.2 串聯電阻的增加

經由十年的曝曬實驗中發現，在 26 組模組當中有兩組其效率降低超過了 10% ，經由量測後發現，其原因為模組串聯電阻 R_s 增加造成太陽能模組填充因數(Fill Factor, FF)降低所導致。

如圖 50 所示，FF 值大約以每年 0.9% 至 1.4% 的速率遞減。在圖 50 中經過 3000 個實驗天數後，可以發現一個 FF 值不降反升的現象，其原因是由於該實驗以酒精清洗模組串聯電極，使原本因銹蝕而接觸不良的電極導電性提高，因此降低了串聯電阻 R_s，也使模組 FF 值有提升的現象。

經過十年後的太陽能模組 I-V 特性曲線圖如圖 51 所示，並經由量測後發現放置於室內的串聯電阻為 0.5Ω，而室外曝曬模組之串聯電阻為 1.2Ω，而模組效率則降低了 20%。

串聯電阻增加經由實驗的分析，可在模組加以正向偏壓的情況下，觀察其溫度的分布情況檢測出來。因為串聯電阻的增加會增加消耗在串聯電阻上的功率，並產生熱，施加一正向偏壓會產生所謂 hot spot 現象，經由紅外線圖的觀察，可以找出串聯電阻增加的太陽能電池。圖 52 與圖 53 為因為串聯電阻增加而造成 FF 降低 20% 之模組的紅外線圖，其中在圖 53 我們可以很明顯的發現 hot spot 的現象。

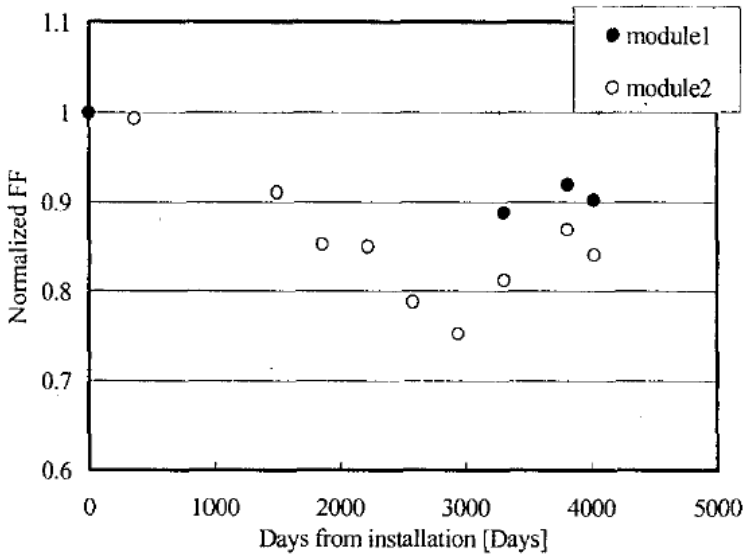

圖50 模組 Fill Factor 降低量測圖[13]

6.7.3 太陽能模組的變色

經過長時間的室外曝曬實驗後，結晶矽太陽能模組依有發現變色的現象，因為模組有變成白色的傾向，因此此現象依稱為所謂白化(Milky White)的現象，如圖 54、圖 55，發生類似變色的現象之模組，經由量測都有超過 25%的效率降低，主因則是因為短路電流的降低，如圖 56，經由圖 55 與圖 56 我們可以發現變色越嚴重的太陽能電池其短路電流依越小。經過十年曝曬實驗後發生變色之模組與放置於室內模組的 I-V 特性曲線圖如圖 57 所示。

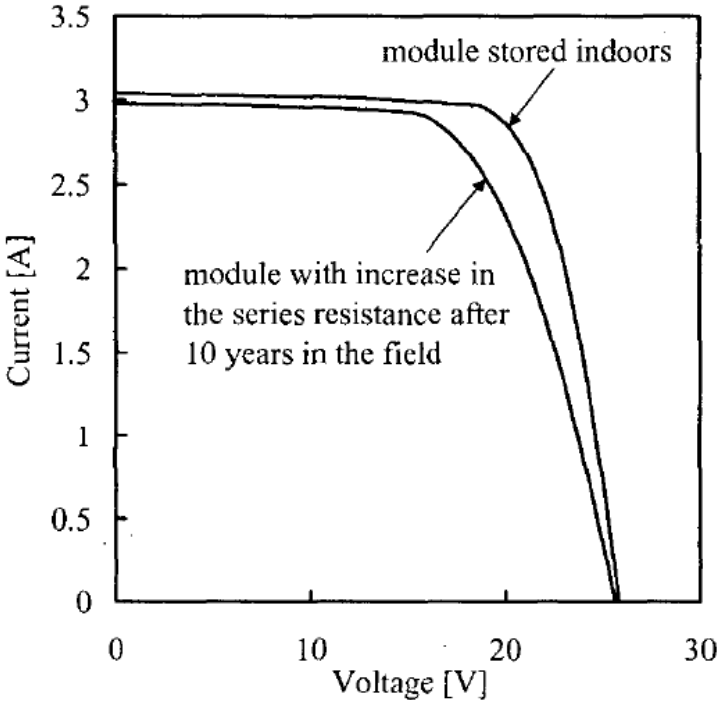

圖51 串聯電阻增加之模組 I-V 特性曲線圖[13]

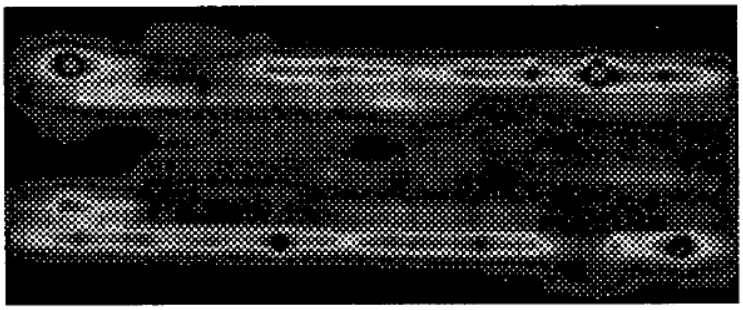

圖52 9*4 太陽能模組紅外線圖[13]

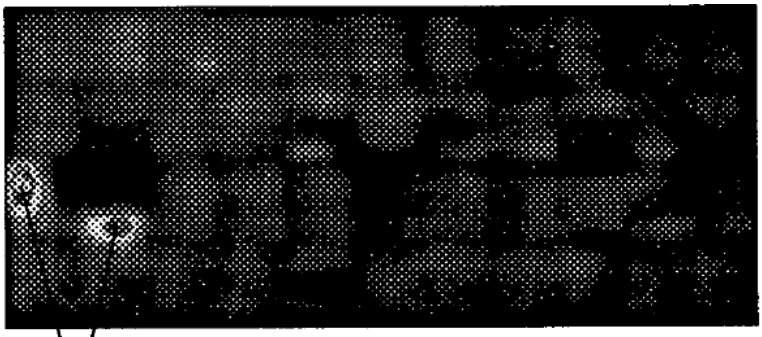

圖53　9*4 太陽能模組紅外線圖[13]

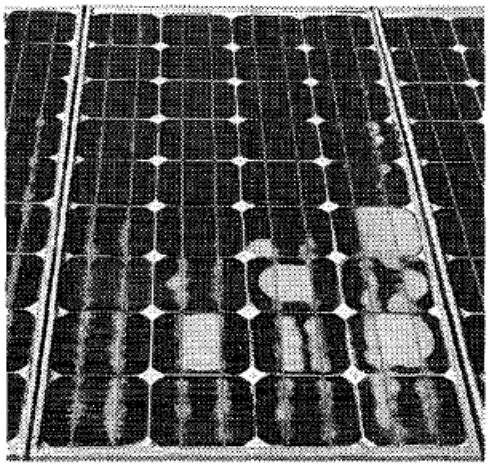

圖54 模組變色白化現象[14]

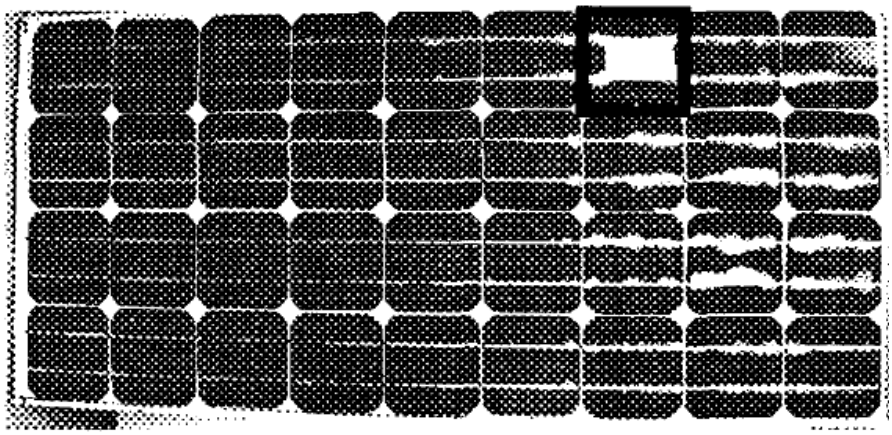

圖55 模組變色白化現象[13]

2.98	2.97	2.98	3.11	2.97	2.97	2.65	2.83	2.89
2.95	2.88	2.97	2.95	2.89	2.92	2.97	2.89	2.94
3.00	2.95	2.95	2.98	2.98	3.02	2.97	2.83	2.91
2.98	3.02	3.00	2.91	3.03	2.97	2.98	2.91	3.00

圖56　模組上各太陽能電池的短路電流(Amp.) [13]

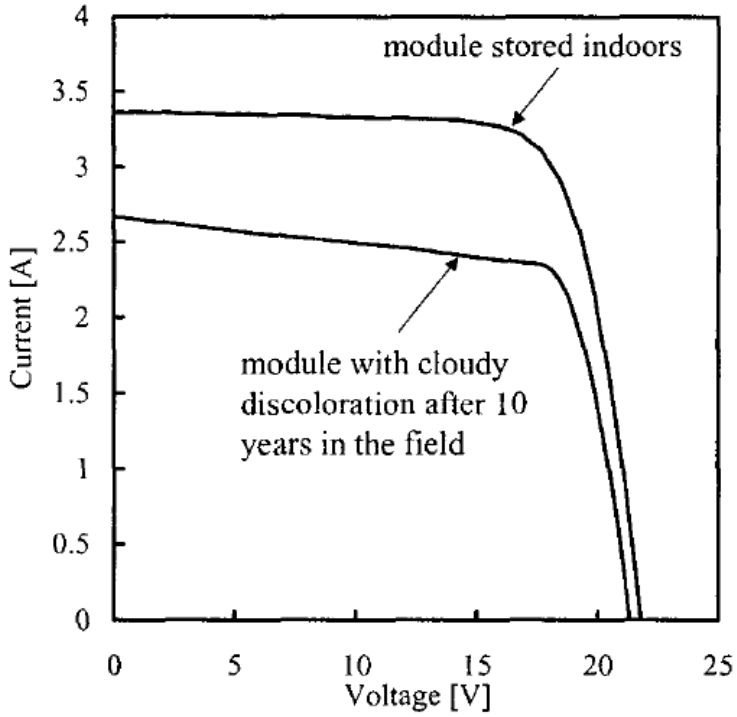

圖57 變色模組之 I-V 特性曲線圖[13]

經由電子顯微鏡的觀察後發現，此一白化的現象是因為太陽能電池中，電池本身與 EVA 發生了分層裂化的現象(delamination)，而發生白化現象之太陽能電池，因為使原本的透光率降低，造成發電效率降低，其短路電流大約會少於沒有白化現象的 10% 左右，最後造成整個模組超過 20%的效率降低。

此太陽能模組白化的現象，除了可由肉眼的觀察檢測出來外，

也可藉由如同串聯電阻增加時的熱分布監測方式進行檢測。因為白化的電池其發電效率的降低，短路電流降低，其電池會從原本電流源的角色轉換為負載的角色，並消耗功率，產生 hot spot 現象，因此依可藉由模組紅外線圖以檢測其發生白化現象的電池，如圖 58。

6.8 太陽能模組老化因子間之交互作用

6.8.1 Na^+離子與環境溫度交互影響

由 6.1 節可得 superstrate 結構的玻璃基板會與 TCO 層直接接觸，造成 TCO 腐蝕的主要原因為其本身化學反應所致，主要推測參與化學反應的因子為 $Na^+ + H_2O + SnO_2$:F，使 SnO_2:F 因化學反應生成 SnO，其中 Na^+離子為來自前端玻璃釋出(soda-lime glass)，而 H_2O 為外在環境的水蒸氣經由模組邊緣滲透進入。經實驗[1]證實溫度越高產生的漏電流 I_L 越大，因此越多 Na^+離子通往 TCO 層參與反應，故環境溫度增加將加速 TCO 腐蝕。

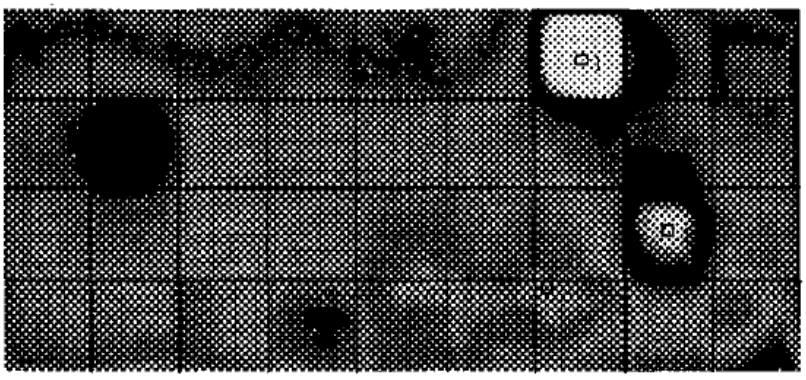

圖58 白化現象模組之紅外線圖[13]

6.8.2 Na^+離子與水氣交互影響

而在 6.5 中，經研究發現，沿海氣候的大氣中會含有高鈉含量，且由於為了改良過去高含鐵量玻璃的製成，故在玻璃製程中加入了較多的鈉以助益其化學作用，此外進行 n 型參雜使得有較高的磷含量，當模組被水氣侵入的量越多，將增加其導電度，且玻璃本身析出之鈉離子越多，因此有更多 Na^+離子與 TCO 參與反應，造成模組老化的速度加快。

6.8.3 溼度、溫度與含氧量之交互影響

6.2 節中所述環境中之濕度與氧氣含量對模組老化的影響，分別為乾熱、濕熱測試(濕度高低)與浸水測試(含氧量)，經實驗結果證實，濕度較高或是含氧量較高之環境中會造成模組老化程度較嚴重，因此在溼度、溫度高且含氧量亦高的環境下，模組老化速度會更加迅速。

6.8.4 水氣後與鋁氧化合物 Al_2O_3 之交互影響

如 6.4 節中所述，水氣侵入後與鋁背面電極發生化學作用，產生鋁氧化合物 Al_2O_3，進而造成模組介面間的空隙被擴增，使得水氣有更多的空間得以進入，故當環境溼度越高，生成之鋁氧化合物含量亦隨之提升，進而造成介面間的剝落情況越嚴重，於是又使得水氣侵入的量更多，交互影響形成惡性循環，加速模組老化情形。

柒、 各月份工作要項

本計畫工作各月份之產出及工作要項，如表 8 所示，其中工作要項包括(1)相關文獻收集，研析太陽能電池模組製作流程，觀察模組所使用材料並探究其可能劣化的因素。(2) 研析 CIGS、CdTe 與微晶矽型薄膜太陽能模組TCO 腐蝕原因及其對模組的影響。(3) 研究文獻中加速 TCO 腐蝕現象因子，偏壓測試、溫度測試、濕度測試、金屬框架與氧氣等影響。(4) 持續探究太陽能模組常見影響性能劣化相關文獻（如鹽霧、水蒸氣等），撰寫期中報告。(5) 研究結晶矽型模組 EVA 變色劣化問題。(6) 研析結晶矽型與結非晶矽薄膜太陽能電池模組中，太陽能電池、EVA 和玻璃之間剝落產生間隙問題，即探究其原因(7)分析太陽能模組因紫外線造成損壞的現象，並探討文獻中提及各應對方法之優缺點，及撰寫期末報告。

表8　本計畫工作各月份之產出及工作要項

月份	執行內容概要
5 月	相關文獻收集、研析太陽能電池模組製作流程。
6 月	研究太陽能電池效能檢測方法、認證規範，與探究模組中材料可能劣化因素
7 月	研析 CIGS、CdTe 與微晶矽型薄膜太陽能模組 TCO 腐蝕原因
8 月	研究文獻中加速 TCO 腐蝕現象因子、撰寫期中報告。
9 月	探究太陽能模組常見影響性能劣化相關文獻（如鹽霧水蒸氣）、結晶矽型模組 EVA 變色劣化問題之研究。
10 月	研析結晶矽型與結非晶矽薄膜太陽能電池模組中，太陽能電池、EVA 和玻璃之間剝落產生間隙問題、探究其原因。
11 月	分析太陽能模組因紫外線造成損壞的現象、探討文獻中提及各應對方法之優缺點、撰寫期末報告。

捌、結論與建議

本計畫研究重點包括微晶矽型與 CIGS 薄膜太陽能電池模組之 TCO 層腐蝕老化現象，與晶矽型與非晶矽薄膜太陽能電池模組之常見老化現象，造成的環境因子包含溫度、紫外線、水氣、鹽度以及模組材料製程等，主要之結論與建議包含下列各項：

1. 由於 Na^+離子與 TCO 產生化學反應為使其損壞主因，因此模組漏電流大小與玻璃種類為造成 TCO 腐蝕的兩大主因。而由於結晶矽無 TCO 作為前端電極，且有 EVA 黏膠作為隔絕，因此可避免漏電流的影響。

2. Substrate 種類的薄模太陽能電池因其結構與 Superstrate 有所不同，Substrate 種類之 TCO 與玻璃並未直接接觸，因此可減少鈉離子與其發生化學反應造成腐蝕現象。藉由高電壓的負偏壓，可加速薄膜太陽能電池模組的 TCO 損壞測試。

3. 水蒸氣對 TCO 的腐蝕的影響有兩種，一種是水蒸氣經由模組邊緣滲透進入並與 Na^+發生化學反應，另一種為環境溼度會造成金屬框架與玻璃的導電性增加，使漏電流增加以加快破壞速率。將模組邊緣接縫處密封，阻止水分滲透，可消除造成侵蝕的水氣進入模組。另外據實驗金屬外框與氧氣皆會增加太陽能電池模組老化的速率。

4. 使太陽能發電模組負極接地，可產生一個電場將帶正電荷的鈉離子被負電場吸附住，較不易往 TCO 層移動，可防止侵蝕情況的發生。

5. 水氣入侵太陽能模組將導致介質間附著力下降，開路電壓幾乎維持在一個定值，僅短路電流逐漸下降。模組中發生剝落的區域宇其他部分會產生不匹配之現象，使溫度升高而造成損壞。另外水氣亦會使腐蝕匯流排間的接點使串聯電阻上升。

6. Staebler-Wronski 光劣化效應會使得模組輸出功率在首度使用後便先下降約 15%左右。受到水氣侵入影響會生成鋁氧化物而使介面間縫隙增加，導致更多的水氣侵入。而水氣侵入產生遮蔽或氣

泡皆可能產生熱點現象損害模組

7. 在靠海的高鹽度環境下，太陽能模組表面在經過一段運作時間後總會有較高含量的鈉和磷，當鈉或磷的含量愈多時，附著力愈減弱。表面磷含量主要是由於進行 n 型摻雜所造成，至於表面鈉含量則是導因於沿海氣候的大氣中所含有之鈉，此外，在製造太陽能電池過程中由化學成分助益的擴散作用也是造成鈉與磷含量過高的原因。因此在製造太陽能電池的過程中有效的監控摻雜的濃度或是雜質的擴散能有效的限制，將可延長太陽能電池模組的使用壽命。

8. 太陽能模組介面之間產生剝落後，水氣會侵入空隙之間，與鈉或磷產生化學作用，產生電池間金屬電極腐蝕等現象，，造成輸出效率降低，故需要加入 SO2 來抑制這些元素的活性，然而除了增加 SO2 含量尚需配合適當的製程環境因數，才能達成其效用。

9. 使用標準固化的 EVA 的褐色化現象比起快速固化來的嚴重，其原因為標準固化程序在固化完成後，其固化劑剩餘濃度比起快速固化高出許多，而剩餘固化劑會因產生較高濃度的紫外光激發有機發色團，紫外光激發有機發色團受紫外光照射而激發後，會因此改變其原本分子鍵結的結構，產生變色，為導致 EVA 褐色化的主要原因。

10. 在原本 EVA 製程中都會混入紫外光吸收體(cyasorb)可吸收紫外光以保護有機發色團，但紫外光吸收體亦會隨著光強度的增強而發生光分解的現象，為了穩定紫外光吸收體，可以抗氧化劑及自由基清除劑混入 EVA 當中。

11. 濾光玻璃可濾除特定波長以下的紫外光，使紫外線無法穿透至 EVA 層導致破壞。濾光玻璃的截止波長選用越大時，越能有效抑制 EVA 褐色化的現象，但濾除的紫外光則無法進行發電。因此以太陽能模組發電效率的角度來看時，在選用濾光玻璃的同時，必須同時對紫外光的發電能力進行評估與取捨，尚能達到最高的整體效率。

12. 太陽能模組經過十至十二年長時間的曝曬實驗後，共發現三種主要老化的現象，分別是初始的短路電流下降、串聯電阻的增加、太陽能模組的變色現象。其中所有模組都發生了初始的短

路電流下降現象，但此現象乃因為玻璃的光學特性改變，造成紅光與紅外光的穿透率降低，影響發電效率，而此現象經過一段時間後此現象便趨於穩定，故並不影響長期的模組可靠度。模組串聯電阻的增加或太陽能模組的變色現象，其效率皆損失超過 10%。

參考文獻

[1] C. R. Osterwald, T. J. McMahon, J. A. D. Cueto, J. Adelstein, and J. Pruett, "Accelerated Stress Testing of Thin-Film Modules with SnO_2:F Transparent Conductors" , *Presented at the National Center for Photovoltaics and Solar Program Review Meeting, 24-26 March 2003, Denver, Colorado*, Report numbers: NREL/CP-520-33567, DOE Contract number: AC36-99-GO10337, May 2003.

[2] N. G. Dherea, V. V. Hadagal, and K. Jansenb , "Performance Degradation Analysis of High-voltage Biased Thin-film PV Modules in Hot and Humid Conditions" , *Photovoltaic Specialists Conference, 2005. Conference Record of the Thirty-first IEEE*, Page(s):507 – 510, Jan. 2005.

[3] C.R. Osterwald, T.J. McMahon, and and J.A. del Cueto, "Electrochemical Corrosion of SnO2:F Transparent Conducting Layers in Thin Film Photovoltaic Modules" , *Solar Energy Materials and Solar Cells*, Volume 79, Number 1, pp. 21-33(13), August 2003.

[4] J. H. Wohlgemuth, M. Conway, and D. H. Meakin, "Reliability and Performance testing of Photovoltaic Modules", *Photovoltaic Specialists Conference, 2000. Conference Record of the Twenty-Eighth IEEE*, Page(s):1483 – 1486, Sept. 2000.

[5] N. G. Dhere, V. V. Hadagali and S. M. Bet, "Leakage Current Pathways, Magnitudes And Their Correlation to Humidity And Temperature In High Voltage Biased Thin Film PV Modules," *Florida Solar Energy Center*, USA.

[6] R. Feist, S. Rozeveld, M. Mushrush, R. Haley, B. Lemon, J. Gerbi, B. Nichols, R. Nilsson, T. Richardson, S. Sprague, R. Tesch, S. Torka, C. Wood, S. Wu, S. Yeung, M. T. Bernius, "Examination of lifetime-limiting failure mechanisms in CIGSS-based PV minimodules under environmental stress" *Photovolatic Specialists Conference, PVSC '08. 33rd IEEE*, 2008.

[7] J. P. Kalejs, "Thin Edge-Defined Film-Fed Growth(EFG) Octagons" , *NREL technical monitor Mobil Solar Energy Corporation*, 1991.

[8] E. E. V. Dyk, J.B. Chamel, and A.R. Gxasheka, "Investigation of Delamination in an Edge-defined Film-fed Growth Photovoltaic Module" , *Solar Energy Materials & Solar Cells* vol. 88 pp.403-411, 2005.

[9] E.E. V. Dyka, A. Audouarda, E.L. Meyera, and C.D. Woolardb, "Investigation of the Degradation of a Thin-film Hydrogenated Amorphous Silicon Photovoltaic Module" , *Solar Energy Materials & Solar Cells* vol.91 pp.167-173, 2007.

[10] A. Kolodziej, "Staebler-Wronski Effect in Amorphous Silicon and its

Alloys" ,*Opto-electronics Review* vol.12 pp.21-32, 2004.

[11] N. G. Dhere and N. R. Raravikar, "Effect of Glass Na Content On Adhesional Sterength of PV Modules" , *IEEE Photovoltaic Specialists Conference* vol. 19-24 pp. 231-234, 2002.

[12] F.J. Pern, "Factors that Affect the EVA Encapsulant Discoloration Rate upon Accelerated Exposure" , *Solar Energy Materials and Solar Cells* vol. 41 pp.587-615, 1996.

[13] K. Morita, T. Inoue, H. Kato, I. Tsuda, and Y. Hishikawa, "Degradation Factor Analysis of Crystalline-Si PV Modules through Long-term Field Exposure Test", *Photovoltaic Energy Conversion, Proceedings of 3rd World Conference*, vol. 2 pp. 1948-1951, 2003.

[14] Y. Hishikawa and K. Morita, "Initial Drop in I_{sc} of the Field Test c-Si PV Modules in Japan", *Photovoltaic Energy Conversion, Proceedings of 3rd World Conference*, vol. 3 pp. 2916-2921, 2003.

附件

A. Investigation of Delamination in an Edge-defined Film-fed Growth Photovoltaic Module

B. Investigation of the Degradation of a Thin-film Hydrogenated Amorphous Silicon Photovoltaic Module

C. Effect of Glass Na Content On Adhesional Sterength of PV ModulesFactors that Affect the EVA Encapsulant Discoloration Rate upon Accelerated Exposure

D. Factors that affect the EVA encapsulant discoloration rate upon accelerated exposure

E. Degradation Factor Analysis of Crystalline-Si PV Modules through Long-term Field Exposure Test

F. Initial Drop in I_{sc} of the Field Test c-Si PV Modules in Japan

A. Investigation of Delamination in an Edge-defined Film-fed Growth Photovoltaic Module

Available online at www.sciencedirect.com
SCIENCE DIRECT®
Solar Energy Materials & Solar Cells
ELSEVIER
Solar Energy Materials & Solar Cells 88 (2005) 403–411
www.elsevier.com/locate/solmat

Investigation of delamination in an edge-defined film-fed growth photovoltaic module

E.E. van Dyk*, J.B. Chamel[1], A.R. Gxasheka

Department of Physics, Nelson Mandela Metropole University, PO Box 77000, Port Elizabeth 6031, South Africa

Received 7 November 2004
Available online 28 January 2005

Abstract

In this study, we have carefully analysed the performance degradation in an edge-defined film-fed growth (EFG) module due to delamination and moisture ingress. Our results showed that this degradation is directly related to the delamination as well as the moisture ingress. We also found that during hot, dry periods (December–January), there is a small reversal in degradation, which is due to the regression of the moisture ingress. The presence of moisture in the delaminated regions has led to the deterioration in cell interconnects. This is observed by the increase in series resistance with time.

Keywords: Photovoltaic modules; EFG technology; Delamination; Current–voltage characteristics

1. Introduction

Photovoltaic (PV) modules deployed outdoors are expected to produce energy for periods longer than 20 years, but environmental factors such as humidity, high levels of ultraviolet (UV) radiation and temperature variation have a detrimental effect on these devices and can as a result induce irreversible degradation. It is therefore

*Corresponding author. Tel.: +27 41 5042579; fax: +27 41 5042573.
E-mail address: ernest.vandyk@nmmu.ac.za (E.E. van Dyk).
[1]Permanent address: ECAM, 40 montée St-Barthélémy, 69005 Lyon, France.

0927-0248/$ - see front matter
doi:10.1016/j.solmat.2004.12.004

important to detect defects and monitor the evolution of any degradation in order to better understand their origin and effect on device performance. In this study, we investigated the delamination in an edge-defined film-fed growth (EFG) PV module that was observed while monitoring the module performance during 30 months in which the module was deployed outdoors at the Photovoltaic Outdoor Research Facility at the Nelson Mandela Metropolitan University. This paper discusses the observed delamination and associated effects on module performance. We found that the delamination reduces module performance and that moisture ingress further degraded power output and also leads to increased series resistance.

2. Experimental

The PV module used in this study comprises 36 EFG-Si solar cells connected in series. The module has an aluminium foil back cover and aluminium frame. In addition to the hermitical seal of encapsulant between back cover and glass front, the frame is attached to laminant (glass/encapsulant/cells/encapsulant/foil) using silicone sealer. The manufacturer's module specifications are listed in Table 1 together with the baseline measurements that are used for reference.

From the data in Table 1 and the module's physical dimensions it is possible to extract two important parameters, viz. the fill factor (FF) and the aperture area efficiency (η). FF is defined as the ratio of P_{max} to the product $I_{sc} \times V_{oc}$ and yields information about p–n junction quality as well as the possible presence of parasitic resistances. We have defined η relative to the exposed glass area, the so-called aperture area that is $0.39\,m^2$ for the module used in this study. Using the module specifications and dimensions yield $FF = 0.75$ and $\eta = 12.8\%$. The measured baseline values are $FF = 0.74$ and $\eta = 12.48\%$. In addition to the good efficiency of EFG solar cells, their square shape enables a higher concentration of the cells in the aperture area and hence an improved aperture area efficiency.

In a previous study [1,2] the module performance was monitored for an extended period of time. During this period (October 2001 to November 2002) it was observed that the module was undergoing degradation. In the current study, the degradation was investigated further. This involved deployment of the module outdoors for

Table 1
Electrical characteristics rated by the manufacturer at standard test conditions (STC: $1000\,W/m^2$ irradiance, 25 °C cell temperature and air-mass 1.5 global spectrum). Baseline STC measurements are also shown

Performance parameter	Manufacturer	Baseline
Maximum power (P_{max})	50 W	48.64 W
Open circuit voltage (V_{oc})	20.7 V	21.11 V
Short circuit current (I_{sc})	3.2 A	3.10 A
Voltage at maximum power (V_{max})	17.0 V	21.1 V
Current at maximum power (I_{max})	3.0 A	3.1 A

further monitoring of physical and performance degradation. During this monitoring period, the module was periodically subjected to thorough indoor assessment [3] to establish the extent and evolution of the degradation. The module has been subjected to 1790 sun-hours (kWh/m^2) in total: 1430 kWh/m^2 during the initial study and 360 kWh/m^2 during the current study. Other studies [4,5] on the durability and degradation of field-aged modules have analysed the degradation mechanisms in detail. In this paper, we focus on the performance degradation associated with the observed physical degradation.

3. Results

The extent of the physical degradation is shown by the photographs in Fig. 1 that were recorded towards the end of the study. In (a), the whole module is shown and the different regions in which delamination has occurred are clearly visible. Some of these regions are magnified in (b)–(d). The extent of the delamination varies with distance from the frame, (b) and (c), indicating that the delamination originates at points along the frame of the module and then grows with time, assisted by daily thermal cycling. The growth of the delamination also occurs along the busbars as depicted in (d). The space between the delaminated laminates, coupled with poor water tightness of the frame at places allows moisture penetration. Fig. 1(c) is an example of this where the discolouration due to moisture ingress is clearly visible. The presence of moisture will accelerate delamination and contribute to power degradation due to photon absorption in the encapsulant.

The delamination observed in Fig. 1 has grown progressively with time and is illustrated in Fig. 2. In the figure, the region depicted in Fig. 1(b) is shown and the extent of delamination at various stages during monitoring is illustrated by the broken lines. Soon after outdoor deployment the delamination started and extended to line 1 (October 2001) and a year later the delamination had grown to line 2. During the current study the delamination progressed to line 3 (July 2004).

In addition to the progressive growth of delamination, the moisture ingress also appeared to vary with time. In Fig. 1(c) we noted the discolouration due to moisture ingress. During the summer months, December 2003 to January 2004, we observed a regression of this discolouration although the overall delamination continued to grow. This is shown in Fig. 3 which depicts the same region as Fig. 1(c) during the test period, with the moisture ingress at various stages indicated by the dashed line. We postulate that this regression of discolouration is due to the regression of moisture ingress caused by the hot, dry weather that is typical for Port Elizabeth during this time. This regression of moisture ingress was monitored and started increasing again during February 2004. February and March are typically more humid and wet. By March 2004 the moisture ingress had progressed to beyond where it was 5 months before and the delamination had also progressed during this time. This supports our hypothesis that the regression of moisture ingress is due to the hot-dry weather.

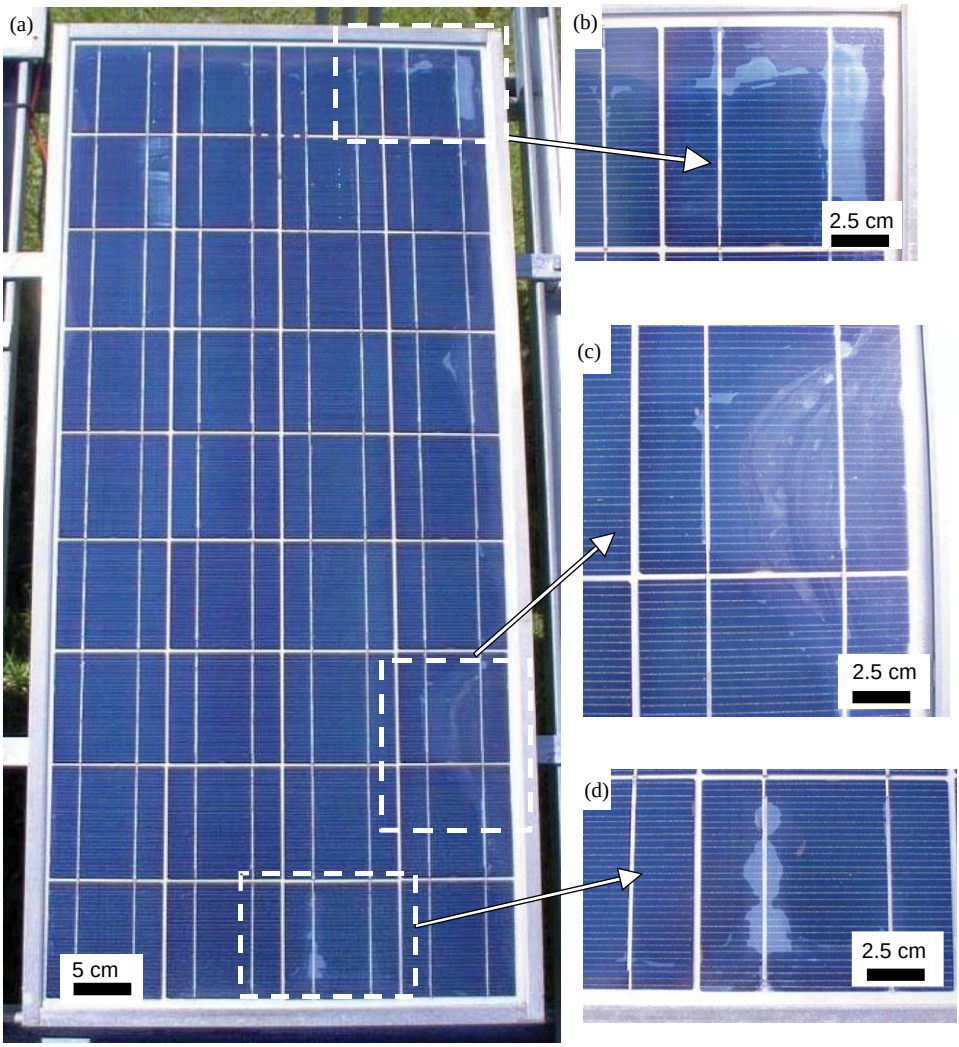

Fig. 1. Photograph of the EFG module: (a) shows regions with delamination and moisture ingress; (b) to (d) show enlarged areas of pronounced delamination and moisture ingress that has grown with time. The photographs were taken in January 2004.

The evolution of the four main electrical parameters during the monitoring period is shown in Fig. 4. The parameters are all normalized with respect to the baseline standard test conditions (STC) measurements. The performance parameters, short circuit current I_{sc}, open circuit voltage V_{oc}, fill factor FF and maximum power P_{max}, enable one to track the degradation in performance and yield information relating to the effects of the aforementioned delamination. From the figure it is clear that the performance degradation observed in the initial study [1,2] continued, although there was a slight recovery in performance that may be associated with the aforementioned

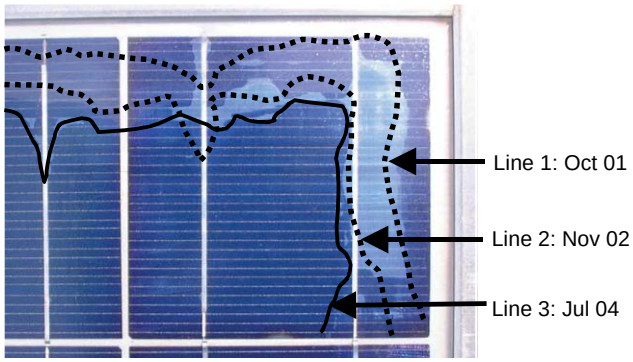

Fig. 2. Progression of delamination in the area shown in Fig. 1(b). The delamination at various stages of the outdoor exposure is indicated on the photograph by lines 1 through 3.

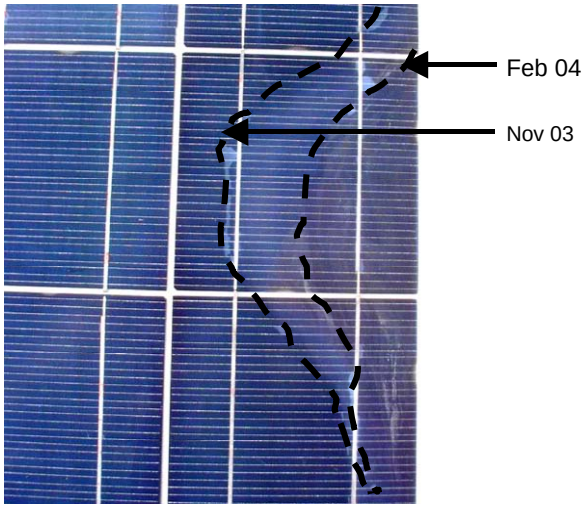

Fig. 3. Spreading of moisture ingress in the area shown in Fig. 1(c). Note that almost the entire cell is affected by the moisture ingress. The regression in moisture ingress is indicated by the lines showing the extent of ingress at different times.

regression in moisture ingress during the December to January 2004 period. The V_{oc} remained relatively constant during the monitoring period, while there was an overall change observed for I_{sc}. This may be explained by the increased delamination and associated discolouration of the laminant that results in a decrease in the number of photons from the incident irradiance being available to reach the solar cells below the affected parts. Photon current is almost proportional to irradiance, while voltage has a logarithmic dependence on irradiance. The decrease in FF is indicative of the increasing presence of parasitic resistances and was investigated further by the careful analysis of current–voltage (I–V) characteristics.

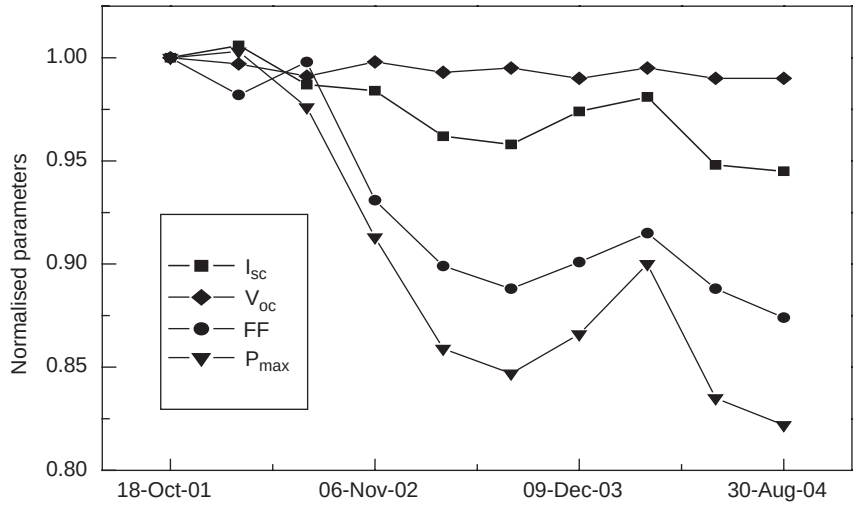

Fig. 4. Module electrical parameters relative to the initial STC measurements as function of time.

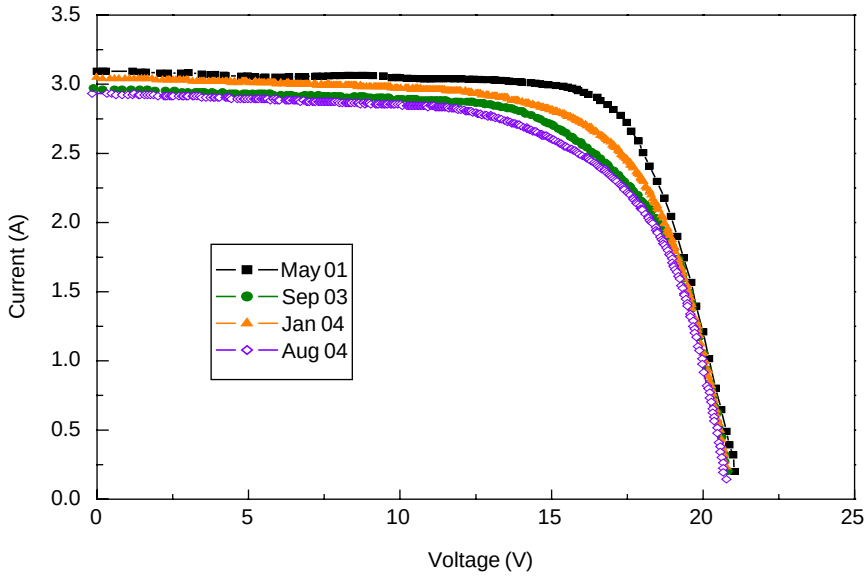

Fig. 5. *I–V* characteristics of the module at different times of the study. The decrease in performance is clearly visible, as well as the improvement in January 2004.

The degradation resulted in more than 16% decrease in the maximum output power, P_{max}.

The *I–V* characteristics of the module taken at various stages during the monitoring are shown in Fig. 5. The degradation discussed above is also evident,

with I_{sc}, FF and P_{max} following the observed trends, confirming the hypothesis that there is a regression in moisture ingress. The slope at I_{sc} is low for all of the I–V curves and also remains relatively constant. This means that there are not likely to be any cells in the module that have low shunt resistance (R_{sh}) and that R_{sh} has not changed during the outdoor exposure. If there are cells with low R_{sh}, the efficiency will decrease with a decrease in irradiance [6]. To confirm that there are no low shunts in any of the cells, we measured η as function irradiance. This showed that the module average shunt resistance has not degraded. The slope at V_{oc}, however, does change with time, indicating that the series resistance (R_s) changes. The slope alone does not yield the value R_s, but gives an indication of the value, with a higher slope being due to lower R_s and visa versa. The R_s values of the module that were determined during the test period were extracted from I–V curves taken at different irradiances and relating the change in voltage to a fixed change in current [7]. R_s increased from 0.4 Ω in 2001 to 0.9 Ω in 2004. This increase in R_s resulting from delamination and moisture ingress is likely to be due to corrosion of busbar contacts. This is illustrated in Fig. 6 where the corrosion at a busbar is shown.

Although the I–V curves of Fig. 5 do not show direct evidence of cell mismatching that could arise due to the delamination and moisture ingress, it is reasonable to expect that there will be some mismatch in the current. This is due to the fact that less light reaches the cell where delamination and moisture ingress has occurred. When series-connected solar cells operate in this manner, the mismatched cells will operate at slightly higher temperatures. To investigate this, the back of module temperature was monitored with the module placed under short-circuit conditions while mounted outdoors when the irradiance was close to 1000 W/m^2. Fig. 7 shows the temperature distribution in the module. The extent of the delamination as shown in Fig. 1 can be seen in the background. The values indicated in the figure represent the deviation, in °C, from the module's average temperature of 41.1 °C. There is a variation in temperature that is consistent with the observed discolouration. The regions where there is significant discolouration are operating at higher temperatures. The cell that is almost entirely covered by discolouration (Fig. 1(c)) is clearly mismatched, hence the higher temperature (+6.0 °C). These enhanced temperatures

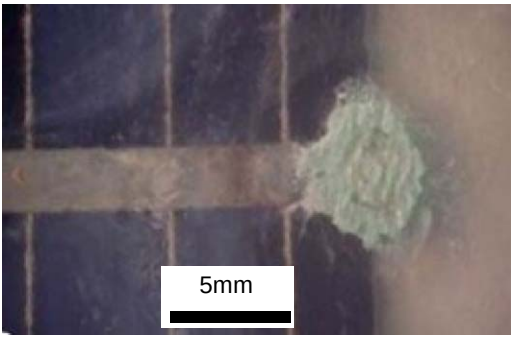

Fig. 6. Corrosion at cell interconnect due to moisture ingress, causing an increase in series resistance.

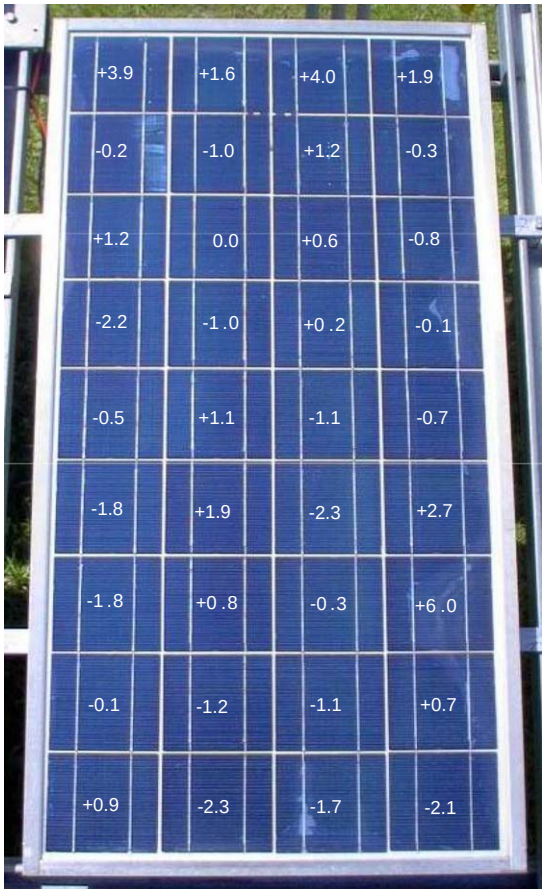

Fig. 7. Solar cell temperature variation across the module while exposed to 1000 W/m^2. The values indicated are the individual cell's temperature deviation from the average temperature of 41.1 °C.

will accelerate the delamination locally, resulting in the spread of the delaminated regions resulting in further moisture ingress and performance degradation.

4. Conclusion

The investigation and analysis of the degradation of an EFG-Si module over a long period of time was conducted. It was observed that delamination progressed with time of outdoor exposure. The growing delamination resulted in moisture ingress, which in turn lead to corrosion of metallic contacts. The study also showed that during summer months, which are typically hot and dry, the moisture ingress regresses, resulting in improved performance, while in other seasons the normal

growth in delamination trend continues. Analysis of the measured I–V characteristics confirmed that there were no cells with low shunt resistance in the module. The measured series resistance, however, increased from 0.4 Ω in 2001 to 0.9 Ω in 2004. This increase in R_s is attributed to observed corrosion of contacts. Temperature distribution across the module was consistent with the observed discolouration where affected regions were operating at higher temperatures than unaffected regions. With the support of experimental data and analysis it can be concluded that degradation of performance parameters of the EFG-Si module was, to a large extent, caused by the observed delamination.

Acknowledgements

The authors acknowledge the financial support of the National Research Foundation (GUN: 2063500) of South Africa, Eskom's Tertiary Education Support Programme and the Department of Trade and Industry in South Africa.

References

[1] E.E. van Dyk, A.R. Gxasheka, E.L. Meyer, Renewable Energy 30 (2005) 399–411.
[2] A.R. Gxasheka, E.E. van Dyk, E.L. Meyer, Renewable Energy 30 (2005) 611–620.
[3] E.L. Meyer, E.E. van Dyk, IEEE Trans. Reliability 53 (2004) 83–92.
[4] N.G. Dhere, H.P. Patil, S.M. Bet, A.U. Pai, V.V. Hadagali, U.S. Avachat, in: Proceedings of the NCPV and Solar Program Review Meeting (NREL/CD-520-33586, 2003), pp. 958–961.
[5] D.L. King, M.A. Quintana, J.A. Kratochvil, D.E. Ellibee, B.R. Hansen, Photovoltaic Module Performance and Durability Following Long-Term Field Exposure, http://www.sandia/gov/pv/docs/PDF/prmking.pdf (2004).
[6] E.L. Meyer, E.E. van Dyk, in: Proceedings of the 17th European Photovoltaic Solar Energy Conference, WIP, München and ETA, Florence, 2002, pp. 528–531.
[7] R.J. van Overstraeten, R.P. Mertens, Physics, Technology and Use of Photovoltaics, Adam Hilger Ltd., Bistol and Boston, 1986.

B. Investigation of the Degradation of a Thin-film Hydrogenated Amorphous Silicon Photovoltaic Module

Available online at www.sciencedirect.com
ScienceDirect
Solar Energy Materials & Solar Cells 91 (2007) 167–173
Solar Energy Materials and Solar Cells
www.elsevier.com/locate/solmat

Investigation of the degradation of a thin-film hydrogenated amorphous silicon photovoltaic module

E.E. van Dyk[a,*], A. Audouard[a,1], E.L. Meyer[a,2], C.D. Woolard[b]

[a]*Department of Physics, Nelson Mandela Metropolitan University, P.O. Box 77000, Port Elizabeth 6031, South Africa*
[b]*Department of Chemistry, Nelson Mandela Metropolitan University, P.O. Box 77000, Port Elizabeth 6031, South Africa*

Received 16 March 2006; accepted 8 August 2006
Available online 8 September 2006

Abstract

The degradation of a thin-film hydrogenated single-junction amorphous silicon (a-Si:H) photovoltaic (PV) module has been studied. We investigated the different modes of electrical and physical degradation of a-Si:H PV modules by employing a degradation and failure assessment procedure used in conjunction with analytical techniques, including, scanning electron microscopy (SEM) and thermogravimetry. This paper reveals that due to their thickness, thin films are very sensitive to the type of degradation observed. Moreover, this paper deals with the problems associated with the module encapsulant, poly(ethylene-*co*-vinylacetate) (EVA). The main objective of this study was to establish the influence of outdoor environmental conditions on the performance of a thin-film PV module comprising a-Si:H single-junction cells.

Keywords: Photovoltaic modules; a-Si:H; EVA encapsulant; Degradation; Failure analysis

1. Introduction

Photovoltaics (PV) is incontestably one of the biggest actors in renewable energy today. The main objective of the PV industry focuses on three guidelines: reduction of the cost of PV cells and modules, development of high-efficiency cells and modules, and increasing the reliability of PV technologies.

In order to evaluate the reliability of different PV technologies, we monitor and analyse the degradation and/or failure of PV modules at the Nelson Mandela Metropolitan University in South Africa. During this research, degradation of several PV modules has been observed in different studies that focus on various PV technologies. One of these studies involved the degradation of thin-film PV modules [1], and during that study, the electrical degradation of a hydrogenated amorphous silicon (a-Si:H) PV module was observed and discussed. Subsequent to that investigation, the a-Si:H module was exposed to outdoor conditions for almost 2 years mounted on a north-facing rack, tilted to an angle of 34°, the latitude of the location in Port Elizabeth. Port Elizabeth has a mild climate with an annual average rainfall of 624 mm, average ambient temperature of 22 °C (max.) and 14 °C (min.), and the average humidity varies between 81% and 63% from morning to afternoon, respectively. After this period the module degraded to such an extent that it was no longer producing meaningful power. About 30% of the module was affected by delamination and moisture ingress from the edges. The moisture ingress, in addition to the UV radiation, resulted in the encapsulation becoming brittle. The poly(ethylene-*co*-vinylacetate) (EVA) encapsulant delaminated from the other layers in the module structure. The moisture ingress resulted in oxidation of the aluminium back contact of the cells. The oxidation followed the moisture as it penetrated the module. This mechanism was also, then, responsible for the removal of some of the silicon. This physical degradation was directly responsible for the loss in power-generating capability of the module

*Corresponding author.
E-mail address: ernest.vandyk@nmmu.ac.za (E.E. van Dyk).
[1]Permanent address: ECAM Lyon, 40 Montee Saint Barthelemy, 69005 Lyon, France.
[2]Permanent address: Fort Hare Institute of Technology, University of Fort Hare, Alice, South Africa.

0927-0248/$ - see front matter © 2006 Elsevier B.V. All rights reserved.
doi:10.1016/j.solmat.2006.08.001

since the module was almost short-circuit by the presence of parasitic resistances created by the aluminium oxide covering the module. Furthermore, in affected regions of the module, almost all the silicon disappeared as a result of flowing with the moisture ingress.

2. Experimental

The module used in this study was an a-Si:H PV module employing a single-junction, p–i–n structure. The module was rated at 14 W but, in anticipation of power loss due to the Staebler–Wronski effect [2], was estimated by its manufacturer to produce 15% more than its rated power when first deployed. In previous studies [1,3,4] the module was part of investigations in which several modules' performance was monitored while deployed outdoors [3] and also subjected to a thorough assessment procedure [4], while electrical degradation was observed and discussed in Ref. [1]. This study investigates the physical degradation of the a-Si:H PV module and correlates the electrical and physical degradation. At the beginning of this study, the module was subjected to a degradation and failure assessment during which, I–V characteristics of the module were measured. The module was then deployed outdoors and periodically taken down for indoor assessment. During the outdoor test period the module degraded gradually up to point where it no longer produced meaningful power, constituting failure. This failure was found to be due to excessive physical degradation. About 30% of the module showed signs of delamination and corrosion. In order to facilitate further investigation, the module was delaminated and samples of the cell structure and encapsulant were taken from the damaged or "affected region" and from the region not affected, that we call unaffected region. These samples were first subjected to scanning electron microscopy (SEM) analysis to determine their structure and composition. Thermogravimetric mass loss measurements were then conducted on the EVA samples to determine the presence of volatile components inside the EVA.

3. Results and discussion

3.1. Electrical degradation

After initial indoor assessment at its acquisition, the module was deployed outdoors and periodically subjected to indoor assessment. Table 1 lists the standard test conditions (STC: 1000 W/m^2, 25 °C cell temperature and Air Mass 1,5 Global Spectrum), power measured at various stages of outdoor exposure. The initial I–V measurements showed that P_{max} was already almost 10% below the rated power of 14 W. It is also clear from the table that the module degraded considerably when first deployed outdoors as would be expected due to the Staebler–Wronski effect. In the first 13 days of outdoor exposure (80 sun-hours) the maximum power (P_{max}) degraded by approximately 50% of its value prior to outdoor exposure. The performance parameters continued to degrade with time, with most of the degradation taking place during the first month (130 sun-hours) of outdoor deployment [1].

Table 1
Degradation of maximum power

Measurement time	Power (W)
Initial	12.53
Prior to outdoor exposure	10.86
After 80 sun-hours	5.56
After 130 sun-hours	5.15
Final, after 3500 sun-hours	2.64

Fig. 1 shows the I–V characteristics at STC of the module at its acquisition and at the last measurement made on it before it failed. The last I–V curve shows dramatic reduction in performance parameters of the module after the observed physical degradation had taken place as compared to initial measurements. P_{max} decreased from 12.53 to 2.64 W, I_{sc} from 1.13 to 0.28 A, and V_{oc} from 24.3 to 21.0 V. Associated with a decrease in these parameters is an increase in the effect of parasitic resistance. The slope at short circuit has increased, indicating an increase in shunting paths or decreased shunt resistance showing the deterioration in the p–n junction quality of the cells in the module. There is also a large increase in the series resistance, R_s, as depicted by the decrease in the slope of the I–V curve at V_{oc}. As discussed later, the increase in R_s may be ascribed to the formation of aluminium oxide covering parts of the module. After the last I–V curve was measured it was not possible to do any further I–V or electrical measurements on the module.

3.2. Physical degradation

Fig. 2 shows a schematic of the structure of a single-junction hydrogenated a-Si cell of the type employed in the module used in this study [5]. The cell structure is of the p–i–n superstate type,with an undoped intrinsic (i) layer of a few hundred nanometre sandwiched between very thin p- and n-doped a-Si that are typically a few tens of a nanometre thick. The p- and n-doped layers establish an electric field over the intrinsic layer, and also provide contact to the end terminals on either side [6]. Fig. 3 shows the back of the module prior to the frame being removed and the module delaminated for further analysis. From the figure it is clear that there is physical damage to the module. This damage is due to delamination between the solar cell structure, EVA laminate and glass, resulting in moisture ingress and corrosion.

3.2.1. Scanning electron microscopy (SEM)

Fig. 4(a) shows a cross-sectional SEM micrograph of a sample from the unaffected part of the module. In the figure the different layers are identified and are, as indicated: glass substrate, transparent conducting oxide

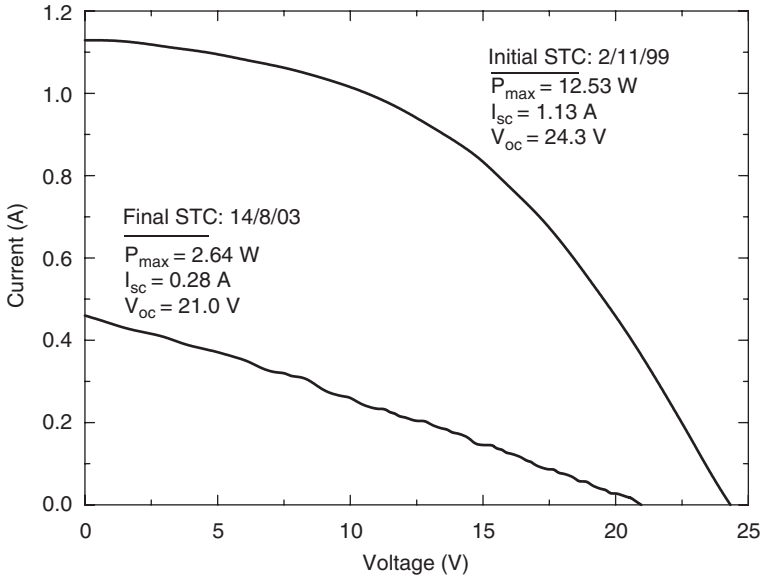

Fig. 1. Initial and final *I–V* curves of the module, measured under standard test conditions.

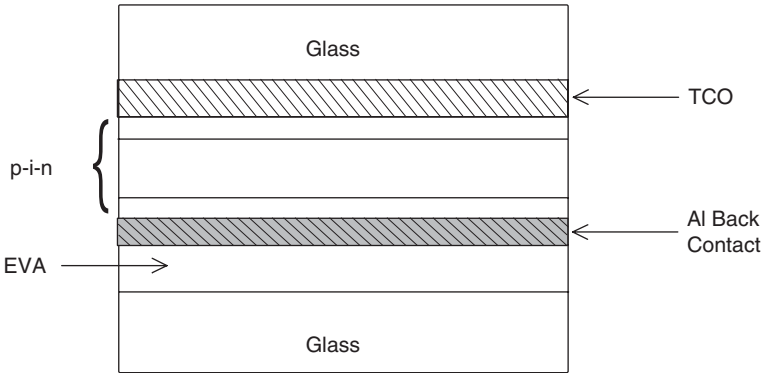

Fig. 2. Cell structure of the a-Si:H module [5].

Fig. 3. Photograph of rear of module showing delamination and moisture ingress.

(TCO) that is a tin oxide (SnO_2) layer, silicon, and aluminium back contact covered by the EVA polymer encapsulant. From Fig. 4(a) it is also clear that the silicon/aluminium/EVA interface is not regular. The aluminium back contact layer, being very thin ($<1\,\mu m$), is more affected by the irregularity of the silicon layer. The micro-irregularity is not expected to affect the EVA–Si bonding strength; however, there is an increase in effective surface for moisture to be retained [5]. This moisture can then diffuse through the EVA bulk and along the EVA/substrate interface. Fig. 4(b) shows a micrograph of a sample from the affected region used for energy-dispersive spectral (EDS) analysis.

As shown in Fig. 3, the main moisture ingress was from the top left region of the module, with the moisture infiltration being between the EVA and silicon layers, where the aluminium back contact is situated. Activated by the electric field generated by the cells and the water

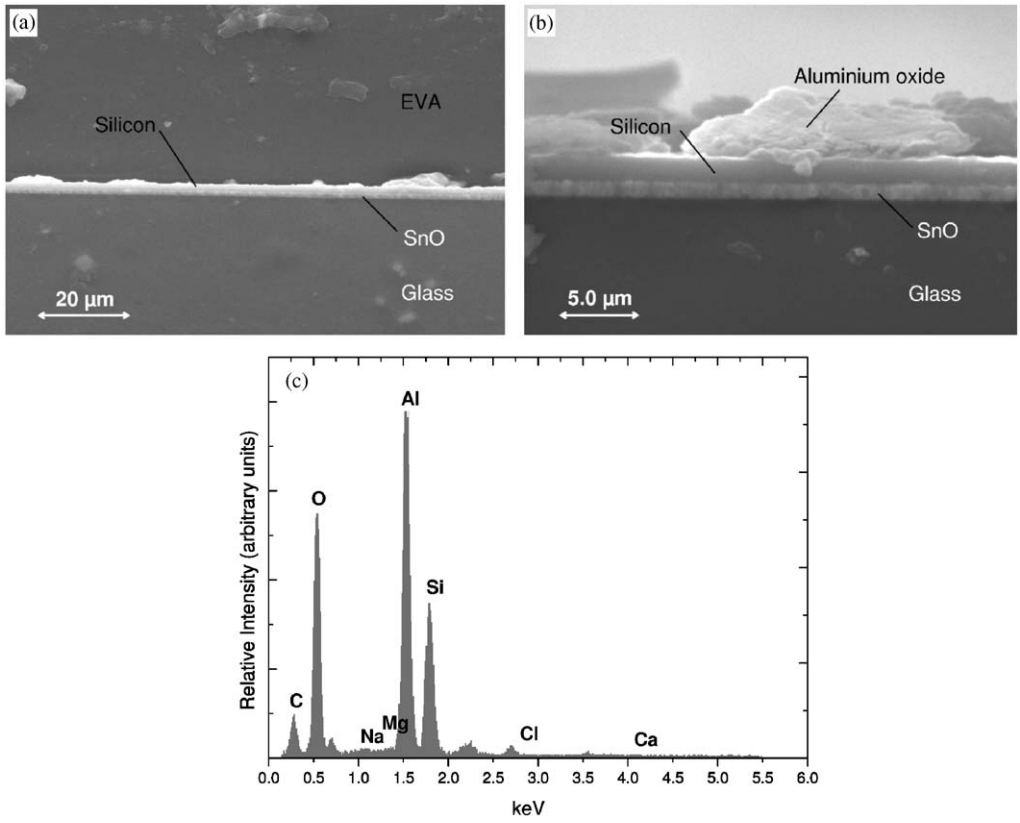

Fig. 4. (a) Cross-sectional SEM micrograph of part of a cell in the unaffected region of the module. (b) Cross-sectional SEM micrograph of part of cell in the affected region of the module. (c) EDS spectrum revealing aluminium oxide created in the affected region of the module.

present in the moisture, the aluminium back contact oxidized and formed aluminium hydroxide $Al(OH^-)_3$ as shown in Fig. 4(b) by the reactions [7]:

The anodic process : $Al \rightarrow Al^{3+} + 3e^- \ (E = +1.66\,eV)$.

The cathodic process :

$\frac{1}{2}O_2 + H_2O + 2e^- \rightarrow 2OH^- (E^0 = 0.40\,V)$.

Precipitation : $Al^{3+} + 3OH^- \rightarrow Al(OH^-)_3$.

Further conversion on ageing is likely

$2Al(OH)_3 \rightarrow Al_2O_3 + 3H_2O$.

At the beginning, some aluminium oxide (oxide alumina, Al_2O_3) was probably created with the simple presence of oxygen before moisture penetrated the module. The formation of the refractory oxide alumina (Al_2O_3) on aluminium improves the oxidation resistance [8], but in this case, the layer of aluminium was so thin that the entire aluminium layer oxidized. The EDS spectrum shown in Fig. 4(c) was obtained from a region in the aluminium oxide shown in Fig. 4(b). From the compositional analysis, we clearly see the presence of oxygen, aluminium, silicon, and some carbon. The carbon originates in the EVA, while the silicon comes from the a-Si:H layer. Further EDS analyses showed that there was no compositional difference between the affected and unaffected regions for the glass substrate and TCO layer, and for the a-Si layer when the layer was not removed. The SEM analysis, therefore, enabled us to determine the evolution of the aluminium layer during the degradation. The degradation of the EVA is detailed in Section 3.2.2.

With continued outdoor exposure, the moisture ingress increased and the aluminium oxidation spread, resulting in more moisture penetrating the layers of the module. Fig. 5(a) shows the result of the flow of aluminium oxide brought on by the moisture ingress. Another interesting observation is that the scribe line limits the flow in certain regions. In addition, temperature variations due to meteorological conditions and cell mismatches in the module would also contribute to the overall degradation. It is postulated that this results in the a-Si:H, which is linked to the aluminium, flowing with the moisture penetration yielding regions with no a-Si:H. These regions of the module appear semi-transparent. This phenomenon is illustrated in Fig. 5(b) that shows a region where there is no a-Si: H.

3.2.2. *Encapsulant degradation analysis*

With a visual inspection of the a-Si:H corroded module, we clearly saw that the EVA layer was also affected by the penetration of moisture. In the affected region, the EVA, which is a co-polymer, became yellow-brown due to UV exposure [8], and also very stiff (and thus breakable). This

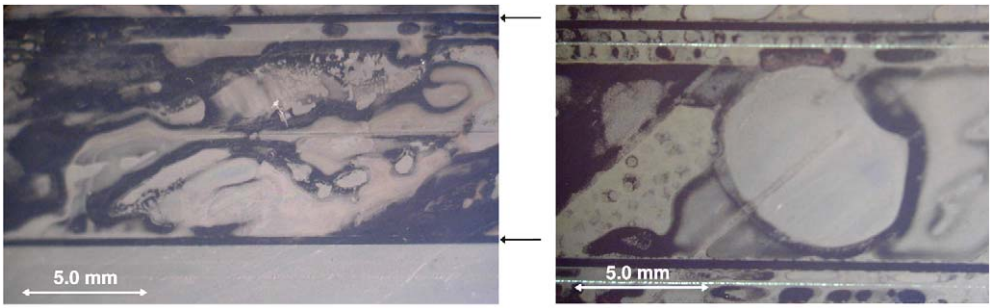

Fig. 5. (a) Micrograph showing the moisture induced aluminium oxide flow and limitation of flow by scribe lines. (b) Micrograph showing a region where there is no Si.

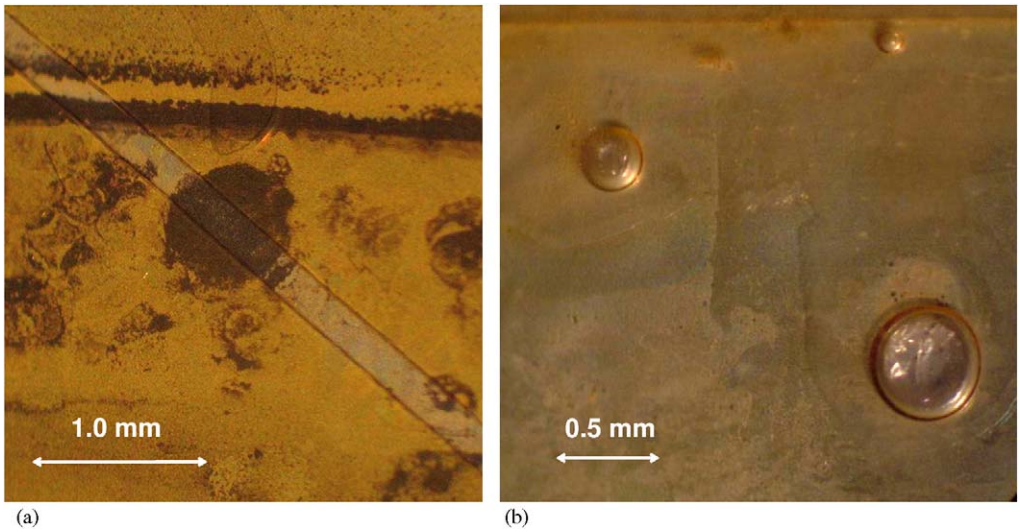

Fig. 6. (a) Micrograph showing a crack in the EVA. (b) Micrograph showing a bubble in the EVA.

yellow-brown colour is ascribed to the formation of conjugated polyene structures and/or α,β-unsaturated carbonyl groups [9]. The interstitial moisture ingress between the silicon and the EVA created some stresses and pressure was exerted on the EVA. The encapsulant became fragile and even broke in some regions of the affected part of the module. This is illustrated in Fig. 6(a) which shows an optical micrograph of a section of the affected region. The water and oxygen present in the moisture, in addition to the UV irradiation generated some changes in the structure and composition of the EVA. We speculate that photothermal deacetylation of acetic acid from the EVA co-polymer was initiated locally. Subsequent photooxidative attack resulted in localized crosslinking of the EVA encapsulant, rendering it brittle. Increases in the degree of crosslinking in areas of yellow-brown photodecomposed EVA films have been noted by other authors [10].

Deacetylation led to the accumulation of volatile organic components such as acetic acid. The accumulation of these compounds and the presence of water resulted in the formation of bubbles under heating. Fig. 6(b) clearly shows bubbles created on the surface of the encapsulant in the affected region of the module.

Unaffected and affected samples were heated in a thermogravimetric analyser (TGA) in a nitrogen atmosphere at 5 °C min^{-1}. At low temperatures (below 120 °C) EVA is stable, so any mass changes that occur at these temperatures would be due to the loss of volatile inclusions. Fig. 7 shows the mass of the unaffected and affected samples as a function of temperature. It is clear that both samples lose some mass below 100 °C. This mass loss is ascribed to the evaporation of acetic acid (produced upon deacetylation [11]) and/or water that may have ingressed into the encapsulant. It is noticeable, however, that this mass loss is significantly greater for the affected sample. The step change in mass below 100 °C is equivalent to 0.23% for the unaffected sample and 1.50% for the affected sample. The mass loss that starts to occur near 150 °C is the breakdown of the actual EVA polymer (thermal deacetylation) [11].

3.2.3. *Hot-spot formation*

During the study, it was also observed that hot-spots formed across the module, but with a higher density in the affected region. Fig. 8(a) shows hot-spots formed in the affected region of the module. In these hot-spots a small

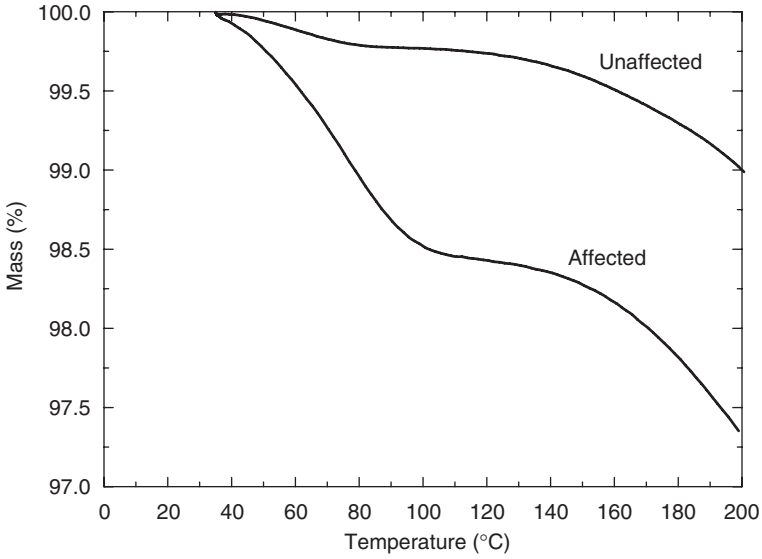

Fig. 7. Thermogravimetric analysis of the EVA from both unaffected and affected regions of the module.

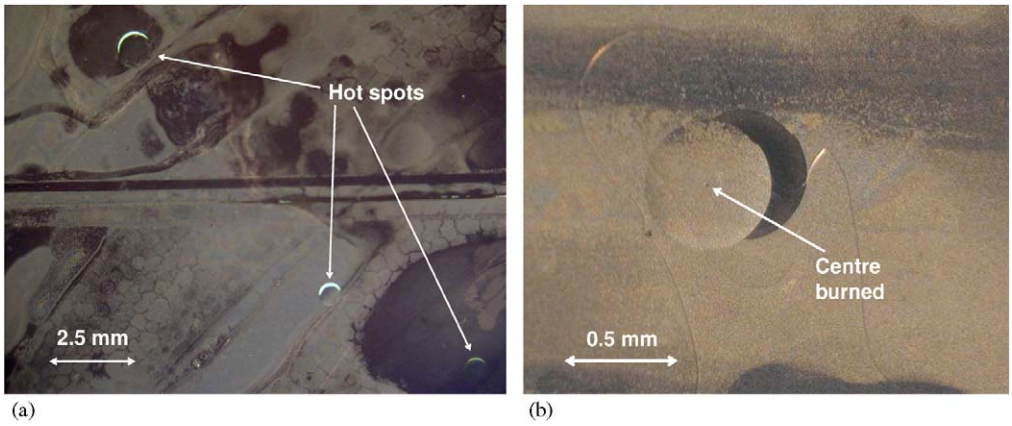

Fig. 8. (a) Micrograph showing hot-spots formed during outdoor exposure. (b) Micrograph showing a hot-spot that have moved with delamination. Note the burn mark in the centre of the hot-spot.

amount of cell was delaminated from the rest of the cell. The penetration of moisture and subsequent delaminating of the module layers accelerated the delamination or removal of hot-spot material from the thin film. The effect of hot-spotting is, therefore, worse in the affected region. Fig. 8(b) shows a hot-spot that has delaminated and moved with the aforementioned flow and delamination. In the figure, the delamination is clearly seen as along with a small dot in the centre of the hot-spot. We postulate that this type of hot-spot was formed by a water droplet on the front surface of the module as illustrated in Fig. 9. A water drop on the front surface acts as a lens and focuses the light as illustrated. This concentration of light has the effect of shading part of the cell under the drop as well as heating the spot where the light is focused. The shaded area heats up compared to the rest of the module due to mismatch in current generation, resulting in thermal stresses which cause the hot-spot to be removed or cut from the thin-film

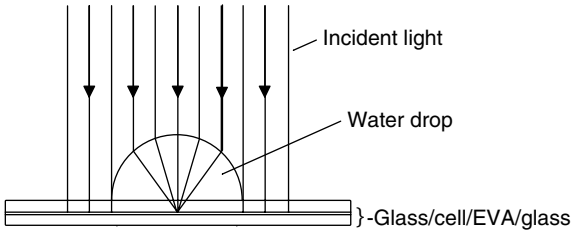

Fig. 9. Schematic illustrating the formation of hot-spots.

cell. Subsequently, when delamination occurs, the hot-spots move as shown in Fig. 8. The "dot" in the centre of the hot-spot shown in Fig. 8(b) is then expected to be caused by the concentration of light at that point, which burns the material. This is then visible as the dot in the centre of the hot-spot.

4. Conclusions

This study applied several techniques to investigate the degradation modes of a thin-film hydrogenated single-junction amorphous silicon PV module, from initial outdoor deployment to failure of the module. It was observed that after an initial electrical degradation due to the Staebler–Wronski effect, some moisture penetrated the module which resulted in the degradation of the constituent layers. In addition to the moisture ingress, there were several other factors that contributed to the degradation, viz., irregular silicon layer and aluminium back contact thickness, bad isolation of the module, embrittlement of the EVA, and the poor adhesion to the front glass. Photothermal degradation of EVA has been observed to lead to the production of volatile acetic acid and subsequent crosslinking [12], which if significant enough could render the EVA brittle. Furthermore, it was found that, although the module suffered severe physical degradation, the silicon did not play a major role in the physical degradation process. The module was also found to be susceptible to hot-spot formation. Due to the nature of the physical degradation, these hot-spots became detached from the rest of the module and moved relative to the surrounding material.

Acknowledgements

This work has been supported by the National Research Foundation (GUN: 2063500) of South Africa, Eskom (Tertiary Education Support Programme), and the Department of Trade and Industry in South Africa. The authors wish to acknowledge Dr. P. Couvrat, Head of the Department of Materials Science from the Engineering School of ECAM Lyon (France), for his support, as well as Messrs. F.J. Vorster, A.R. Gxasheka, and J.C. Chamel for useful discussions. The assistance of Dr. M.C. Wagener and Dr. M.S. Branch with SEM is also acknowledged.

References

[1] E.L. Meyer, E.E. van Dyk, Renew. Energy 28 (2003) 1455.
[2] D.L. Staebler, C.R. Wronski, Appl. Phys. Lett. 31 (1977) 292.
[3] E.E. van Dyk, E.L. Meyer, in: Proceedings of the 28th IEEE Photovoltaic Specialist Conference, IEEE Press, New York, 2000, p. 1525.
[4] E.L. Meyer, E.E. van Dyk, IEEE Trans. Reliab. 53 (2004) 83.
[5] D. Carlson, R. Romero, F. Willing, D. Meakin, L. Gonzalez, R. Murphy, M. Al-Jassim, in: Proceedings of NCPV and Solar Program Review Meeting, American Institute of Physics, New York, 2003, p. 946.
[6] R. Messenger, J. Ventre, Photovoltaic Systems Engineering, CRC Press, Boca Raton, 2000, p. 348.
[7] L.L. Shreir, Corrosion, George Newnes Ltd., London, 1963.
[8] T. Kojima, T. Yanagisawa, Sol. Energy Mater. Sol. Cells 81 (2004) 119.
[9] F.J. Pern, Polym. Deg. Stab. 41 (1993) 125.
[10] F.J. Pern, A.W. Czanderna, Sol. Energy Mater. Sol. Cells 25 (1992) 3.
[11] M. Rodriguez-Vázquez, C.M. Liauw, N.S. Allen, M. Edge, E. Fontan, Polym. Deg. Stab. 91 (2006) 154.
[12] R.H. Liang, S. Chung, A. Clayton, S. Di Stefeno, K. Oda, S.D. Hong, A. Gupta, Polym. Sci. Technol. 20 (1983) 267.

C. Effect of Glass Na Content on Adhesional Sterength of PV Modules Factors that Affect the EVA Encapsulant Discoloration Rate upon Accelerated Exposure

EFFECT OF GLASS Na CONTENT ON ADHESIONAL STRENGTH OF PV MODULES

Neelkanth G. Dhere, Nachiket R. Raravikar
Florida Solar Energy Center
1679 Clearlake Road, Cocoa, FL 32922-5703, USA.
Alex Mikonowicz
Shell Solar
4650 Adohr Lane, Camarillo, CA 93010, USA
Chris Cording
AFG Industries Inc., AFG-Technical Development
700 AFG Road, Church Hill, TN 37642, USA

ABSTRACT

Effect of reduction of soda-ash content and more effective fixing of sodium in superstrate sodalime glass surface on durability of PV modules was studied. Damp-heat acceleration-tested PV modules having higher soda-ash content glass or normal SO_2-treated glass were most severely stained. Their adhesional strength was the lowest and delamination was most severe. High concentrations of impurities correlated with regions of delamination. Increasing the intensity of SO_2 treatment reduced the surface roughness, degree of staining, powder formation, and delamination; and increased the adhesional strength. The best approach is to reduce the sodium content as well as to fix the remaining sodium by an adequate sulfur-dioxide treatment and having fixed it not to disturb it during subsequent processes.

INTRODUCTION

Over the last seven years, PV Materials Laboratory of Florida Solar Energy Center has been carrying out systematic and detailed study of the glass/encapsulant/Si-cell/encapsulant/backing-layer composite with an objective to lay the scientific basis for further improvement of the manufacturing technology of PV modules. Through this study, wealth of data has been collected at FSEC on properties of new, acceleration-tested, and field-deployed PV modules fabricated by PV manufacturers in US, Japan and Europe. It included modules deployed in harsh coastal conditions, hot and humid, hot and dry, and moderate climates. Specifically, adhesional strength and impurity segregation at cell/encapsulant and glass/encapsulant interfaces, as well as on elastic properties of encapsulant samples extracted from PV modules have been studied [1-10].

Analysis of samples from delaminated regions in PV modules deployed in harsh coastal climates showed the highest surface concentrations of sodium and phosphorous. Often significantly high sodium and phosphorous concentrations were observed at the surface of crystalline silicon (c-Si) solar cells up to depths of few thousand angstroms. Phosphorous surface concentrations resulted from the n-type dopant while the very high surface sodium concentration was attributed to atmospheric sodium containing aerosols in the coastal climate [1,2]. However, very high surface sodium concentrations observed in modules deployed in Arizona as well as in damp-heat acceleration-tested modules during subsequent studies clearly pointed toward sodium out-diffusing from sodalime glass [9,10]. The Auger electron spectroscopy (AES) line-scans from c-Si cell samples usually showed correlation between concentrations of sodium and phosphorous. Often these were accompanied by proportionately larger concentrations of oxygen after discounting oxygen in the antireflection titanium-oxide layer [1,2,9,10]. The phenomenon of chemically-assisted diffusion seemed to be responsible for the excessively high sodium and phosphorous concentrations. This pointed to a strong probability of formation of compounds such as sodium phosphates and hydro-phosphates.

The high sodium and phosphorous concentrations both at the surface and throughout the depth of a few thousand angstroms always correlated with low adhesional strengths at c-Si/encapsulant interface. In fact, there was a correlation between low adhesional strength on the one hand and high sodium and phosphorous concentrations on the other [Figure 1]. EVA adheres to glass by attaching to silica bonding sites on the glass surface. The diffusion of active species such as sodium and phosphorous can satisfy some of the bonds at the EVA and silicon surfaces. This surface passivation, in turn, reduces the strength of the adhesional bonds. This indicated that the durability of PV modules could be improved if precautionary measures were taken to control the sources of impurities into the structure of PV modules, as well as, if the diffusion of inadvertent impurities was limited. The present study was undertaken to test this hypothesis.

PV manufacturers desire maximum light transmission through cover glass to optimize electricity production.

0-7803-7471-1/02/$17.00 ©2002 IEEE

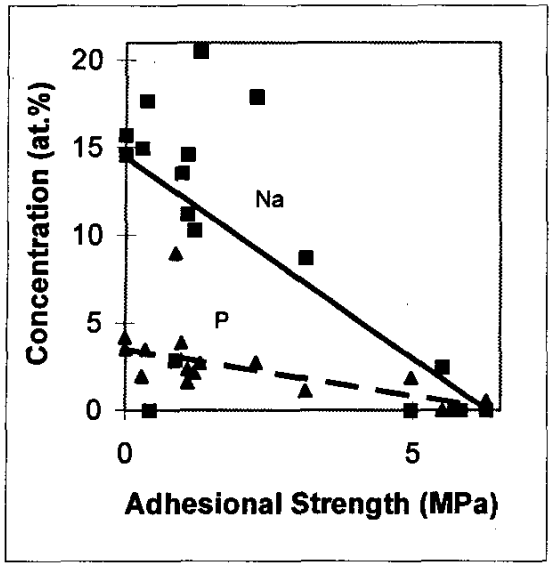

Fig. 1. Correlation between adhesional strength at c-Si cell/EVA interface with concentration of Na and P.

Light transmission in glass is reduced by iron contamination, which gives glass a greenish tint. Therefore, most PV manufacturers buy special low iron glass for cover plates for PV modules. Dolomite ($CaMg[CO_3]_2$) a mineral that was normally used in glass manufacturing typically contains excess iron, and is often unsuitable for low iron glass production. When dolomite was removed in order to fabricate low-iron glass, other compensating adjustments had to be made to the glass composition, such as increasing the sodium content. As a result, sodium oxide (Na_2O) concentration in low iron glass used in PV modules was typically raised to >15%. Sodium is a mobile ion that can cause a reactive surface layer. Usually SO_2 treatment is carried out during fabrication of sodalime glass to fix the sodium and thus to make the surface relatively inert. This paper presents a study of the effect of reduction of soda ash content and more effective fixing of sodium on the adhesional strength and staining of glass during damp-heat acceleration testing.

EXPERIMENTAL TECHNIQUE

Different types of glass superstrates were specially prepared by varying the soda-ash content or by increasing the intensity of SO_2 treatment. The formulation of specially prepared 1/8" thick, 1'x1' superstrate glass employed for preparation of PV modules were altered as follows: 1: Krystal Klear Float; 2: Krystal Klear Float with lower Na_2O; 3: Solite with normal SO_2; 4: Solite with high SO_2 (4scfh in annealing lehr and 30 psi in the tempering furnace); 5: Solite with very high SO_2 (5scfh in annealing lehr and 80 psi in the tempering furnace). PV modules were encapsulated using slow-cure ethylene vinyl acetate (EVA) and the above mentioned five types of glass. Each module contained four different types of crystalline silicon (c-Si) solar cells. Titanium oxide anti-reflection (AR) coating was deposited on two of the four cells. One AR-coated c-Si cell and one non-AR-coated cell were cleaned with isopropyl alcohol. AR-coated cells were labeled A and non-AR-coated cells were labeled N. Cells cleaned with isopropanol were labeled C and the cells that were not cleaned were labeled N. Thus the four cells were labeled AC, NC, AN, NN as follows: with (A) or without (N) AR-coat and with (C) or without (N) cleaning with isopropyl alcohol. Influence of bus lines and solder bonds was avoided by not attaching them. The modules were damp-heat accelerated tested at 85^{0}C and 85% relative humidity for 1000 hours. Accelerated-tested modules were inspected visually and photographed. Adhesional shear strength at the weaker of the two interfaces viz. glass/EVA or Si/EVA interfaces was calculated from the maximum torque required to extract samples using an extraction process initially developed by the Sandia National Laboratories and subsequently improved at FSEC. EVA and glass samples were examined by optical microscopy. The surface composition of EVA was analyzed by X-ray photoelectron spectroscopy (XPS).

RESULTS AND DISCUSSION

The surfaces of damp-heat acceleration-tested modules of type1 Krystal Klear Float glass and 3 Solite with normal SO_2 treatment were the roughest and most severely stained with powder non-uniformly sticking to the surface. Charles has studied water vapor corrosion ("stain") of sodalime glass [11]. In theses modules, delamination at the EVA/Glass interface was clearly visible especially at the EVA/Glass interface in the narrow strips between cells. At some places, delaminated portion also extended inside peripheral region of solar cells. White spots were observed in delaminated areas. The glass showed heavy chipping and degeneration into fine milky white powder with fine glass particles attached to the delaminated portion of EVA. EVA could be easily removed along with the backing sheet in the periphery and central portion of the module of type 1 using Krystal Klear Float glass. Delamination at EVA/Glass interface was observed all along the periphery and center of module in the case of type 3 module having Solite glass with normal SO_2 treatment.

Increasing the SO_2 flow rate in the annealing lehr and in the tempering furnace for Solite glass of type 4 and 5 PV modules progressively reduced the surface roughness, degree of staining, powder formation, and delamination. Delamination was observed at the glass/EVA interface all along the periphery of the modules 4 and 5 but not as prominently in the central region. Not much powder was observed on glass surface of module 5.

There was no powder formation and the staining was

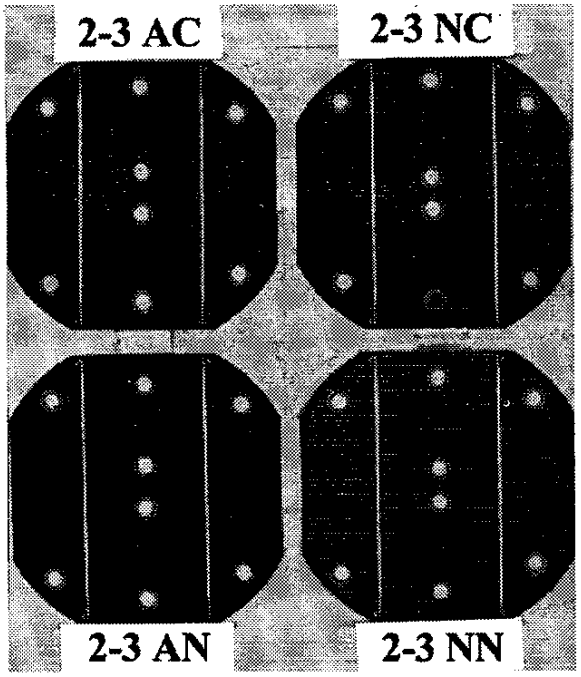

Fig. 2. Images of cells AC, NC, AN, and NN of the module of type 2: Krystal Klear Float with lower Na_2O

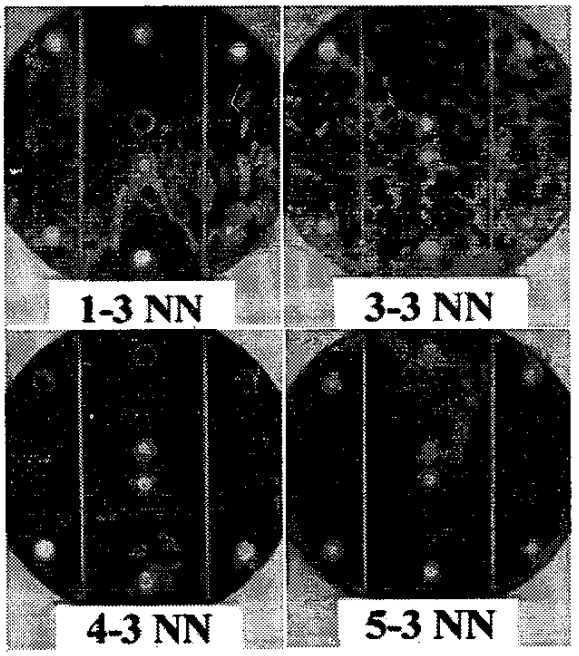

Fig. 3. Images of cells NN of modules of type 1: Krystal Klear Float; 2: Krystal Klear Float with lower Na_2O; 3: Solite with normal SO_2; 4: Solite with high SO_2 and 5: Solite with very high SO_2.

the least showing interference colors at an inclined angle in module of type 2 Krystal Klear Float with lower Na_2O. Also delamination was very low as compared to other modules. Figure 2 provides a photograph of a damp heat-tested module of type 2, with the four types of c-Si cells. Photographs of type NN cells of modules of type 1, 3, 4, and 5 in Figure 3 clearly depict varying degree of staining in different modules.

As expected, AR coated cells appeared dark blue whilst the non-AR-coated cells appeared dull gray. Adhesional failure at the glass/EVA interface was observed in more samples in the peripheral region than in the middle region. In the middle region, the average adhesional strength at the cell/EVA interface was the least (3.89-3.94 Mpa) in modules of type 1 Krystal Klear Float glass and 3 Solite with normal SO_2. The average adhesional strength at the glass/EVA interface in the peripheral region was the least (3.2 Mpa) for module of type 3 Solite with normal SO_2. Increasing SO_2 flow rate to 4 scfh in the annealing lehr and pressure in the tempering furnace to 30 psi for module of type 4 Solite glass with increased SO_2 showed low to moderate improvement in the adhesional strength. High adhesional strength (4.89-5.3 Mpa) was obtained in the case of the modules of type 2 Krystal Klear Float with lower Na_2O and 5 Solite with very high SO_2. The data on high adhesional strength for the module of type 5 Solite with very high SO_2 does not take into consideration delamination observed in one corner. Therefore, relying totally on very high SO_2 treatment would not be effective.

XPS energies and atomic concentrations of elements identified on the glass-side surface of a typical EVA sample (13NNP) from the peripheral area of module of type 1, were as follows: C (1s), 284.5 eV, 73.1%, O (1s), 532 eV, 20.7%, Si (2p3), 101.5 eV, 2.6%, Na (1s), 1072 eV, 3.6% (Fig. 4). Sodium atomic concentration on the glass-side surface of a typical EVA sample measured by XPS in the other modules 2, 3, 4, and 5 respectively were 1.4%, 2.2%, 3.9%, 3.6%. The high concentrations of precipitated impurities correlated with regions of complete delamination.

Excessive amounts of sodium are detrimental to adhesion. The high concentration of sodium on EVA surface is from sodalime glass. Such impurity precipitation would deplete the sites of adhesional bonds between EVA and silicon cell surface.

It may be noted that voids resulting from the delamination provide a preferential location for accumulation of moisture and precipitation of active impurities. These impurities can greatly increase the possibility of corrosion failures in metallic contacts.

Based on the above study and with significant industry investigation, AFG completely redesigned their low iron glass composition and lowered the sodium content to ~13% for the PV industry. This constitutes a reduction of ~2%. Subsequently, low-Na glass is being supplied to all PV manufacturers.

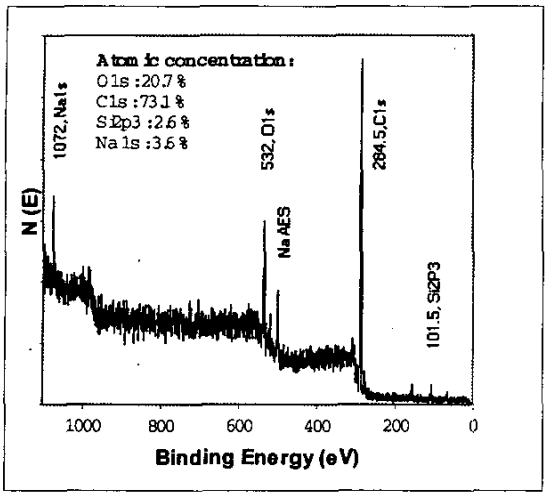

Fig. 4. XPS spectrum of EVA on glass side of module of type 1: Krystal Klear Float glass.

The reduction in the soda ash content by ~2% would certainly improve the PV durability of PV modules. As discussed above, high surface sodium concentration can result from atmospheric sodium containing aerosols in the coastal climate. Therefore, the concentration of dopant and other impurities must be carefully monitored and controlled.

So_2 treatment of glass tends to fix sodium and thus to neutralize the active layer on the surface of sodalime glass. However, glass surface can be damaged during some thin-film module manufacturing processes, such as edge delete by sand blasting. This seems to have resulted in sodium migration and severe delamination of SnO_2:F layer from glass surface together with the remainder of the thin films cells in high-voltage bias and damp-heat tested thin-film PV modules [3,12].

CONCLUSIONS

High concentrations of precipitated impurities at Si/EVA and glass/EVA interfaces correlated with complete delamination in PV modules. Surface roughness, staining, powder formation, and delamination of superstrate glass and surface Na concentration of EVA in damp-heat tested PV modules can be reduced with lower sodium content and by increasing the intensity of sulfur dioxide treatment in the lehr and in the tempering furnace. Very high SO_2 treatment by itself would not be sufficient. The best approach is to reduce the sodium content as well as to fix the remaining sodium by an adequate sulfur dioxide treatment and having fixed it not to disturb it during subsequent processes. It is also essential that the concentration of dopant and other impurities should be carefully monitored and controlled.

ACKNOWLEDGMENTS

This work was supported by the US Department of Energy through Sandia National Laboratories (SNL). The authors are thankful to Michael A. Quintana and David L. King of SNL for useful discussions.

REFERENCES

[1] N. G. Dhere and N. R. Raravikar, "Adhesional Strength and Surface Analysis of a PV Module Deployed in Harsh Coastal Climate" *Solar Energy Materials and Solar Cells*, **67**, 2001, pp 363-367.

[2] N. G. Dhere, K. S. Gadre, and A. M. Deshpande, "Durability Of Photovoltaic Modules", *Proc. 14th European Photovoltaic Solar Energy Conference, (EPVSEC)*, 1997, pp. 256-259.

[3] N. G. Dhere, M. B. Pandit, A. H. Jahagirdar, V. S. Gade, A. A. Kadam, S. S. Kulkarni, N. S. Mehta, S. M. Bet, and H. P. Patil, "Overview of PV Module Durability and Long Term Exposure Research at FSEC", *Proc. NCPV Program Review Meeting, Denver, CO, 2000, pp. 313-314.*

[4] M. A. Quintana, D. L. King, F. M. Hosking, J. A. Kratochvil, R. W. Johnson, B. R. Hansen, N. G. Dhere, and M. B. Pandit, "Diagnostic Analysis Of Silicon Photovoltaic Modules After 20-Year Field Exposure", *Twenty-eighth IEEE PVSC*, 2000, pp. 1420-23.

[5] N. G. Dhere, K. S. Gadre, N. R. Raravikar, S. R. Kulkarni, P. S. Jamkhandi, M. A Quintana, and D. L. King, NCPV Photovoltaic Program Review, Proceedings of the 15th Conference, Denver, CO, Sept. 1998. AIP Conference Proceedings 462, 1999, pp. 593-94.

[6] N. G. Dhere and K. S. Gadre, Comparison of Mechanical Properties of EVA Encapsulant in New and Field-Deployed PV Modules, *Proc. 2nd World Photovoltaic Solar Energy Conf. Vienna, Austria*, 1998, pp. 2214-2217.

[7] N. G. Dhere, M. E. Wollam, and K. S. Gadre, "Correlation between Surface Carbon Concentration and Adhesive Strength at the Si Cell/EVA Interface in a PV Module", *Twenty-sixth IEEE PVSC*, 1997, pp. 1217-1220.

[8] N. G. Dhere and K. S. Gadre, "Tensile Testing of EVA in PV Modules", *Proc. Int. Solar Energy Conf. Solar Engineering, ASME, Albuquerque, NM*, 1998, pp. 491-497.

[9] N. G. Dhere, "PV Module Durability In Hot And Dry Climate", *Sixteenth EPVSEC*, 2000, pp. 1046-49.

[10] N. G. Dhere and M. B. Pandit, "Study of Delamination in Acceleration Tested PV Modules", *Seventeenth EPVSEC*, 2001, (to be published).

[11] R. J. Charles, "Static Fatigue of Glass I & II", *J. Appl. Phys.* **29**, (1958), pp. 1549-60.

[12] J. A. del Cueto and T. J. McMahon, "Analysis of Leakage Currents in Photovoltaic Modules under High-Voltage Bias in the field", *Prog. In Photovoltaics: Res. & Appl.*, **10**, 2002, pp. 15-28.

D. Factors that affect the EVA Encapsulant Discoloration Rate upon Accelerated Exposure

ELSEVIER Solar Energy Materials and Solar Cells 41/42 (1996) 587–615

Solar Energy Materials and Solar Cells

Factors that affect the EVA encapsulant discoloration rate upon accelerated exposure

F.J. Pern

Measurements and Characterization Branch, Photovoltaics Division, National Renewable Energy Laboratory, 1617 Cole Blvd., Golden, CO 80401, USA

Abstract

Several factors that affect the discoloration rate of the ethylene-vinyl acetate (*EVA*) copolymer encapsulants used in crystalline-Si photovoltaic (*PV*) modules upon accelerated exposure have been investigated primarily by employing UV-visible spectrophotometry, spectrocolorimetry, and fluorescence analysis. A variety of film samples including the two typical (*unprimed*) EVA formulations, A9918 and 15295, were studied. The films were laminated, cured, and exposed to either a concentrated 1-kW Xe or an enhanced-UV light source. The results indicate that the extent of EVA discoloration can be affected by factors of two general categories: chemical and physical. In the chemical category, the degradative factors include (1) EVA formulation, (2) presence and concentration of curing-generated, UV-excitable chromophores that depend on the type of curing agent used, (3) loss rate of the UV absorber, Cyasorb UV 531™, (4) curing agent and curing conditions, and (5) photobleaching reactions due to diffusion of air into the laminated films. In the physical category, the factors involve (6) UV light intensity, (7) UV-filtering effect of glass superstrates, (8) gas permeability of polymeric superstrates, (9) film thickness, and (10) lamination–delamination (maybe chemical and/or mechanical effect, too).

Photodecomposition of the Cyasorb was first verified in cyclohexane solutions and then in Elvax 150™ (*EVX*) films (the copolymer without any additives and curing agent). Cyasorb decomposition rates in cyclohexane solutions are exponentially proportional to the light intensity, but can be greatly reduced by a free-radical scavenger, Tinuvin 770™, and furthermore by an antioxidant, Naugard P™. The discoloration rate of EVA increases with increasing loss of Cyasorb UV 531 and is faster for the EVA A9918 films that have a greater concentration of UV-excitable chromophores generated from a slower curing than for the EVA 15295 films that are fast cured. In general, the loss rate of the UV absorber and the rate of discoloration from light yellow to brown follow a sigmoidal pattern. A reasonably good correlation for changes in transmittance at 420 nm, yellowness index, and fluorescence peak area (or intensity ratio) is obtained as the extent of EVA discoloration progresses.

No discoloration was observed for the laminated EVX films that contain no stabilizers and curing-generated chromophores. The discoloration rate of both types of EVA can be largely reduced by UV-filtering glass superstrates that remove UV < 320 nm. Photobleach-

0927-0248/96/$15.00
SSDI 0927-0248(95)00128-X

ing reactions are responsible for the non-discoloration of unlaminated EVA, the visually clear perimeter around the edges of laminated samples, and the EVA films laminated with gas-permeable polymer film superstrates. Delamination of EVA films from the top glass superstrate was observed after prolonged UV exposure.

1. Introduction

Browning of the ethylene-vinyl acetate (*EVA*) encapsulant used in crystalline-Si (*c-Si*) photovoltaic (*PV*) modules can reduce the efficiency because of decreased light transmittance. The worst known case is the browning of EVA in the c-Si PV modules deployed at Carrisa Plains, CA, which used a V-trough-mirror configuration to increase the solar flux onto the modules. Consecutive decreases in the annual power output of nearly 10%/year have been well documented since 1986 [1–6]. Recently, browning of the EVA has also developed in the c-Si PV modules of similar mirror-enhanced configuration deployed in the Negev desert at the Ben-Gurion National Solar Energy Center, Sede Boqer, Israel [7]. The effect of EVA browning on PV module efficiency has been a subject of debate [8,9]. Degradation mechanisms of the EVA encapsulant have been investigated and discussed [10,11]. Previous systematic studies [12–15] have included post-mortem analyses of field-degraded, yellow to dark brown EVA to understand the chemical and physical changes in the material, laboratory-simulated degradation to characterize the degradation mechanisms, and accelerated exposure of laminated solar cells to quantify the effect of EVA discoloration on cell efficiency. In this work, three non-invasive spectrophotometric analytical methods — absorption/transmission, colorimetry, and fluorescence analysis (*FA*) — were employed to investigate factors that affect the discoloration rate of EVA in the laminated samples that were subjected to accelerated exposure. Results are summarized below on the photodecomposition of Cyasorb UV 531™, its stabilization by antioxidants, progress of EVA discoloration, temporal evolution of discoloring chromophores, their effects on optical transmittance of EVA, and mitigation of EVA discoloration by UV-filtering glass and gas-permeable polymer films as superstrates.

2. Experimental

2.1. Sample preparations

A number of film samples were studied, including the two commercially available (***unprimed***) EVA formulations, A9918 and 15295 [16–18]. These formulated and as-extruded films are ~ 0.46 mm (18 mils or 0.018 inch) thick. For the films formulated in our laboratory, the components of stabilizers were varied according to the needs of our experimental design and were cast from solutions of Du Pont's Elvax 150 (*EVX*) in high purity (99.9 + %, HPLC grade) cyclohexane. A constant thickness film maker with a 0.50-mm ring spacer was used to process at

80°–90°C the solution-cast films between two thin aluminum foils into films of uniform thickness suitable for lamination. A manually controlled, hydraulic mini-press with two heated platens was used to laminate the films at ~ 115°C for ~ 10 min between a superstrate and a substrate of either 25 mm × 25 mm × 1.56 mm (1″ × 1″ × 1/16″) or 50 mm × 50 mm × 3.16 mm (2″ × 2″ × 1/8″). The superstrates include quartz, borosilicate, indium-doped tin oxide (ITO)-coated, window, and cerium oxide (ceria)-doped UV-filtering glasses, and Du Pont's "Oriented" T^2 Tefzel™ films. All glass slides were thoroughly cleaned prior to use with a detergent, Nochromix™ (Godax Laboratories, Inc.)-sulfuric acid solution (not used for ITO), isopropanol, and deionized water in a ultrasonicator. Either one-layer or two-layer 0.2-mm thick aluminum spacers were used to control the laminated film thickness under applied hydraulic pressure. Curing was conducted for the laminated films containing a curing agent by heating for ~ 40 min at ~ 145°C followed by ~ 3–5 min cooling for the EVA A9918 using Lupersol 101™ (Elf Atochem) and ~ 10–12 min at ~ 145°C followed by cooling for the EVA 15295 using Lupersol TBEC™. Solutions of high purity cyclohexane were prepared in the experiments to study the photodecomposition of Cyasorb UV 531™ (American Cyanamid), which will be referred to as "Cyasorb" in the text below.

Plain EVX films heated in the *absence* of a curing peroxide (Lupersol) *are not suitable for PV encapsulation*. Inclusion of EVX films in this work was intended to contrast the damaging effects of Lupersol-curing-generated chromophores and stabilizers on EVA discoloration as discussed in the text.

2.2. Light sources and accelerated exposure

Three light sources were used for the accelerated exposure: (a) An Oriel 1-kW Xe arc lamp with a power supply (Model 8266) operated at 1000 W, where the light beam was concentrated and filtered by a ~ 8-cm path length, aqueous $CuSO_4$ solution (~ 2.6 mg/ml) attached to the condensor and cooled by flowing cold tap water. The concentrated and $CuSO_4$-filtered light will be referred to as "*C-Xe*" hereafter. In some experiments, the C-Xe light was also filtered with a 1/8″-thick 305-nm long-pass (*LP*) filter or a 1/8″ borosilicate plate before reaching the sample plane with a beam size of ~ 1″ in diameter. For other experiments, the light beam was filtered further with neutral density (*ND*) filters of various optical density (*OD*) as indicated in the text. (b) An Oriel enhanced-UV, 1-kW Xe arc lamp, solar simulator (Model 82866) with a dichroic filter to remove most visible and IR light (refer to as "*SS-Xe*" hereafter). A 1/8″-thick borosilicate glass plate was used as filter when needed. (c) Hereaus DSET Suntest CPS tabletop exposure systems operating with a 1.8-kW Xe arc tube burner.

The irradiance of the three light sources filtered by a 1/8″ borosilicate plate (to remove the UV wavelengths below ~ 285 nm) was measured at the test planes with an OL752 spectroradiometer. Fig. 1 shows the measured spectra for the three light sources and a global normal (*GN*), solar spectrum on a cloudless sunny day in August, Golden, CO, USA. By referring to the GN solar irradiance as 1-sun

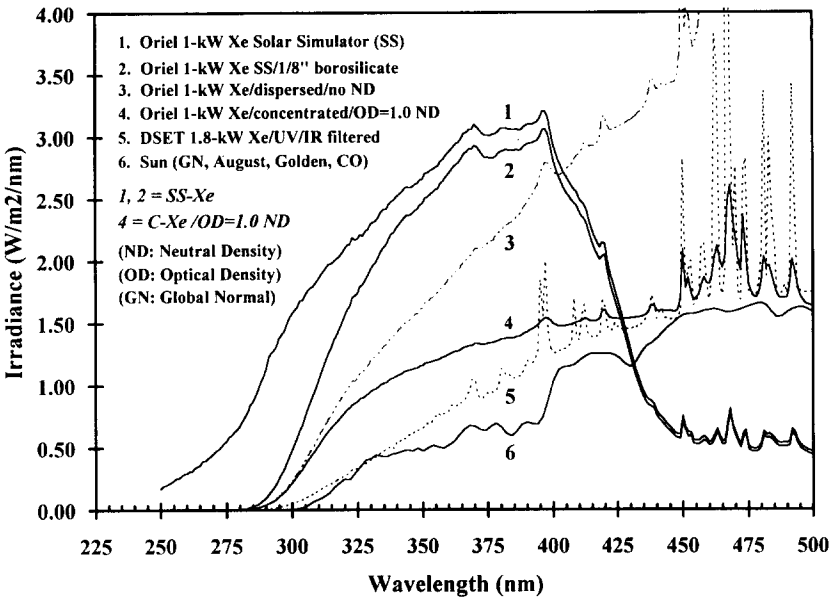

Fig. 1. Spectral irradiance measured at the test plane for three Xe arc light sources. (a) An Oriel 1-kW Xe arc, enhanced-UV solar simulator with dichroic filter to remove most visible and IR light (*SS-Xe*). Curve 1: no filter; curve 2: filtered with a 1/8″ borosilicate plate. (b) An Oriel 1-kW Xe arc, condensable light source filtered by an aqueous $CuSO_4$ solution to remove IR. Curve 3: dispersed (unconcentrated) light beam; curve 4: concentrated into ~1″ diameter and filtered with an OD = 1.0 neutral density (ND) filter, used to reduce the light intensity for the spectroradiometric measurements. The concentrated and $CuSO_4$-filtered light will be referred to as *C-Xe*. (c) A 1.8-kW Xe arc tube burner in a DSET Suntest CPS system operated at maximum power setting (~765 W/m^2) filtered with a special UV and an IR-reflecting filter, curve 5. Curve 6 shows a global normal, solar spectrum measured in August.

intensity, the integrated irradiance of the light from 300 nm to 400 nm is ~17.6-sun for the concentrated 1-kW *C-Xe* light measured at the test plane without an OD = 1.0 ND filter, ~2.3-sun with the ND filter, ~5.5-sun for the solar simulator (*SS-Xe*) without a borosilicate plate, and ~4.8-sun with the borosilicate filter. The total irradiance is 1% higher for the C-Xe and ~7% higher for the SS-Xe if integrated over the range of 285 nm to 400 nm. The Suntest CPS system produced a light intensity of ~1.4-sun from a new lamp operated at 750 W/m^2, which decreased gradually to ~1.1-sun when the lamp was aged by ~1100 h. In the experiments to study the photodecomposition of Cyasorb, cyclohexane solutions and EVX films containing Cyasorb in tightly capped quartz cuvettes were exposed to filtered C-Xe light. Some EVX films containing Cyasorb in cuvettes were exposed in the chamber of DSET Suntest CPS systems. The samples of laminated/cured films were exposed to either the C-Xe or the enhanced-UV SS-Xe light. Black panel temperatures (*BPT*) were monitored and measured for the samples during exposure.

2.3. Spectrophotometric characterization

The exposed samples were analyzed periodically for their absorption or transmittance with a Hewlett-Packard Model 8452A UV/VIS spectrophotometer (190 nm to 820 nm at a resolution of 2 nm), color indices with a HunterLab UltraScan™ spectrocolorimeter from 375 nm to 750 nm, and fluorescence characteristics with a SPEX Model FL112 Fluorolog-II spectrofluorometer using a "front face" emission monitoring geometry for the samples that were secured in a fixed position by a solid sample holder. The entrance and exit adjustable slit widths were all set at 0.5 mm, resulting in a calculated bandpass of 1.89 nm for the excitation (single-grating monochromator) and 0.85 nm for the emission (double-grating monochromator). The standard deviations are ≤ 0.0003 in the UV/VIS absorbance measurements and ≤ 0.01 in the color index measurements.

3. Results and discussion

3.1. Materials and effects of thermal processing

In the encapsulation process for c-Si PV modules using a double-bag vacuum laminator, a time-temperature and pressure profile is typically employed to initiate the outgassing, lamination, and curing of the EVA layers [18]. A cross-linked polymeric matrix in the EVA is produced in the curing step to provide the physical properties (e.g., mechanical strength) required of a PV module pottant. In the current industrial practice, the lamination time is typically $\sim$ 8–10 min at < 120°C and the curing time at ~ 145°C is $\sim$ 40–50 min for EVA A9918 and $\sim$ 8–10 min for EVA 15295. (A shorter 'one-step' processing for lamination/curing at $\sim 155° \pm 10$°C may be used at the PV manufacturer's discretion.) The difference in curing time between the two commonly used EVA formulations results from using Lupersol 101 for EVA A9918 and Lupersol TBEC for EVA 15295 [17,18]. Fig. 2a compares the *calculated* time-dependent residual concentration for Lupersol 101 and Lupersol TBEC at the typical curing temperature of ~ 145°C. Nearly complete consumption of Lupersol TBEC is achieved in ~ 20 min because of a lower activation energy and a shorter half-life. For EVA A9918, the *calculated* concentration of residual Lupersol 101 is still $\sim 42\%$ after 45 min curing. In addition to the higher residual concentration of Lupersol 101, a significantly higher concentration of UV-excitable chromophores is produced in the EVA A9918 than EVA 15295 as shown by fluorescence analysis in Fig. 2b [19]. The chemical structures for the two curing peroxides are also given in Fig. 2b. As illustrated in Fig. 3a, the consequence is that Cyasorb, with two major absorption peaks at 288 nm and 328 nm in a cyclohexane solution (Fig. 3b), will not be able to completely shield (protect) the chromophores in EVA A9918 from being excited by long-wavelength UV light; therefore photo-initiated Norrish degradation reactions may occur

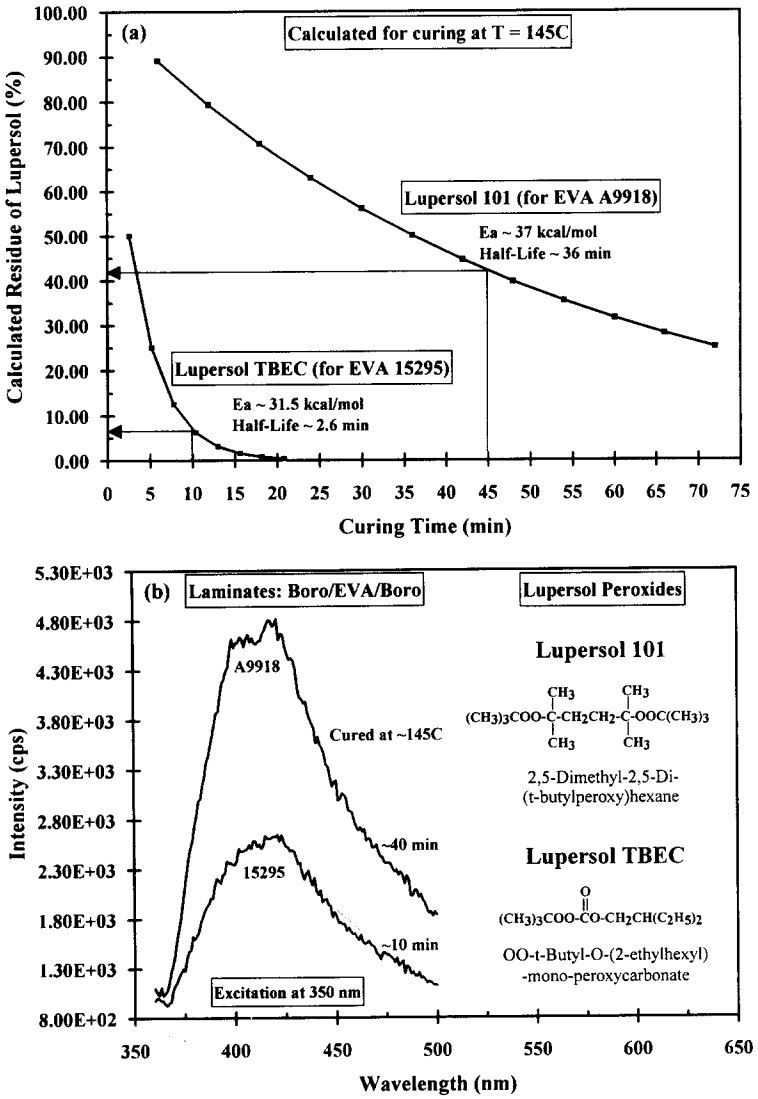

Fig. 2. (a) Calculated residual concentrations of Lupersol 101 and Lupersol TBEC peroxides for curing at 145°C, based on the activation energy and half-life derived from Elf Atochem's technical literature. (b) Fluorescence emission spectra of the borosilicate-laminated and cured EVA A9918 (after ~ 40 min at 145°C) and EVA 15295 (after ~ 10 min at 145°C), respectively, obtained at an excitation wavelength of 350 nm. The chemical structures of the two Lupersol peroxides are also shown.

[20,21]. Jointly, these factors result in a greater photothermal stability of the cured EVA 15295 than that of EVA A9918 as reported recently [22], which will be discussed further below.

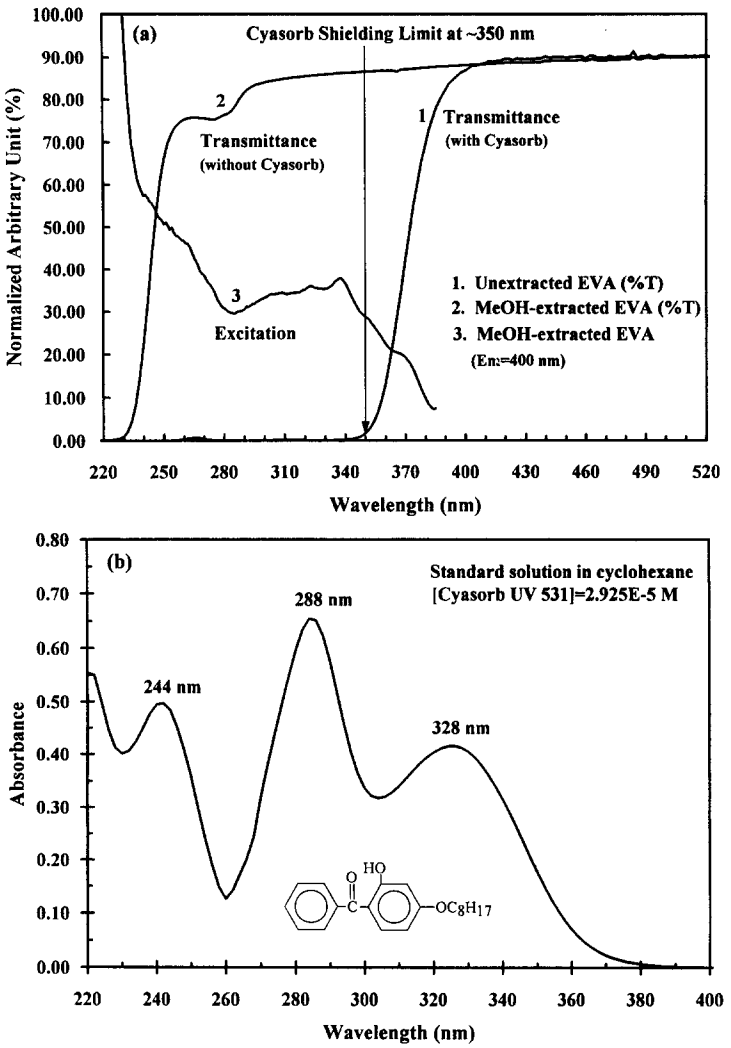

Fig. 3. (a) Transmittance spectra for a cured EVA A9918 film before (curve 1) and after (curve 2) methanol extraction and an excitation spectrum (curve 3) monitored at 400 nm emission for the methanol-extracted film. (b) The chemical structure and absorption spectrum of the UV absorber, Cyasorb UV 531, in a cyclohexane solution.

3.2. Degradation and discoloration

3.2.1. Photodecomposition, stabilization of Cyasorb, and effect of light intensity

The use of Cyasorb is intended to protect the polymer from photodegradation by absorbing the UV light and dissipating the light energy into heat via a

mechanism of rapid "keto-enol" tautomerism [20]. Cyasorb is also a quencher for the UV-excited chromophores as confirmed by fluorescence analysis for cured EVA before and after extraction with methanol or tetrahydrofuran [13]. However, it decomposes rapidly photochemically when present alone in the cyclohexane solutions or EVX thin films prepared in cuvettes. Fig. 4(a and b) show the decomposition profiles of Cyasorb in cyclohexane solutions exposed to the C-Xe light filtered with a 305-nm (Fig. 4a) or 345-nm (Fig. 4b) LP filter. As is seen, the 345-nm LP filter can reduce, but not effectively eliminate, the decomposition of Cyasorb by longer UV wavelengths. The Cyasorb molecules probably decompose into some yet-unidentified, mono-substituted aromatic components, which can be smelled and absorb UV < 300 nm with a strong peak in the 210–240 nm range and two very weak peaks in the 270–290 nm region (Figs. 4 (a) and (b)). However, Pickett and Moore reported that benzoic acid was observed as the major identifiable product from Cyasorb photodecomposition in poly(methyl methacrylate) [23]. Fig. 4c shows the faster decomposition of Cyasorb by shorter UV light (> 305 nm using a 305-nm LP filter) and the deviation of the decomposition rate for the absorption peak at 244 nm from those for the other two peaks at 286 nm and 328 nm, as a result of the absorption by the decomposition products. Fig. 5 illustrates (a) the time-dependent photodepletion of Cyasorb embedded in an EVX film and (b) the photodepletion rates of the three absorption peaks. From these results, it is concluded that the absorption peak at 328 nm is more suitable to quantify the Cyasorb concentration in cyclohexane solutions, EVX, or EVA films to avoid the influence from the absorption by the decomposition products below ~ 300 nm.

The photodecomposition rate of Cyasorb in cyclohexane solutions was quantitatively studied by exposure to different intensities of the 1-kW C-Xe light. The light intensity level was attenuated by using neutral density filters of various optical density. The results, and the derived curve-fit parameters, are shown in Fig. 6, indicating the photodecomposition rate of Cyasorb in cyclohexane is exponentially proportional to the light intensity.

Stabilization of the Cyasorb in cyclohexane solutions and EVX films was also studied, and the results are shown in Fig. 7. The photodecomposition rate of Cyasorb in cyclohexane solutions is somehow higher when EVX is present, as seen in Fig. 7a (compare curves 1 and 2), indicating a marked difference in the kinetics and a detrimental matrix effect exerted by the EVX copolymer. Decomposition rates of UV absorbers, including Cyasorb, are found by Pickett and Moore to be highly dependent on the polymer matrix that can have influence on the hydrogen bonding effects and free radical generation [23]. Addition of antioxidant Naugard P provides only a relatively small degree of stabilizing effect (curve 3). However,

Fig. 4. Photodecomposition of Cyasorb in cyclohexane solutions exposed to the concentrated 1-kW Xe light filtered by an aqueous $CuSO_4$ solution (i.e., *C-Xe* in Fig. 1b) with (a) a 305-nm long pass (LP) filter and an OD = 0.5 ND filter, or (b) a 345-nm LP filter, at a black panel temperature (BPT) of $55° \pm 2°C$. (c) The decomposition of Cyasorb in (a) and (b) are plotted for the three absorption peaks at 244 nm, 288 nm, and 328 nm.

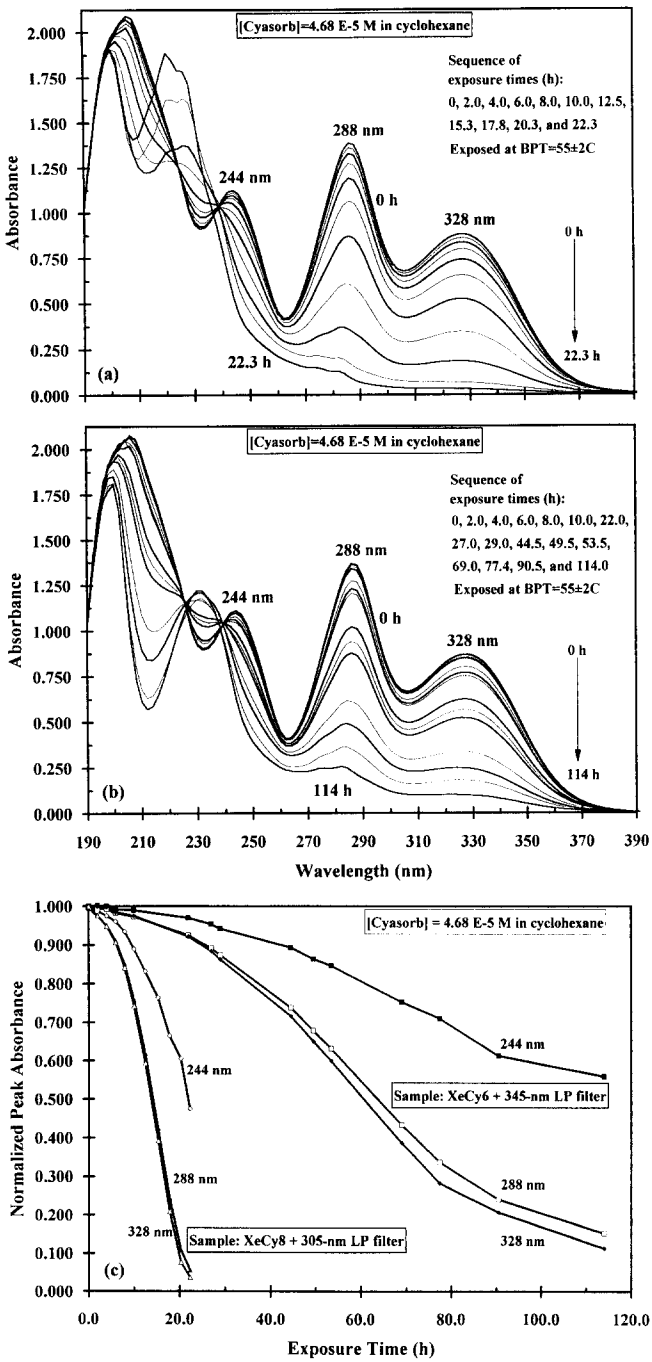
[Cyasorb]=4.68 E-5 M in cyclohexane
Sequence of exposure times (h): 0, 2.0, 4.0, 6.0, 8.0, 10.0, 12.5, 15.3, 17.8, 20.3, and 22.3
Exposed at BPT=55±2C
288 nm
244 nm
0 h
328 nm
0 h
22.3 h
22.3 h
(a)
Absorbance
[Cyasorb]=4.68 E-5 M in cyclohexane
Sequence of exposure times (h): 0, 2.0, 4.0, 6.0, 8.0, 10.0, 22.0, 27.0, 29.0, 44.5, 49.5, 53.5, 69.0, 77.4, 90.5, and 114.0
Exposed at BPT=55±2C
288 nm
244 nm
0 h
328 nm
0 h
114 h
114 h
(b)
Absorbance
Wavelength (nm)
[Cyasorb] = 4.68 E-5 M in cyclohexane
244 nm
244 nm
Sample: XeCy6 + 345-nm LP filter
288 nm
288 nm
328 nm
328 nm
Sample: XeCy8 + 305-nm LP filter
(c)
Normalized Peak Absorbance
Exposure Time (h)

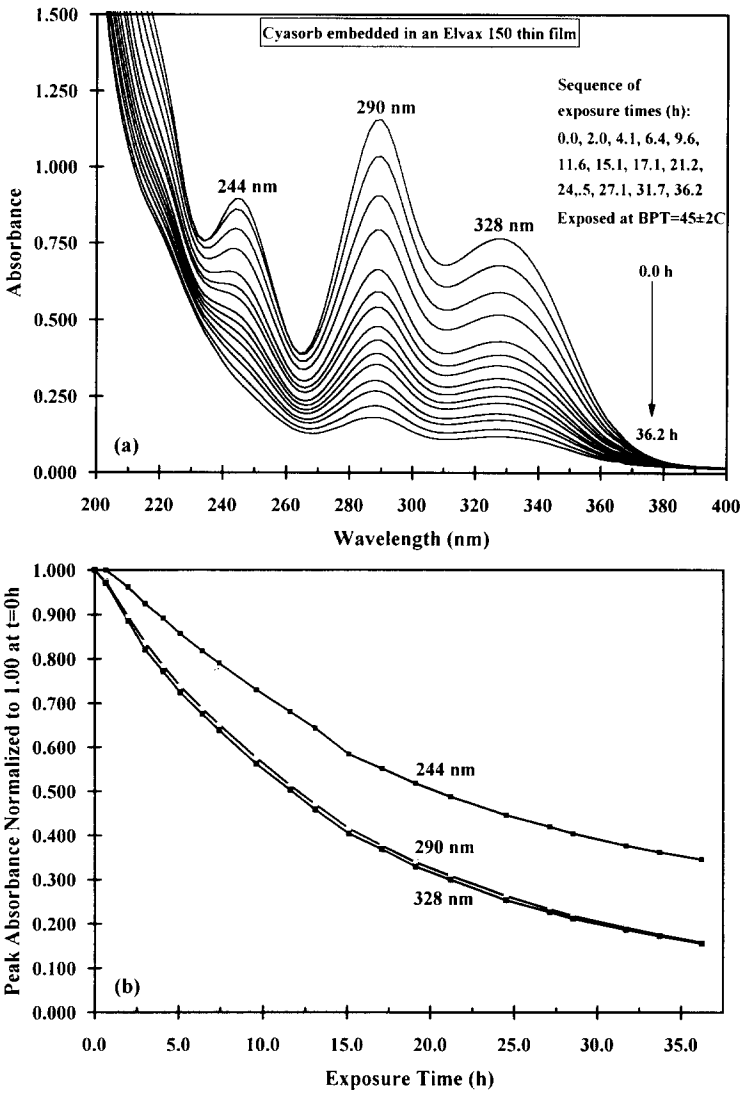

Fig. 5. (a) Absorption spectra as a function of exposure time from 0 to 36 h at BPT = 45° ± 2°C, showing the photodecomposition of Cyasorb embedded in an Elvax 150 (EVX) film that was prepared on one side of a cuvette by a solution casting method. The light source was the *C-Xe* in Fig. 1b. (b) Peak absorbance normalized to 1.00 at $t = 0$ h for each of the three absorption maxima, 244 nm, 290 nm, and 328 nm.

the Cyasorb can be more effectively, but not completely, stabilized by the free-radical scavenger Tinuvin 770 (curve 4). When both Tinuvin 770 and Naugard P are present, the stabilization effect is further enhanced (curve 5). Similar stabilization effects are also observed for Cyasorb embedded in EVX thin films exposed to

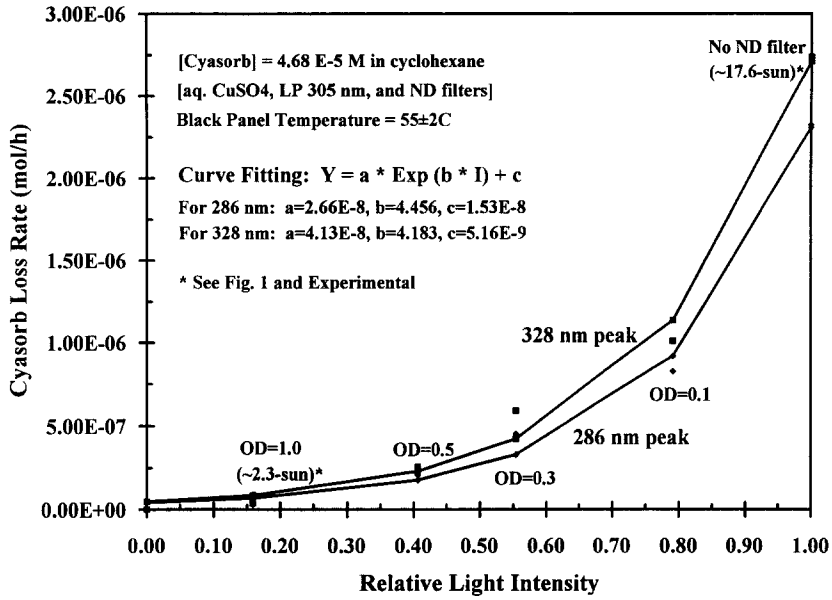

Fig. 6. Light intensity dependence and results of curve fitting for the photodecomposition rates of Cyasorb in cyclohexane solutions exposed at BPT = 55°±2°C to the *C-Xe* light filtered with a 305-nm LP filter and various ND filters to provide different light intensities.

the concentrated C-Xe (Fig. 7b) or to a ~1.2-sun DSET Xe light (Fig. 7c). The stabilization effect on Cyasorb is critically affected by the concentration ratio of the stabilizers relative to Cyasorb as shown in Fig. 7b and 7c. An optimized concentration ratio of stabilizers for Cyasorb stabilization has been hence derived [24] and experimental verification of its effectiveness is presently underway.

In the absence of any stabilizers, no cross-linking was found for the exposed, plain EVX films, which dissolved easily in tetrahydrofuran (*THF*) just like unexposed samples. In contrast, EVX thin films that incorporated Cyasorb or other UV absorbers, such as Tinuvin™ 326 and 327, but *without* a free-radical scavenger (a UV light stabilizer) became highly cross-linked and mostly insoluble in THF. The cross-linking was largely reduced when a UV light stabilizer, such as Tinuvin 770, was present.

Based on these observations, it is concluded that the Cyasorb, acting as a UV absorber and a quencher, can promote the cross-linking of EVX and most likely involves a free radical mechanism. While Cyasorb can be decomposed by the attack from the free radicals generated photochemically in the EVX matrix, it can be protected by the presence of Tinuvin 770 to neutralize the free radicals that are formed. The Tinuvin can greatly reduce, but not completely eliminate, the photodecomposition of Cyasorb. These results also explain why various field-degraded PV modules show large to complete loss of Cyasorb and a substantial increase in the degree of cross-linking in a large number of yellow–brown, brown, and dark brown EVA films [12,13].

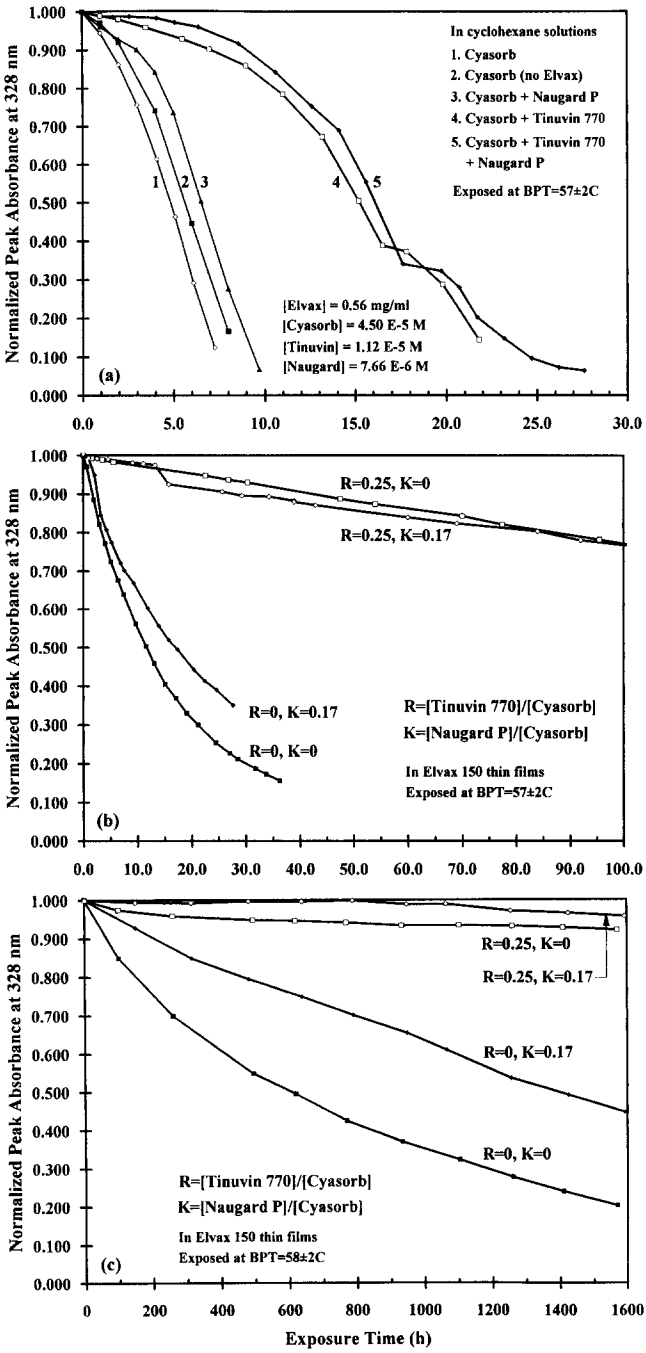
Normalized Peak Absorbance at 328 nm
In cyclohexane solutions
1. Cyasorb
2. Cyasorb (no Elvax)
3. Cyasorb + Naugard P
4. Cyasorb + Tinuvin 770
5. Cyasorb + Tinuvin 770 + Naugard P
Exposed at BPT=57±2C
[Elvax] = 0.56 mg/ml
[Cyasorb] = 4.50 E-5 M
[Tinuvin] = 1.12 E-5 M
[Naugard] = 7.66 E-6 M
(a)
R=0.25, K=0
R=0.25, K=0.17
R=0, K=0.17
R=0, K=0
R=[Tinuvin 770]/[Cyasorb]
K=[Naugard P]/[Cyasorb]
In Elvax 150 thin films
Exposed at BPT=57±2C
(b)
R=0.25, K=0
R=0.25, K=0.17
R=0, K=0.17
R=0, K=0
R=[Tinuvin 770]/[Cyasorb]
K=[Naugard P]/[Cyasorb]
In Elvax 150 thin films
Exposed at BPT=58±2C
(c)
Exposure Time (h)

3.2.2. Discoloration and spectrophotometric characterization of exposed EVA laminates

Fig. 8a shows the spectral changes in transmittance measured as a function of exposure time for a sample of EVA A9918 that is formulated with three stabilizers (Cyasorb, Tinuvin 770 and Naugard P), laminated between two quartz slides, cured at 145°C, and exposed to the C-Xe light filtered with a borosilicate plate. The increase in transmittance below ~ 375 nm results from a decreased concentration of Cyasorb due to photodecomposition. The decrease in the transmittance at wavelengths > 375 nm is accompanied by the appearance of a light yellow color. The color gradually darkens to a light brown as the transmittance of a *broad band* in the visible range continues to decrease. The net spectral changes after subtraction from the original at t = 0 h are given in Fig. 8b, showing the large depletion of Cyasorb in the 250–375 nm region and the formation of discoloring elements absorbing from 375 nm to the infrared wavelengths. These changes are more evident when the transmittance at some wavelengths are plotted as a function of exposure time (Fig. 9a), where the depletion of Cyasorb is observed at 326 nm along with the curve at 420 nm that corresponds to absorption by the discoloring chromophores that are formed. The presence of decomposition products from Cyasorb and the effect of their absorption of UV at < 300 nm can be inferred from the relatively slow depletion rate shown for the curve at 288 nm.

The extent of discoloration of the exposed EVA laminates can be numerically represented by the color indices (a simplified Adam-Nickerson chromaticity system or CIELAB [25] that is used here) as shown in Fig. 9b, in which the brightness, or lightness (L^*), decreases as the yellowness index (*YI*) increases. A positive increase in the magnitudes of a^* and b^* denotes an increase in redness and yellowness, whereas a negative decrease of a^* and b^* denotes an increase in greenness and blueness, respectively. The changes in the color indices can be used to represent an increase or decrease in the length of conjugations that absorb visible light of long or short wavelengths. In Fig. 9b, the a^* shows a small decrease initially before gaining redness later, that probably results from an initial photodecomposition of some originally existing chromophores at low concentrations that absorb in the IR region. As the film color darkens gradually from light yellow to light brown upon exposure, the indices of YI, a^*, and b^* increase correspondingly while L^* decreases. When curve-fitted, the YI (or b^*) curve exhibits a sigmoidal pattern followed by a slight linear slope during the course of color development from light yellow to light brown. The sigmoidal shapes appear to match the curve shapes for the transmittance changes at 326 nm and 420 nm (Fig. 9a). In effect, the increase in YI and loss in transmittance at 420 nm are essentially mirror images.

Fig. 7. Photodecomposition of Cyasorb and its stabilization by individual or joint presence of Tinuvin 770 and Naugard P in (a) cyclohexane solutions and (b) EVX films exposed to the *C-Xe* light at BPT = 57° ± 2°C, and (c) EVX films exposed to a 1.8-kW Xe light at BPT = 58° ± 2°C in a DSET tabletop exposure system. The cyclohexane solutions contained Elvax 150 and were used to cast the EVX films in cuvettes used in (b and c). The concentrations of each component or their ratios are indicated in the figures.

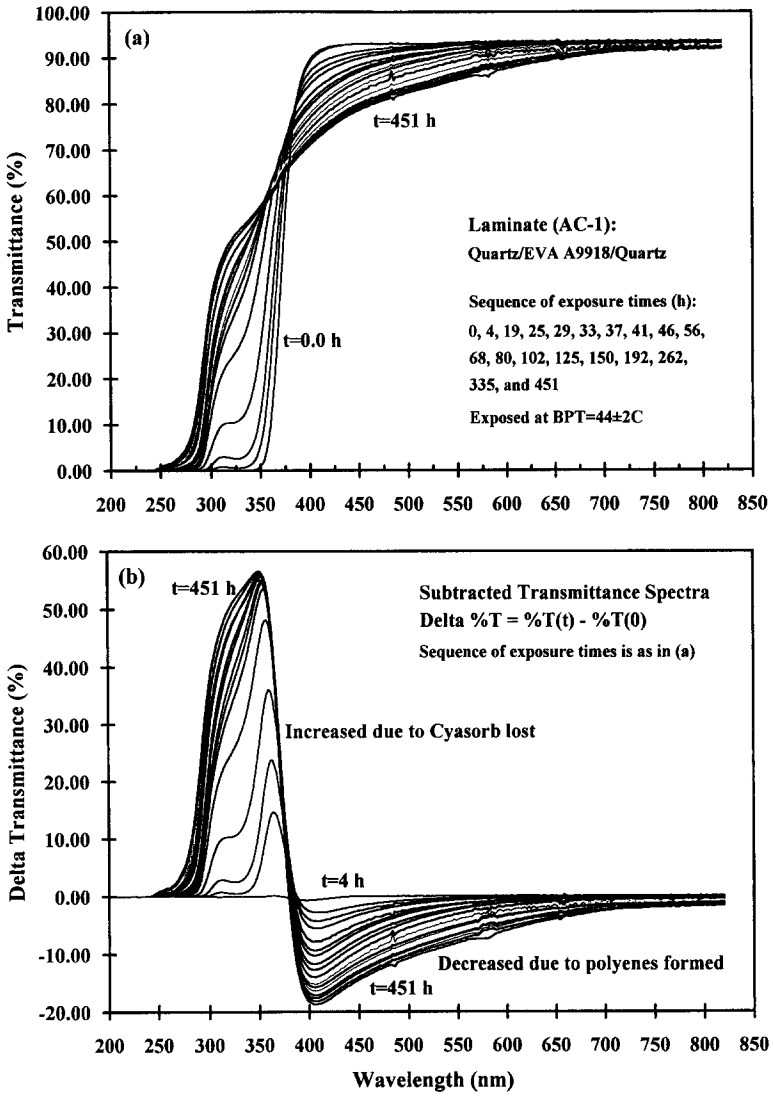

Fig. 8. (a) Transmittance spectra for an EVA A9918 sample that was laminated between two $1'' \times 1'' \times 1/16''$ quartz slides, cured, and exposed to the *C-Xe* light filtered with a $1/8''$ borosilicate plate for 1088 h at BPT = 44° ± 2°C. (b) Subtracted transmittance spectra from the original film transmittance at $t = 0$ h.

As expected, when the light intensity is increased, the discoloration occurs earlier and the rate is faster (not shown).

3.2.3. Effects of formulation and stabilizers on EVA discoloration

As pointed out earlier, cured EVA A9918 has a greater concentration of UV-excitable chromophores and a higher residue of curing peroxide than the

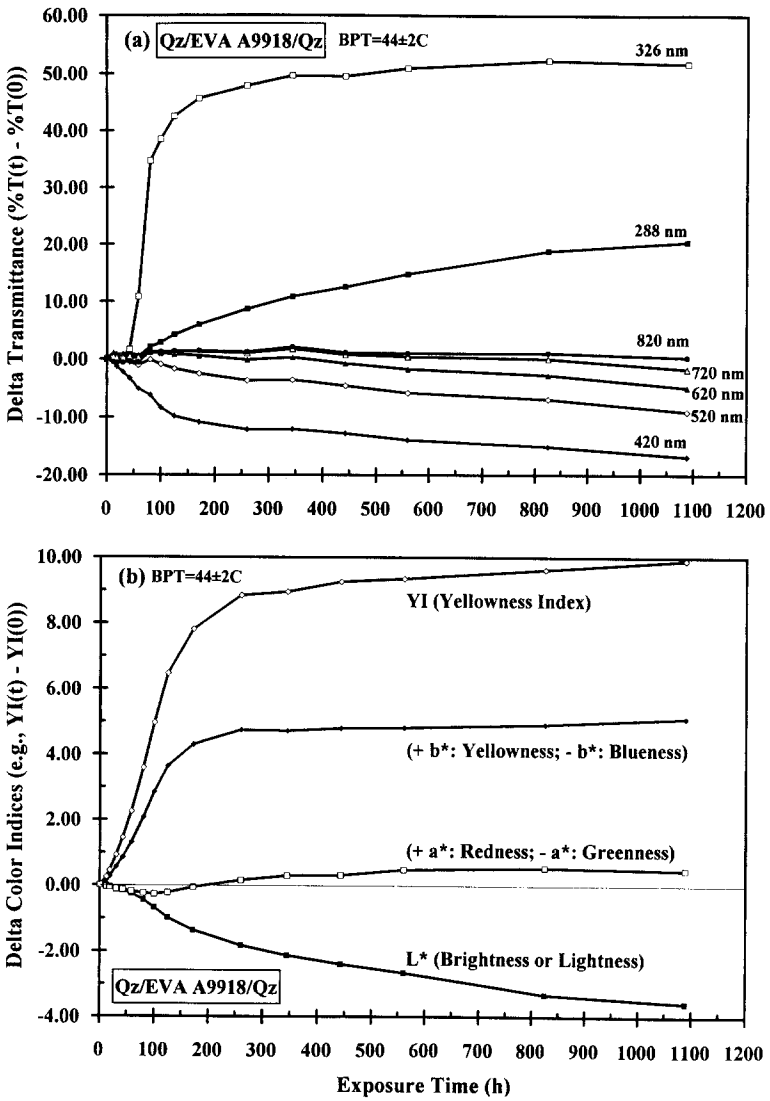

Fig. 9. (a) Net changes of the transmittance at various wavelengths from the spectra in Fig. 8a. (b) Net changes of color indices-yellowness index (*YI*), a*, b*, and L*-measured for the sample in Fig. 8a as a function of exposure time. See text for an explanation of the color indices.

cured EVA 15295 (Fig. 2b). Because enhanced photodegradation rates of polymers are frequently associated with high concentrations of UV-excitable chromophores, peroxides, and hydroperoxides in a polymer [20,21], a faster degradation/discoloration rate of the EVA A9918 is expected. The discoloration is attributed to the formation of a mixture of conjugated polyenes and polyenic α,β-unsaturated carbonyls [26,27]. However, as will be discussed more below, possible contributions

from other discoloring elements such as dimerized or phototransformed moieties of stabilizer(s) are not ruled out. Analytically, the fluorescence emission intensity is generally proportional to the concentration and the emission peak wavelength to the structure of luminescent chromophores (lumophores). Therefore, the photodegradation rates of the two EVA laminates (A9918 and 15295) under UV exposure can be easily differentiated by monitoring their fluorescence characteristics. Fig. 10a compares the emission spectra obtained with an excitation wavelength $\lambda = 350$ nm for the laminated and cured samples of the two EVA formulations between two borosilicate slides that were exposed to the enhanced UV (SS-Xe) light. As both EVA laminates gradually developed a color from yellow to light brown, the emission peak at 420 nm showed a large increase initially and then a decrease later, while a new, broad emission peak in the 450–600 nm region evolved that is attributed to the polyenic formations [26,27]. The changes are similar for both formulations but are faster for the EVA A9918.

By plotting the peak intensities at 420, 500, and 550 nm (Fig. 10b), the marked differences in the changing rates of the structures of chromophores are clearly shown as a function of exposure time for the two EVA laminates; three common degradation mechanisms are also indicated. Since the emission peak intensity at 420 nm (curves 1 and 4) is associated with the quenching concentration of Cyasorb on the initially existing lumophores (from curing) [13], a rapid increase in the first 350 h of exposure for the EVA A9918 clearly indicates a rapid loss of Cyasorb from photodecomposition. After reaching a maximum, a decrease in the 420-nm peak intensity is accompanied by an increase in the 450–600-nm peak intensity, which is interpreted as a transformation of the initially shorter chromophores to longer lumophores. These spectral changes in transmittance and fluorescence therefore show that the loss of Cyasorb and the formation of discoloring chromophores occurs earlier and faster in EVA A9918 than in EVA 15295.

The differences in yellow–browning rates between the EVA A9918 and 15295 are further illustrated in Fig. 11 (curves 1 and 2), in which a significantly higher photostability against discoloration is exhibited by EVA 15295 in the first $\sim$ 1500 h of exposure. The two EVA films probably would behave similarly after $\sim$ 2000 h, if delamination had not occurred to the EVA A9918 (curve 1). In addition, a thicker laminate made with two layers of EVA A9918 film ($\sim$ 0.40 mm thick after curing) discolored slower initially, but later became faster than the laminate made of single layer EVA (compare curves 3 and 4 to curve 1). On the other hand, no discoloration is observed for the plain EVX film laminates (curve 5) that contained no stabilizers and Lupersol, and therefore no curing-generated chromophores. Without chromophores absorbing UV > 285 nm, the EVX films are transparent to the SS-Xe UV light (> 285 nm, filtered with a borosilicate plate) and thus are not expected to discolor under the experiment conditions.

3.2.4. Possible causes of EVA discoloration

Using a variety of spectroscopic and chemical analyses, the EVA discoloration has been attributed to the formation of a mixture of polyenic chromophores [26,27], which results from deacetylation of the pendant acetate groups on the

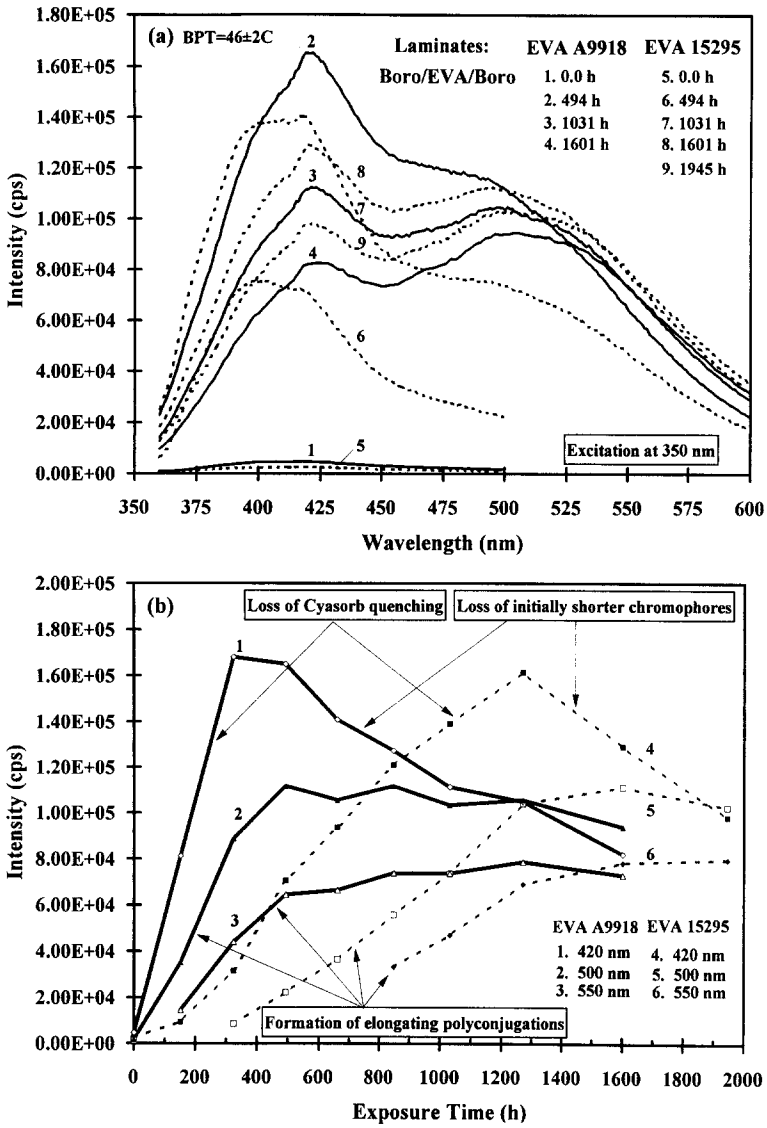

Fig. 10. (a) Fluorescence emission spectra obtained from excitation at 350 nm for EVA A9918 (solid curves 1–4) and EVA 15295 (dashed curves 5–9) that were laminated between two $2'' \times 2'' \times 1/8''$ borosilicate (Boro) glass slides, cured (see Fig. 2b), and exposed to the *SS-Xe* light (see Fig. 1a, curve 2) at BPT = 46° ± 2°C. The measurements were performed by exciting directly through the Boro plate to the EVA side facing the UV light. (b) Fluorescence emission peak intensities at 420 nm, 500 nm, and 550 nm for the two UV-exposed EVA laminates in (a). Three key mechanisms involved in EVA degradation and discoloration are indicated.

EVA polymeric chains as well as transformation of the initially shorter chromophores to the longer chromophores (Fig. 10). The polyene structures are believed to exist as a mixture and partially in conjugation with carbonyl groups

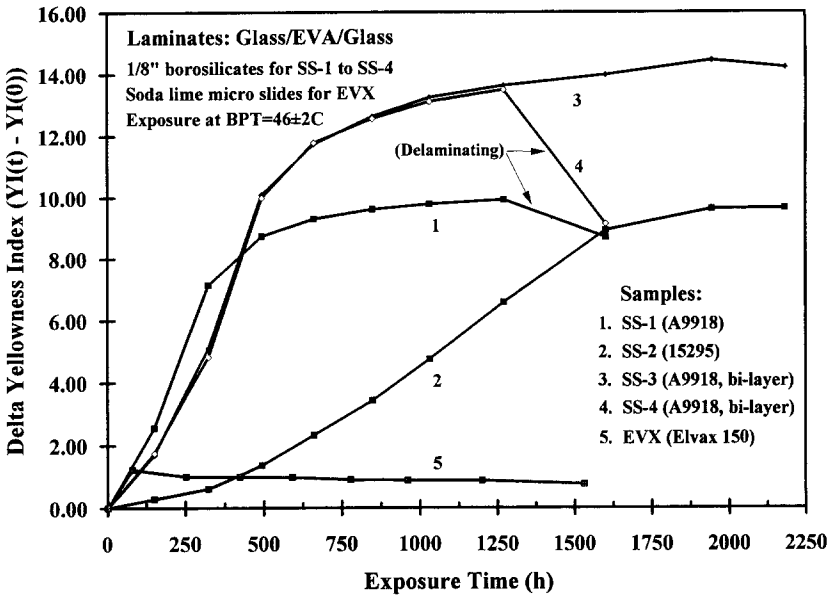

Fig. 11. Net changes in yellowness index (YI) as a function of exposure time to the *SS-Xe* light for four EVA film samples (curves 1, 2, 3, and 4) laminated between two borosilicate glass slides and cured, and a plain Elvax 150 film (curve 5) laminated between two soda lime micro slides. Curve 2 is for EVA 15295 and curves 1, 3, and 4 are for EVA A9918 samples in which samples 3 and 4 used two layers of the EVA films in the lamination. Exposure was conducted at BPT = 46°±2°C as in Fig. 10 for all samples simultaneously.

[26], perhaps similar to those produced in thermally and photochemically degradaed polyvinyl chloride [28,29]. The polyenic chromophores absorb a continuous broad band of visible to infrared light (Fig. 8), give the yellow to dark brown color (Fig. 9b), and produce broad emission peak in the 450–600 nm region (Fig. 10a).

The formation and presence of the polyenic chromophores in the discolored EVA are further evidenced by the largely increased peak magnitudes observed in the electron paramagnetic (spin) resonance (EPR or ESR) analysis. Fig. 12a compares the EPR spectrum of an unexposed, cured EVA A9918 (curve 1) to those of two field-discolored EVA samples (curves 2 and 3). The dark brown EVA sample (curve 3) was extracted with THF prior to the EPR analysis. The THF extraction removed all *soluble* low molecular weight EVX, residual stabilizers, and decomposition products. The large increases in peak magnitudes at 3260 and 3280 Gauss for the two brown EVA samples clearly indicate the presence of a relatively high concentration of free electrons in the conjugated π bondings, which are attributed to the elongated polyenic conjugations. Hanna et al. [30] have reported calculated and experimental EPR results for the polyenic carboxylic acids, $CH_3(CH=CH)_{m-1}COOH$, $m = 2$–5, 7, that were irradiated with X-ray; Kubota et al. [31] also showed EPR results for the benzophenone-sensitized, photodegraded three model compounds that produced the C = C bonds increasingly from one to

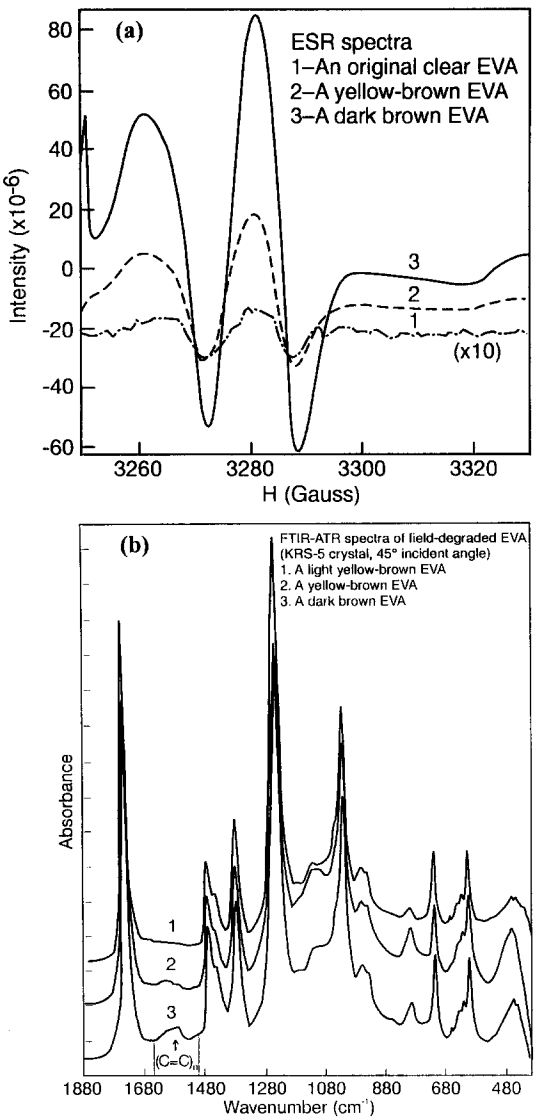

Fig. 12. (a) EPR spectra for samples of (1) an original, unexposed, cured EVA A9918, (2) a yellow–brown EVA, and (3) a THF-extracted, dark brown EVA. (b) FTIR-ATR spectra taken at a 45° incident angle using a KRS-5 crystal for (1) a light yellow–brown EVA, (2) a yellow–brown EVA, and (3) a dark brown EVA. The IR absorption peaks for the polyenic structures appear weakly in the ~1500–1650 cm^{-1} region. All of the discolored EVA films were taken from different field-degraded PV modules.

three (triene). To further verify, or eliminate, the effect of the additives and any decomposition products on the EPR signal intensity, methanol extraction was applied to an uncured EVA A9918, a cured-but-unexposed EVA A9918, and a

yellow–brown EVA film prior to EPR analysis. The results show no EPR peak for the uncured EVA, similar EPR peaks with a ~1.8-time increase in the peak intensity for the cured-but-unexposed EVA A9918, and essentially unchanged in the peak intensity for the yellow–brown EVA after methanol extraction (figures not shown here). These observations further confirm the consequence of curing with Lupersol 101 on generating new chromophores and the presence of polyconjugations *on* the polymeric chains of the discolored EVA.

Detection of the polyenic structures by FTIR-ATR (Fourier transform infrared-attenuated total reflectance) is much less sensitive, and seems to be inconsistent sometimes, probably because of the low absorptivity of the conjugated $-(C=C)_n-$ bonds in the 1500–1650 cm^{-1} region [28] as shown in Fig. 12b for three field-degraded, increasingly brown EVA samples. In addition, the $(C=C)_n$ ($n > 1$) may be more difficult to detect in FTIR if the double bonds are in *trans* configuration [32]. FTIR-Raman analysis was also performed for discolored EVA samples and a number of model compounds that contain short or long C = C conjugations. For example, a light yellow–brown EVA sample produces a weak broad peak in the 1500–1650 cm^{-1} region that centers at ~1600 cm^{-1} (figure not shown), which is not observed for a cured, undegraded EVA. In comparison, 1-acetoxy-1,3-butadiene shows a peak at 1654 cm^{-1}, 2,4-hexadienoic acid at 1626 cm^{-1}, all-trans-retinol at 1590 cm^{-1}, all-trans-retinoic acid at 1570 cm^{-1}, and trans-β-carotene at 1512 cm^{-1}, respectively.

In addition to the above results from UV/VIS, YI, FA, EPR, FTIR-ATR and FTIR-Raman analyses, it should be emphasized that analysis of the UV/VIS absorption spectra of the extracts from polar organic solvents such as methanol and THF or non-polar solvent such as cyclohexane exhibits *no* visible color or any absorption peak(s) in the visible to infrared region for any of the lab-degraded or field-degraded, yellow to dark brown EVA samples. All discolored EVA films essentially retained their initial color after extraction for extensive periods (e.g., 20 days). Besides, the color exists as a relatively thin layer on the light-exposed surface side of the EVA films, which can be easily observed on specimens soaked and swelled in THF, toluene, or cyclohexane. Fig. 13 show the absorption spectra for the cyclohexane extracts of three EVA specimens of different colors and a standard solution of Cyasorb (2.925×10^{-5} M). As is seen, the residual Cyasorb concentration in dark brown EVA is less than that in a lighter brown EVA as the PV module for the former was weathered longer in the field than the latter; the residual Cyasorb concentration is even lower in the lab-degraded, light yellow–brown EVA A9918 that was exposed to the enhanced UV, SS-Xe light. None of the extracts for these three samples produced any absorption peak in the 410–820 nm region. The observations in Fig. 13 also imply that the extent of EVA discoloration is not *linearly* proportional to the lost quantity of Cyasorb from photodecomposition. These results indicate further that the discoloration of exposed EVA is due to structural changes *on* the polymeric chains of the EVA.

Dimerization or phototransformation of stabilizer(s) used in the EVA formulations that may subsequently attach covalently to the EVA polymeric chains (e.g., via a *postulated* mechanism involving recombination of free radicals from Cyasorb

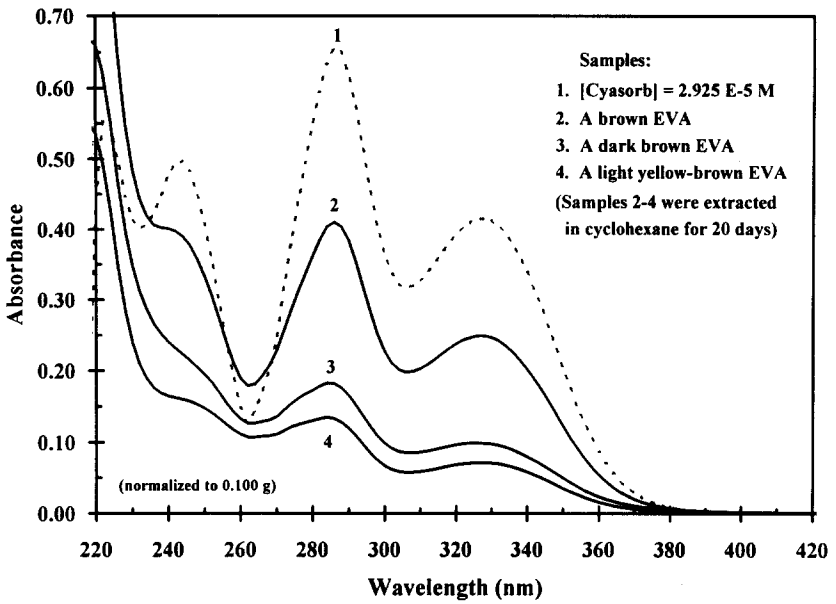

Fig. 13. Absorption spectra of cyclohexane solutions of (1) a standard solution of Cyasorb at a concentration of 2.925×10^{-5} M, (2) a field-degraded, brown EVA, (3) a field-degraded, dark brown EVA, and (4) a lab-degraded, light yellow–brown EVA (sample SS-1 as in Fig. 11). Samples 2–4 were weighed (0.8–0.15 g) and extracted in 10.0 ml cyclohexane at room temperature for 20 days. Their absorbance are normalized by weight to 0.100 g.

and EVX polymer) was also considered previously to account for the discoloration, but has not been verified experimentally, e.g., by FTIR-ATR analysis. One of the probable dimer candidates is the one that arises from photo-induced transformation of the Cyasorb molecules. However, the Cyasorb is found to decompose photochemically (see Figs. 4–10), possibly with benzoic acid as the major product as reported by Pickett and Moore [23]. Besides, there is no *distinctive, individual* absorption peak(s) in the *visible* region observable in any discolored EVA samples as one may expect for a dimer photochemically transformed from compound(s) such as benzoquinone(s) [33]. For examples, Klemchuk and Horng [34] used model compounds that may represent the transformation products of some hindered phenols and showed these quinoidal compounds have *individual* peaks with high extinction coefficients in the UV (240–340 nm) and visible (420–450 nm) regions; Lucki et al. [35] showed that, upon UV irradiation in air, hindered phenols exhibit a strong but changing absorption peak at 270–280 nm and their phototransformed products appear as a shoulder peak at 300 nm. In contrast, all of the discolored EVA, regardless of the extent of yellowing or browning, show two absorption peaks and a shoulder that commonly appear over a broad envelop in the UV region at ~235 nm, ~285 nm, and ~335 nm along with a long, peakless absorption tail into the visible-IR region [see Ref. [26], Fig. 4b]. Except for a greater absorption, the latter two peak positions at 285 nm and 335 nm are

essentially identical to the peaks found for methanol-extracted, cured-but-unexposed EVA [26]. Furthermore, if the discoloring dimers or phototransformed products were present as free molecules in the EVA matrix, then one would expect to extract them out with organic solvents such as THF or cyclohexane; the fact is that all extracts are observed to be clear with no absorption peaks in the visible-IR region. Diffusion of the dimer molecules would also take place and produce a fairly uniform pattern of discoloration over the entire areas or bulk of the EVA laminates; the fact is that clear perimeter and bulk are observed in the discolored EVA from lab-degraded samples and field-degraded PV modules. Another probable form for the "discoloring dimer" model is the covalent attachment to the polymer chains on the light-exposed layers; the fact is that, as indicated earlier above, a continuous peakless transmission (absorption) band, not certain distinctive absorption peaks from a dimer or transformed compound, is observed in the visible-IR region for all discolored EVA films before and after solvent extraction.

Another source of EVA discoloration considered is the decomposition products from Cyasorb and/or other additives. Since the Cyasorb decomposition products absorb UV < 300 nm (Figs. 4 and 5), they do not give the color. Whether, and how, Tinuvin 770 and Naugard P will decompose and produce discoloring components is not known yet. One more question remains unanswered: do these yet-to-be-identified decomposition products photochemically facilitate the EVA degradation and discoloration? More detailed studies are needed to resolve and verify *experimentally* the presence of discoloring moieties, and their structures, other than the polyenic chromophores on the EVA.

In a recent study about the effects of individual stabilizers on the discoloration of solution-cast, laminated and cured EVX films, the results show that when Lupersol 101 and Cyasorb are both present, a synergistic effect on the EVA yellowing is observed. When present separately, neither one induces significant yellowing in the laminates. From the new findings, the results described in previous sections, and the facts that the Cyasorb promotes free-radically cross-linking in EVX (Section 3.2.1) and that the Lupersol peroxide can degenerate into free radicals, it seems that Cyasorb and Lupersol may "accelerate" the EVA discoloration probably via an enhanced, free-radical-involving degradation process. Details will be published later.

3.2.5. Effect of EVA discoloration on optical transmittance

An important issue in studying the effects of EVA discoloration on solar cell performance is the *net loss* in the optical transmittance of the exposed EVA that may reduce the photocurrent generated by the solar cells. The results from analysis of the spectral transmittance changes integrated from 280 nm to 820 nm for the borosilicate-laminated samples are shown in Fig. 14. Because of the gradual photodepletion of Cyasorb, a net gain in the total transmittance is initially obtained. Subsequently, the integrated total transmittance shows a progressive loss as the yellow–browning increases and a value of a net increase of ~ 9 is measured for the yellowness index (Fig. 11); these correspond to ~ 600 h UV exposure for a single layer of EVA A9918 (curve 1) and ~ 1600 h exposure for EVA 15295 (curve

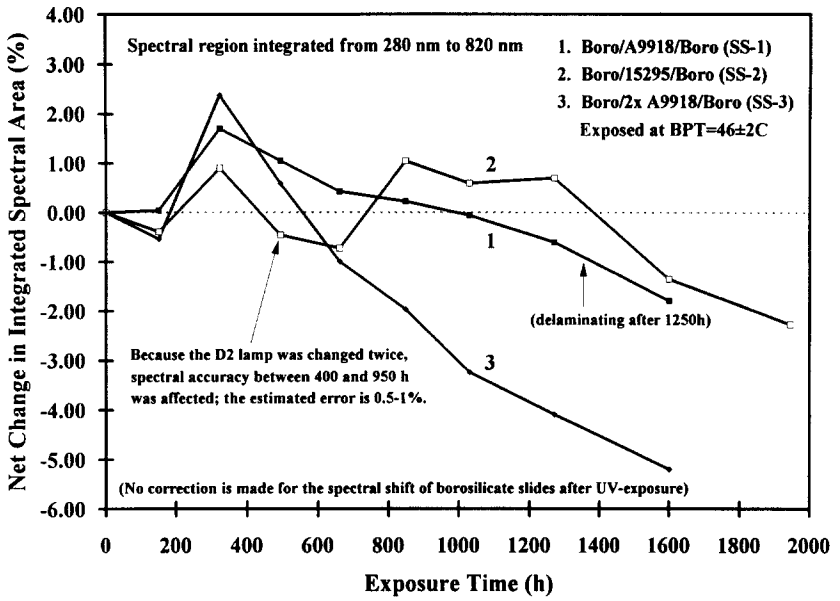

Fig. 14. Net changes of spectral transmittance integrated from 280 nm to 820 nm (subtracted from the original transmittance at t = 0 h) for samples of curves 1, 2 and 3 in Fig. 11 as a function of exposure time at BPT = 46° ± 2°C.

2). An important implication here is that a quantitative relation can be established between the increase in YI and the total (integrated) transmittance loss on the exposed, discolored EVA laminates.

3.2.6. Effects of lamination, delamination and photobleaching

If the EVA films are *not* laminated between glass plates, discoloration has never been observed. The same results are observed for samples that are only sandwiched between two glass plates (i.e., no lamination and curing at elevated temperatures) and exposed to enhanced UV light in the air for more than 4000 h at a BPT of ~ 56 ± 3°C. This is attributed to the photooxidation of originally existing chromophores and any new ones before they become discoloring polyenes. Further evidence for the photobleaching reactions is the observation of the clear band of EVA around the perimeter of both field-degraded [13] and lab-degraded specimens where air diffusion is allowed [10 and this work]. In this work, the clear band is ~ 3–5 mm wide compared with a width of ~ 3–10 mm around the solar cells in many field-degraded PV modules studied.

Delamination of the EVA occurred on two borosilicate laminates and resulted in a rapid decrease in the yellowness index (**YI**) after ~ 1250 h (curves 1 and 4 in Fig. 11). Eventually, the delamination could be seen visually. The delamination probably results from two factors: (1) exposure to the UV light and ambient conditions (air and humidity) gradually reduces the adhesion strength, and (2) the

EVA films and the glass slides used were unprimed so the initial adhesion strength was relatively low at the interface of EVA and glass. In a recent study using a prototype vacuum laminator, nearly an order of magnitude difference in adhesion (or, pull) strength was measured between the primed and unprimed EVA laminated on the same borosilicate glass superstrates. As the films gradually delaminate from the glass surfaces, air (oxygen) diffuses more readily to the yellow–browned EVA, resulting in photobleaching reactions that decrease the YI. The photobleaching reactions cause an oxidative breakdown of the polyenic chromophores in the presence of air [19].

3.3. Correlation of the spectrophotometric results

One of the objectives of this study is to establish a correlation for the results acquired from the three spectrophotometric measurements in transmittance, color indices (primarily yellowness index), and fluorescence emission (peak intensity and/or area). For the EVA 15295 laminate, all four curves correlate quite well as shown in Fig. 15a after applying some multiplying factors to bring all curves into the same Y-axis scale (net change %). Understandably, curves of transmittance changes (delta %T) at 420 nm and YI correlate very well mutually. For the EVA A9918 laminate (Fig. 15b), curves for changes in transmittance at 420 nm and YI correlate well with the same multiplying factors as for the EVA 15295; but the curves for the peak area ratio (or emission peak intensity ratio) deviate from the curves of delta %T and YI at $T > 1000$ h, which probably resulting from the delamination problem. Better correlation may be obtainable if primed EVA films are used. More effort is needed in this area of correlation study.

3.4. Mitigation of EVA discoloration

Results from on-going efforts to mitigate, chemically and/or physically, the rate of EVA discoloration have shown that the modification of the EVA formulations [24], the use of UV-filtering glass, and gas-permeable polymeric superstrates [19] are useful when employed individually or jointly. Fig. 16 shows (a) the transmittance spectra for superstrates of four glass slides and two Tefzel™ ZMC films, and (b) their respective effects on the EVA discoloration rate. When PPG's short-UV-transmitting Starphire™ (no cerium oxide) is used as a superstrate, a much faster EVA discoloration rate takes place for EVA A9918 than for EVA 15295 (Fig. 16b). Discoloration of EVA A9918 laminates is greatly reduced or nearly eliminated, when the superstrates of UV-transparent quartz (refer to Figs. 8 and 9) and borosilicate with a ~ 290 nm cutoff (refer to Figs. 10 and 11) are replaced by glass plates that can more effectively filter or absorb UV wavelengths below 320 nm, such as window glass that allows 10% T at 320 nm, or PPG's Airphire™ (or Solarphire™), which is a cerium oxide-doped glass that allows 10% T at 342 nm. The slower discoloration rate apparently results from a significant reduction in the shorter-UV wavelength induced photodegradation reactions. For the EVA A9918 laminated with gas-permeable Tefzel™ polymer films as super-

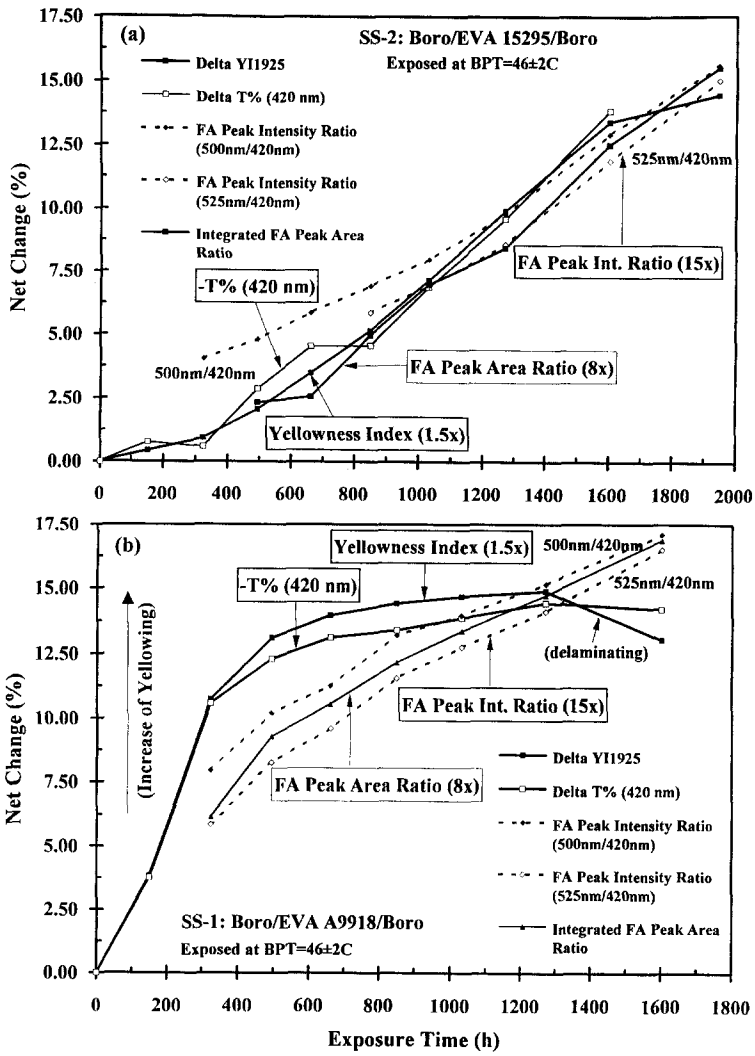

Fig. 15. Correlation plots of net percentage changes in transmittance (%T at 420 nm), yellowness index (YI), and fluorescence emission peak intensity and area ratios for (a) EVA 15295 (sample SS-2) and (b) EVA A9918 (sample SS-1) from Fig. 11. Multiplications of the YI (×1.5) and fluorescence peak ratios (×8 and ×15) curves are used to demonstrate how well the three different measurements can be correlated. The fluorescence peak intensity ratios are for the ratio of the evolving peak in the 500–550 nm range for the polyenic chromophores from EVA degradation to the initial peak at 420 nm. The peak area ratios are for the peak area integrated between 451 nm and 600 nm to the peak area integrated between 360 nm and 450 nm (see Fig. 10a for reference).

strates, no discoloration occurred when exposed to the enhanced UV light as reported preliminarily [19]; more studies have been conducted since that yield the same results. Fluorescence analysis shows that the original chromophores (after

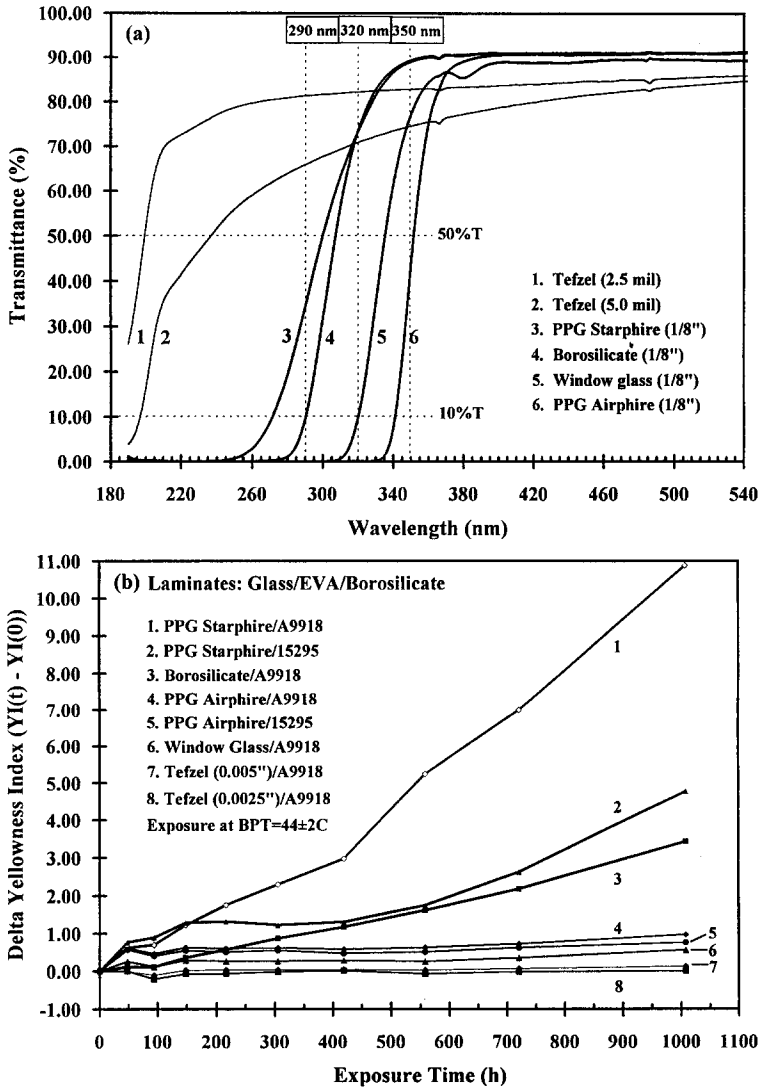

Fig. 16. (a) Transmittance spectra of two Tefzel films and several types of glass. (b) Net changes in the yellowness index for EVA A9918 and 15295 laminated separately either between a superstrate of Tefzel film (or a glass) and a borosilicate (Boro) glass substrate. The glass plates are 3.16 mm (1/8″) thick and the Tefzel films are 2.5 mil and 5.0 mil thick. PPG's cerium oxide (ceria)-doped Airphire™ glass has been renamed Solarphire™. The laminates were exposed simultaneously to the *SS-Xe* light at BPT = 44° ± 2°C.

curing) are effectively destroyed because of the photobleaching reactions. More details will be published later. The above results are very encouraging, but other issues remain to be characterized such as whether the physical properties (e.g., adhesion and mechanical strength) of the EVA layers, and even the solar cell

performance, will be adversely affected by the enhanced diffusion of gaseous elements (e.g., O_2, NO_x, SO_x, H_2O, etc.) such as from the ambient.

Accordingly, more thorough studies are still required to ensure that using various chemical and physical approaches to mitigate discoloration will *also* provide the desired long-term durability of EVA-encapsulated PV modules. Alternatively, new polymeric encapsulants can be developed as replacements for the EVA. For example, ASE Americas (formerly Mobil Solar, Inc.) has successfully selected a different polymer encapsulant for their PV modules that has not discolored in accelerated tests in which EVA A9918 and 15295 both discolor [36].

4. Conclusions

Several factors that affect the rate of EVA discoloration have been identified. The photodecomposition of Cyasorb, its stabilization by antioxidants, EVA formulation and stabilizers used, curing treatment, UV light intensity, hermetic lamination, film thickness, delamination, rate of air diffusion, and rate of photobleaching are all important that influence the *net rate* of discoloration of EVA. Reasonably good correlations are obtained among the transmittance loss, yellowness index increase, and fluorescence peak area (or intensity) ratio and should be useful in quantitatively correlating the extent of EVA discoloration to efficiency loss in PV modules. More extensive work is in progress to elucidate the overall impact on the PV module service lifetime by using a number of chemical and/or physical approaches to stabilize or eliminate the EVA discoloration.

Acknowledgements

The author thanks S.H. Glick and Joy M. Folkvord for assistance, D. Trudell and T. Cannon for the spectroradiometric measurements of Xe arc lamps, T. McMahon for the EPR measurements, and J. Webb for the FTIR and FTIR-Raman measurements. A.W. Czanderna, the leader of the PV Module Materials and Component Durability Task is thanked for reviewing and commenting on the manuscript. R. DeBlasio, the manager of the PV Module and System Performance and Engineering Project, is thanked for his support of this work. This work was performed at NREL under support by the US Department of Energy Contract No. DE-AC36-83CH10093.

References

[1] F. Gay and E. Berman, Chemtech, March (1990) 182–186.
[2] A.L. Rosenthal and C.G. Lane, in: L. Mrig (Ed.), Proc. PV Module Reliability Workshop, Lakewood, CO, SERI/CP-4079, October 25–26 (1990) 217–229.
[3] V. J. Kusianovich, in: L. Mrig (Ed.), Proc. PV Module Reliability Workshop, Lakewood, CO, SERI/CP-4079, October 25–26 (1990) 241–245.

[4] J. Schaefer, L. Schlueter, A. Rosenthal, H.J. Wenger and A. E. Laque, in: Proc. 10th EC Photovoltaic Solar Energy Conf., 1991, p. 1245–1248.
[5] H.J. Wenger, J. Schaefer, A. Rosenthal, R. Hammond and L. Schlueter, in: Proc. 22nd IEEE Photovoltaic Specialists Conf., New York, NY, 1991, pp. 586–591.
[6] A. Rosenthal, M.G. Thomas and S.J. Durand, in: Proc. 23rd IEEE Photovoltaic Specialists Conf., New York, NY, 1993, pp. 1289–1291.
[7] D. Berman, S. Biryakov and D. Faiman, in: Sol. Energy Mater. Sol. Cells 36 (1995) 421–432.
[8] J.H. Wohlgemuth and R.C. Peterson, in: L. Mrig (Ed.), Proc. Photovoltaic Performance and Reliability Workshop, SERI/CP-411-5184 (1992) 313–326.
[9] J.H. Wohlgemuth, in: L. Mrig (Ed.), Proc. Photovoltaic Performance and Reliability Workshop, NREL/CP-410-6033, September 8–10 (1993) 394–398.
[10] F.J. Pern and A.W. Czanderna, in: R. Noufi and H. Ullal (Eds.), AIP Conf. Proc. for the 11th NREL PV Program Review Meeting, No. 268, American Institute of Physics, New York, 1992, pp. 445–452.
[11] A.W. Czanderna, in: L. Mrig (Ed.), Proc. Photovoltaic Performance and Reliability Workshop, NREL/CP-410-6033, September 8–10 (1993) 311–357.
[12] F.J. Pern, in: L. Mrig (Ed.), Proc. Photovoltaic Module Reliability Workshop, SERI/CP-4079, Lakewood, CO, October 25–26 (1990) 279–299.
[13] F.J. Pern and A.W. Czanderna, Sol. Energy Mater. Sol. Cells 25 (1992) 3–23.
[14] F.J. Pern, A.W. Czanderna, K.A. Emery and R.G. Dhere, in: Proc. 22nd IEEE Photovoltaic Specialists Conf., Las Vegas, Neveda, October 7–11 (1991) 557–561.
[15] F.J. Pern, in: L. Mrig (Ed.), Proc. Photovoltaic Performance and Reliability Workshop, SERI/CP-411-5184, Golden, CO, September 16–18 (1992) 326–44.
[16] C.G. Gebelein, D.J. Williams and R.D. Deanin (Eds.), Polymers in Solar Energy Utilization, Ch. 22, 23, and 24 (ACS, Washington DC, 1983).
[17] E. Cuddihy, C. Coulbert, A. Gupta and R. Liang, Flat-Plate Solar Array Project Final Report, Vol. VII: Module Encapsulation (JPL Publication 86–31, October 1986, DOE/JPL-1012-125).
[18] P.B. Willis, Investigation of Materials and Process for Solar Cell Encapsulation, Final Report of JPL Contract No. 954527, S/L Project 6072.1 by the Springborn Laboratory, Inc. to JPL (JPL Publication, 1986, DOE/JPL-954527-86/29).
[19] F.J. Pern and S.H. Glick, in: R. Noufi and H. Ullal (Eds.), AIP Conference Proceedings for the 12th NREL PV Program Review Meeting, No. 306 (American Institute of Physics, New York, 1994) 573–585.
[20] J.F. McKellar and N.S. Allen, Photochemistry of Man-Made Polymers (Applied Science Publishers, London, 1979).
[21] G. Scott (Ed.), Mechanisms of Polymer Degradation and Stabilization (Elsevier Applied Science, New York, 1990).
[22] F.J. Pern, in: L. Mrig (Ed.), Proc. Photovoltaic Performance and Reliability Workshop, NREL/CP-411-7414, Lakewood, CO, September 21–23 (1994) 329–47.
[23] J.E. Pickett and J.E. Moore, Polym. Deg. and Stab. 42 (1993) 231–244.
[24] F.J. Pern, in: L. Mrig (Ed.), Proc. Photovoltaic Performance and Reliability Workshop, NREL/TP-410-6033, Golden, CO, September 8–10 (1993) 358–74.
[25] R.R. Blakey, Measuring Colour, a technical publication by Tioxide Group PLC, England, 1990 (registration no.: 249759).
[26] F.J. Pern, Polym. Deg. and Stab. 41 (1993) 125–139.
[27] F.J. Pern, in: Proc. 23rd IEEE Photovoltaic Specialists Conf., Louisville, KY, May 10–14, 1993, pp. 1113–1118.
[28] Y. Shindo, D.E. Read and R.S. Stein, Die Makromolecukulare Chemie 118 (1968) 272–312.
[29] J.F. McKellar and N.S. Allen, Photochemistry of Man-Made Polymers, pp. 95-101 and Table 2.7 in Ch. 2 and the references cited (Applied Science Publishers, London, 1979).
[30] M.W. Hanna, A.D. McLachlan, H.H. Dearman and H.M. McConnell, J. Chem. Phys. 37 (1962) 361–367.
[31] H. Kubota, K. Takahashi and Y. Ogiwara, Polym. Deg. and Stab. 33 (1991) 115–123.

[32] R.M. Silverstein, G.C. Bassler and T.C. Morrill, Spectrometric Identification of Organic Compounds, Ch. 3 (Wiley, New York, 1981).
[33] J. Pospisil, in: N.S. Allen (Ed.), Developments in Polymer Photocehmistry-2 (Applied Science Publishers, London, 1981) Ch. 3, pp. 53–133.
[34] P.P. Klemchuk and P.-L. Horng, Polym. Deg. and Stab. 34 (1991) 333–346.
[35] J. Lucki, J.F. Rabek and B. Ranby, Polym. Photochem. 5 (1984) 351–384.
[36] M. Azzam, in: L. Mrig (Ed.), Proc. Photovoltaic Performance and Reliability Workshop, NREL/CP-411-7414, Lakewood, CO, September 21–23 (1994) 349–60.

E. Degradation Factor Analysis of Crystalline-Si PV Modules through Long-term Field Exposure Test

6P-A9-50

DEGRADATION FACTOR ANALYSIS OF CRYSTALLINE-Si PV MODULES THROUGH LONG-TERM FIELD EXPOSURE TEST

Kengo Morita[1], Takamitsu Inoue[1], Hiroshi Kato[1], Izumi Tsuda[2], Yoshihiro Hishikawa[2]
1. Japan Electrical Safety & Environment Technology Laboratories,
2. National Institute of Advanced Industrial Science and Technology
5-14-12 Yoyogi, Sibuya-ku, Tokyo 151-8545, Japan

ABSTRACT

Degradation factors that affect the performance loss of crystalline-Si PV modules have been analyzed through long-term field exposure test, in order to contribute to the long-term reliability improvement. Tested PV modules were manufactured in the early 1990's and many modules were stable for 10-12 years exposure. However, some of the modules showed the performance loss which exceeds 10% either due to discoloration caused by the delamination between the solar cell and EVA or due to increase of the series resistance caused by the cracks in electrode soldering. It is demonstrated that the signs of these degradations can be detected before the performance loss become significant by careful visual inspection or the temperature distribution inspection under forward bias condition.

1. INTRODUCTION

Long-term reliability is crucial for mass deployment of PV modules, as directly affects the kWh cost of the PV system. However, it takes many years to evaluate the reliability of new modules in field exposure test, so the technique that can evaluate the reliability of the modules in a short term (i.e. the acceleration test) is necessary. For that purpose, the problems of the modules exposed in the field for a long term were picked up and analyzed to understand the degradation mechanism.

Fig.1 The field exposure test site

2. FIELD TEST DETAILS

26 crystalline-Si PV modules supplied by 3 manufactures were installed on 4 sites in Japan during 1991-1993 and in 1997. The photograph of one of the sites is shown in Fig.1. The modules were connected with the lead acid battery and were periodically carried from the sites to the laboratory for IV characteristic measurements by a solar simulator to find the detailed change. And in order to understand the conditions of a large number of modules, in addition to the above, about 100 modules (4 manufactures) installed in 1991 were removed from the large-scale PV system to the laboratory and measured IV characteristic by a solar simulator. The IV characteristic measurements were performed at standard test condition (AM.1.5, 1kW/m^2, 25°C).

3. RESULTS

The performance (Pmax) changes of almost all crystalline-Si PV modules exposed 10-12 years in the field were less than 10%. This indicates that PV modules are stable for a long term. However, some of degradation factors were observed.

All the modules showed slight initial drop in Pmax due to the reduction in Isc (short circuit current). Typical Isc change of the modules is shown in Fig.2, where Isc is normalized by an initial value. All the modules showed the loss in the Isc by 1~5% within 1 year of the field exposure. Afterwards, the Isc of the modules became stable. On the other hand, no change in Voc (open circuit voltage) and FF (fill factor) were observed.

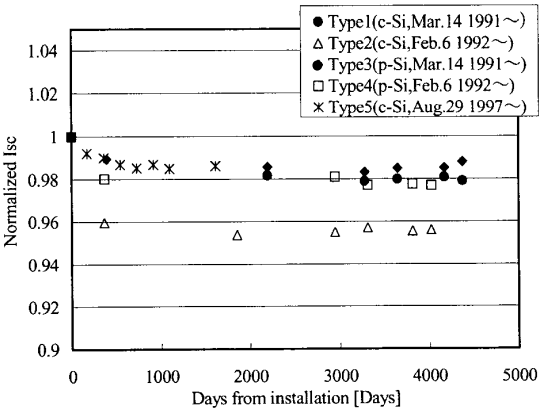

Fig.2 Typical Isc change of the modules by long-term field exposure test

Some of the modules showed performance loss for a long term. 2 types of degradation factors were observed.

First, 2 out of 26 modules in the field exposure test showed performance loss that exceeds 10% due to the reduction in FF (fill factor) caused by the increase in Rs (series resistance). IV characteristic of the module that indicated the increase in the Rs are shown in Fig.3. Compared with the characteristics of the module stored indoors (unexposed), 10 year exposed module shows performance loss (-20%) mainly due to the increase in the Rs. Estimated Rs of the module is about 1.2 ohms, on the other hand, the Rs of the module stored indoors is 0.5 ohms. The degraded modules showed no distinct visual change. The change in the FF by field exposure is shown in Fig.4. Though the data of modules showed large swings, this is due to the increase in resistance caused by corrosion of external contacts to connect with the storage battery. After contacts were washed by alcohol, the values of the FF increased. The FF of the module changes gradually at the rate of 0.9~1.4%/year. In large-scale PV system, the increase in the Rs was also confirmed in the modules. The degree of the degradation was very dependent on the individual module.

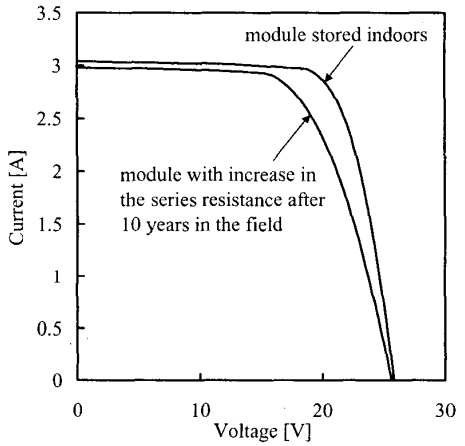

Fig.3 IV characteristic of p-Si module which showed performance loss (-20%) due to the reduction in the FF caused by the increase in the Rs (series resistance) after 10 years in the field

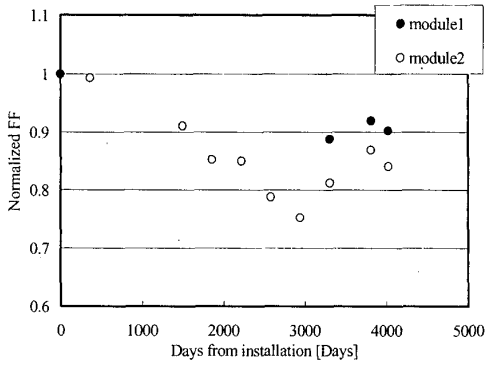

Fig.4 The change in the FF by field exposure

Second, some modules in the large-scaled PV system showed performance loss due to visible discoloration (whitening). IV characteristic of the module with the strong discoloration is shown in Fig.5. Compared with the characteristic of the module stored indoors, the module with the discoloration showed performance loss (-25%) mainly due to the reduction in the Isc. The degree of the discoloration was very dependent on the individual module and there are not many modules with the strong discoloration in this case. In the 26 field exposure test modules, no performance changes due to this type of degradation were observed.

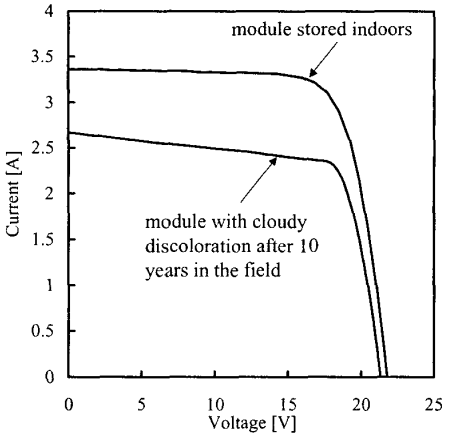

Fig.5 IV characteristic of c-Si with the discoloration after 10 years in the field

4. DEGRADATION FACTOR ANYLSYS

4.1 The initial drop in Isc

To confirm further, the modules manufactured in 2002 were tested and the similar initial drop in the Isc were observed. So to clarify the degradation speed, one-cell modules used the same materials (cell, EVA, glass etc) as usual modules were irradiated to the light (1kW/m^2) by a solar simulator. As a result indicated in Fig.6, the module showed the initial drop in the Isc by 3% within 300 minutes of light exposure and the stable state afterwards. The measured c-Si and p-Si PV modules showed a similar result.

Spectral response of p-Si PV module before and after the light exposure is shown in Fig.7. This indicates that the drop in the Isc is due to the drop in the response in the range of red light and infrared light (700nm~).

To clarify the cause of the initial drop in the Isc, silicon wafer, glass, and glass/EVA/glass laminated sample were exposed to the light for 300 minutes. No changes in the Isc and spectral response that exceed the measurement error were observed with silicon wafer. On the other hand, the change of the optical transmittance of glass after light exposure was observed as shown in Fig.7. The drop is in the range of red light and infrared light (700nm~) that is very similar to that of the module.

Next, two types of laminated glass/EVA/glass sample using the unexposed glass and the degraded (stabilized after exposure for several days outdoor) glass was exposed to the light for 300 minutes in order to confirm whether

EVA degraded or not. As a result, glass/EVA/glass sample employing the unexposed glass showed a similar result as the glass itself. But no change in the optical property was observed with the sample that employs the degraded glass. This indicated that degradation only occurs with the glass and that EVA did not degrade.

Thus in this case, it is concluded that the initial drop in the Isc is caused by the change in optical property of the glass. The optical change of the cerium containing glass was reported by D.E.King et al. (NREL) [1]. It is also well known that light-induced degradation occurs in boron-doped silicon. Further study on the origin of the initial drop is required.

This type of degradation will not affect the long-term reliability because the Isc becomes stable after initial drop.

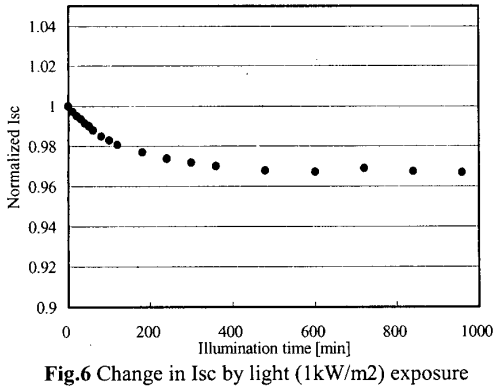

Fig.6 Change in Isc by light (1kW/m2) exposure

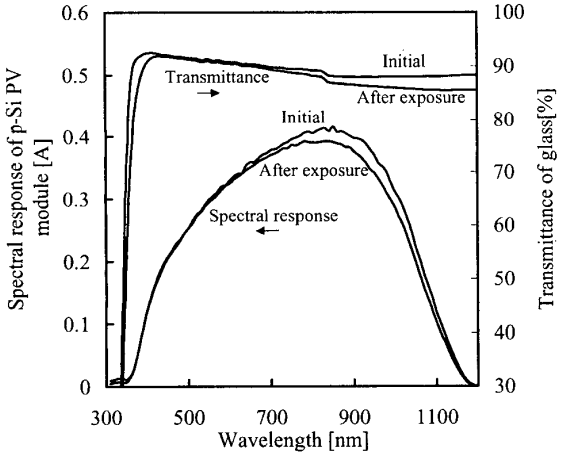

Fig.7 Spectral response of p-Si PV module and optical transmittance of glass before and after the exposure

4.2 Increase in Rs

This type of degradation can be detected by temperature distribution inspection under forward bias condition[2]. When a degraded module is impressed with forward bias by DC power supply, localized heating happens in the parts of the increased Rs. Using IR camera, the degradation parts of the module can be specified. IR image of the degraded module under forward bias condition is shown in Fig.8, which indicates there are many parts where the Rs increased. This module showed the reduction in FF (-20%) due to the increase in the Rs after 10 years in the field. Microscopic observation of the degraded part in the module suggests that the increase in the Rs is due to the degradation in the soldering of electrodes such as microscopic cracks.

In some cases, the modules in which the localized heating was observed showed only small or no change in FF. Fig.9 is the IR image of the module exposed for 12 years which has small sign of localized heating only in 2 parts. This module showed little decrease (-1% drop) in FF. This suggests that the temperature distribution inspection can detect the slight increase in the Rs before the loss in the performance becomes significant. Result of inspecting all the field exposure test modules, 10 out of 26 modules showed the sign of the increase in the Rs.

This degradation factor might affect the reliability of the modules in the range of 20 years or more when progresses.

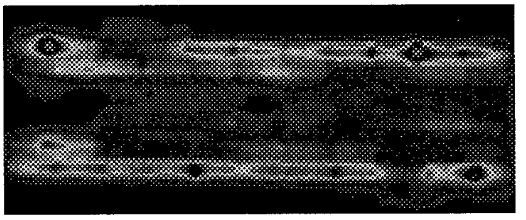

Fig.8 IR image of the module that showed the reduction in FF(-20%) due to the increase in the Rs

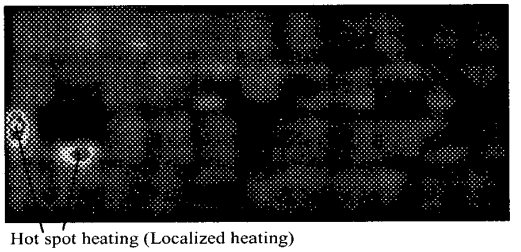

Fig.9 IR image of the module that showed the sign of the increase in the series resistance

4.3 Discoloration (Delamination)

This type of degradation can be confirmed by visual inspection, as the portion of such degradation becomes white. The appearance of the module with the strong discoloration (square marked cells) after 10 years in the field is shown in Fig.10(a).

Electron-probe microanalysis (EPMA) indicated that the discoloration is due to the delamination between the solar cell and EVA. The delamination was also reported by other laboratories[3) 4)]. The Isc of each component cell in this module is identified in a non-destructive method, based on the principle that the current of the module is limited to the current of the cell with the lowest performance[5)]. The Isc of each component cell is shown in Fig.10(b). The Isc of the marked cell that showed the strong discoloration is about 10% lower than that of other cells and this results in the decrease in the Pmax of the degraded module.

At the early stage of degradation, small visual whitening spot (1mm^2) around the grid electrode can be detected by very careful visual inspection as shown in Fig.11. Some of the field exposure test modules showed that, at this stage of degradation, change in Isc after initial

drop was not observed. Result of inspecting all the field exposure test modules, 6 out of 26 modules showed the sign of the discoloration.

Once the degradation progresses, the cell with the strong discoloration shows the reduction in the Isc and is forced into reverse bias condition in operation, this causes hot-spot heating (localized heating) as shown in Fig.10(c). This module showed the further decrease in the Isc of about 10% by re-exposure of 5 months, which indicated that once the discoloration becomes significant, the degradation progresses rapidly.

This degradation factor might also affect the reliability of the modules in the range of 20 years or more when progresses.

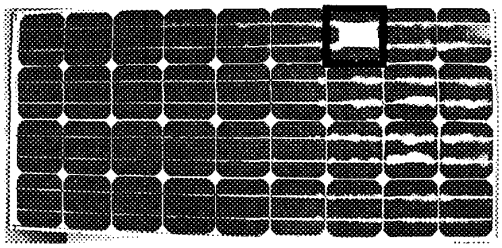

Fig.10(a) The appearance of c-Si PV module with the strong discoloration after 10 years in the field

2.98	2.97	2.98	3.11	2.97	2.97	2.65	2.83	2.89
2.95	2.88	2.97	2.95	2.89	2.92	2.97	2.89	2.94
3.00	2.95	2.95	2.98	2.98	3.02	2.97	2.83	2.91
2.98	3.02	3.00	2.91	3.03	2.97	2.98	2.91	3.00

Fig.10(b) Isc(A) of 36 component cells of the module shown in Fig.10(a)

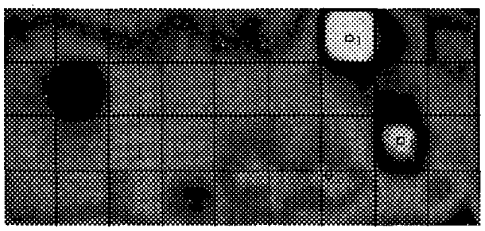

Fig.10(c) IR image of the module shown in Fig.10(a), short-circuited under fine weather in outdoor : T1=52.9°C, T2=50.3°C, T3=44.5°C

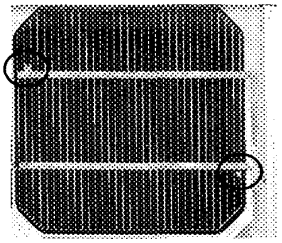

Fig.11 The discoloration of small visual spot ($1mm^2$) around the grid electrode

5. CONCLUSION

The degradation factors of crystalline-Si PV modules manufactured in the early 1990's have been analyzed through long-term field exposure test. Although many modules have been stable for 10-12 years exposure, some of degradation factors were observed.

All the modules showed slight initial drop in Isc (-1~5%) caused by the change in optical property of the glass. The Isc becomes stable after initial drop. This type of degradation will not affect the long-term reliability.

Though there were not a lot of modules, some of the modules showed the performance loss that exceeds 10% either due to the discoloration caused by the delamination between the solar cell and EVA, or due to the increase in the Rs caused by the cracks in electrode soldering. Through the field exposure test, though the slight signs of degradation were observed with some modules tested, no problems that affect strongly the reliability in the range of 10 years were observed. But in the range of 20 years or more these degradation factors when progressed might affect the reliability of the modules. It is crucial to improve acceleration test corresponding to these degradation mechanisms and evaluate the long-term reliability of the modules newly developed.

6. ACKNOWLEDGEMENTS

This work was supported by NEDO as a part of "Photovoltaic technology for mass deployment" Program.

REFERENCES

[1] D.E. King, F.J. Pern, et al., "Optical Changes in Cerium-Containing Glass as a Result of Accelerated Exposure Testing", *Proc. 26th IEEE Photovoltaic Specialists Conf.* (1997), p1117

[2] D.L. King, J.A. Kratochvil, and M.A. Quintana, "Applications for infrared imaging equipment in photovoltaic cell, module, and system testing", *Proc. 28th IEEE Photovoltaic Specialists Conf.* (2000), p1487

[3] N.G. Dhere, "PV module durability in hot and dry climate", *Proc. 16th EU Photovoltaic Solar Energy Conf.* (2000), p2280

[4] M.A. Quintana and D.L. King, et al., "Commonly observed degradation in field-aged photovoltaic modules", *Proc. 29th IEEE Photovoltaic Specialists Conf.* (2002), p1436

[5] K. Morita, Y, Hishikawa et al., *Proceedings of JSES/JWEA Joint Conf.* (2000), p287 (in Japanese)

F. Initial Drop in Isc of the Field Test c-Si PV Modules in Japan

S5O-C9-02

INITIAL DROP IN I_{sc} OF THE FIELD TEST c-Si PV MODULES IN JAPAN

Yoshihiro HISHIKAWA and Kengo MORITA*
National Institute of Advanced Industrial Science and Technology (AIST), Central 2, 1-1-1, Umezono, Tsukuba, Ibaraki 305-8568, Japan
*Japan Electrical Safety & Environment Technology Laboratories (JET), 5-14-12 Shibuya, Tokyo 151-8545, Japan

ABSTRACT

Stability of photovoltaic (PV) modules has been investigated, based on about 2,400 field test PV modules manufactured in 1990's, which show better reliability than the earlier generation modules. The overall system performance showed no distinct change within the 10 years of field test. Some of the modules showed sign of various degradation modes. Among these, the initial drop in I_{sc} indicated that the c-Si modules showed reduction in I_{sc} by 1 - 5% within 1 year of outdoor exposure, then became stable. Experimental results showed that this do not strongly affect the long term stability of the PV modules, as the I_{sc} becomes stable in a very early stage of the operation. Spectral response measurement showed that the drop in I_{sc} is due to the decrease in the response for the red light and infrared light. Possible contributions from the changes in the optical properties of glass and EVA, and the metastability of c-Si solar cells are discussed. Other modes of instability such as the delamination and increase in R_s is also discussed.

1. INTRODUCTION

As PV is penetrating into the market, the long-term stability of photovoltaic (PV) modules is becoming more and more important. Many systematic studies[1-6] on the stability of PV modules were carried out during the 1980's to the early 1990's. Those studies were mainly based on the PV modules manufactured in 1980's. The stability of newer modules are expected to be improved, thanks to the results of those earlier studies. However, systematic information on their reliability, based on a large quantity of modules manufactured in 1990's or later, has not been enough. The purpose of the present work is to summarize the stability issues on the results of PV field tests, based on about 2,400 modules manufactured in 1990's. Special attention is paid on the initial loss in the I_{sc}, where the PV modules showed reduction in I_{sc} by 1 - 5% in the very early stage of outdoor exposure, then became stable.

2. EXPERIMENTAL DETAIL

Laminated one cell modules, small-size modules, glass/EVA/glass laminated samples and ~3t tempered glass samples were used for the indoor measurements of the I_{sc}, optical transmittance, in order to closely investigate the origin of the initial instability of I_{sc}. The field test modules were supplied from several manufacturers. About 2,300 modules (16 systems, ~100 kW_p in total) were located at JQA (Japan Quality Assurance Organization) Hamamatsu site. They were daily measured on the system base. Additional ~100 modules were located at Kitami, Tosu, and Miyakojima sites. They were connected to automatic I-V, irradiance, and temperature measurement apparatus. The modules were exposed outdoors for 8 - 10 years, and were occasionally removed from the systems for detailed indoor I-V measurements. The present study discusses results of the single crystalline silicon (c-Si) and polycrystalline silicon (p-Si) modules, which accounted for the major part of the field test modules.

3. RESULTS AND DISCUSSION

3.1 Stability of the Overall System Performance

Figure 1 shows the typical relative system efficiency of the c-Si and p-Si PV systems in the 100 kW_p PV

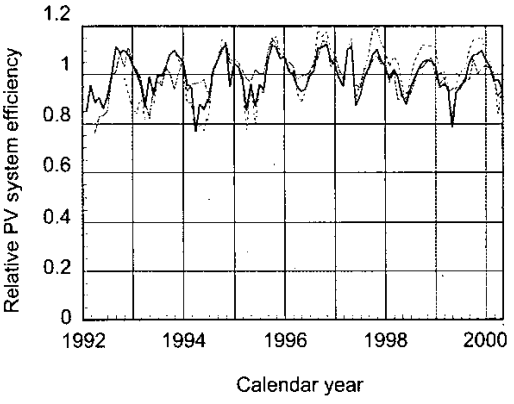

Fig. 1 Typical example of the long term variation of the PV system efficiency. No distinct long term change is observed on the system measurement basis. Each system consists of about 200 PV modules (~10 kWp).

system during the field test. Although the system efficiency showed monthly change due to the effects of temperature and solar spectrum etc., it showed no distinct long term change during the 10 years of field test. This result agrees with many previous studies. On the other hand, the fields test study has also shown that some of the individual modules showed degradation in the output power (P_{max}), as described in the following. This indicates that the degradation in P_{max} of the modules in 10 years was within the uncertainty of the system output power measurements. It should be noted that actually failed modules or modules which showed more than 30% drop in the conversion efficiency, which were sometimes reported in previous studies, were not observed in the present study. This clearly demonstrates that the PV modules manufactured in 1990's in the present study is improved compared to those of older generations.

3.2 Initial drop in I_{sc}

Although the PV performance showed no distinct change on the system basis, detailed indoor I-V measurements of the modules showed reduction in the short circuit current (I_{sc}) of 1 ~ 5% within 1 year of outdoor exposure, as shown in Fig. 2[7]. In order to make clear the slight change in I_{sc}, modules stored indoors were used as control, and measured together with the field test modules. No change in the fill factor FF and open circuit voltage V_{oc} were observed. The I_{sc} became stable afterwards. Although the number of measured modules is limited to ~20, as highly precise measurement using a control group is required, all the measured modules showed some reduction in I_{sc}. Indoor measurement using a small size module and a solar simulator indicates that the I_{sc} becomes stable within a very short period (300 minutes) of light exposure, as shown in Fig. 3. Spectral response of selected modules (Fig. 4) indicate that the drop in I_{sc} is due to the decrease in the response to the red light and infrared light. Measurements on the optical reflectance of a small-size module (Fig. 5), also showed drop in the reflectance in the same wavelength range after 20 days of outdoor exposure. This suggests that the change in I_{sc} is due to the change in the optical properties of the PV modules. As the optical transmittance of glass/EVA/glass laminated samples also showed similar decrease (Fig. 3), change in the optical transmittance of the EVA encapsulant or cover glass is the most probable origin of the drop in I_{sc}. Light exposure experiments on a tempered glass sheet with the same specifications as the currently available PV module cover glass showed drop in the optical transmittance in the same wave-

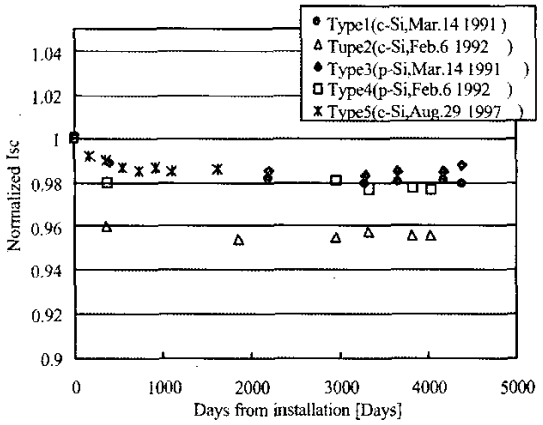

Fig. 2 Change in the short circuit current I_{sc} of 5 c-Si PV modules by outdoor exposure. Different symbols correspond to different modules. The I_{sc} show initial drop by 1% - 5% within 1 year, then becomes stable. Reference modules, which are stored indoors, are used for the control group, in order to improve the accuracy in I_{sc}.

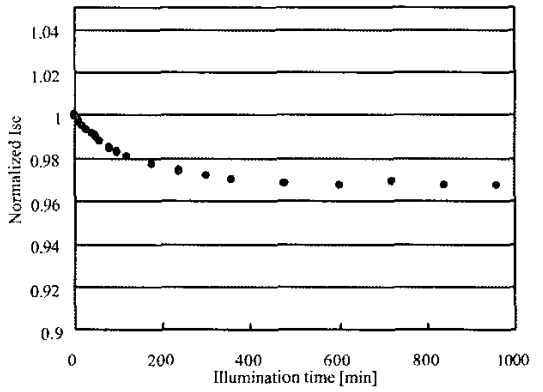

Fig. 3 Change in the short circuit current I_{sc} of a c-Si small size module under a 1 kW/m^2 light exposure by a solar simulator. The drop in I_{sc} occurs within 300 min. of light exposure.

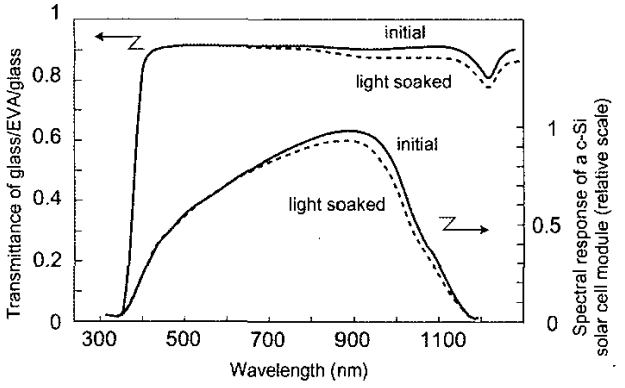

Fig. 4 Spectral response of a c-Si PV module and optical transmittance of a glass/EVA/glass laminated sample before and after light exposure. The spectral response of one cell in the module was measured using a chopped monochromatic light, by biasing other cells in the module. Both spectra changes in the wavelength range of > 600 nm (red and infrared light).

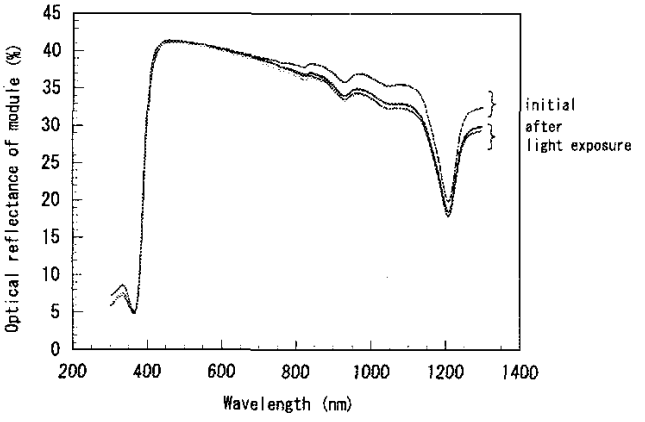

Fig. 5 Optical reflectance of a c-Si small size module before and after 20 days of outdoor exposure. The reflectance was measured in an optical configuration where the probe light passes through the air/glass/EVA, then reflected by tedlar, then passes through EVA/glass/air.

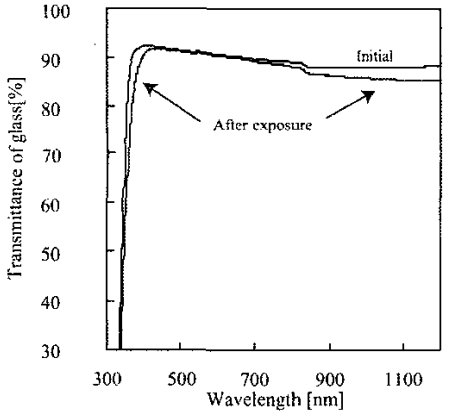

Fig. 6 Optical transmittance of a ~3t tempered glass sheet with the same specifications as the currently available cover glass of PV modules, before and after the light exposure (1 kW/m^2, 300 minutes) by a solar simulator.

length range (Fig. 6), which indicates that the primary origin of the initial drop in I_{sc} of the small size module in this study is the "solarization" of the cover glass. This agrees with the result of D.E. King et al [8] that Cerium-containing glass show drop in the optical transmittance by light exposure. It is noted that the composition of the cover glass in the present study is not identified. As for the field test results (Fig. 2), the instability of the solar cell and EVA cannot be ruled out from the possible origins at the present stage. It is known that c-Si solar cells using substrates with high boron concentration sometimes show instability in the similar wavelength range and similar or faster time range[9]. Relatively high UV intensity of the outdoor sunlight than the solar simulator possibly enhances the EVA discoloration[10]. Further study is required to clarify the origin and reduce the initial drop in I_{sc} in the field. It should be noted that the present results also indicate that, as the I_{sc} become stable after the initial drop in the very fast stage (several hours) of outdoor operation, this degradation mode does not affect the 20 - 30 years reliability.

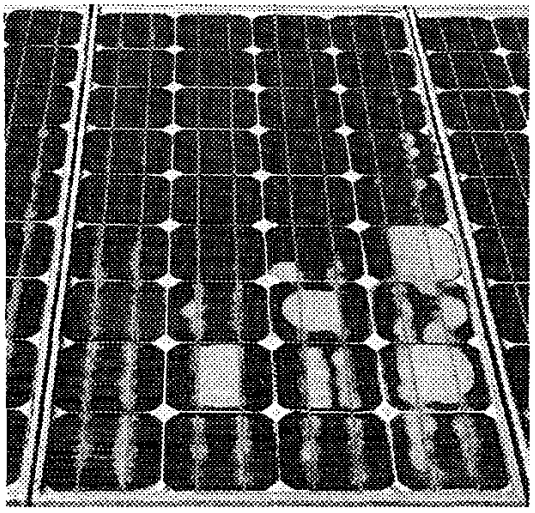

Fig. 7 A module with strong cloudy discoloration due to delamination at cell/EVA interface (extreme case).

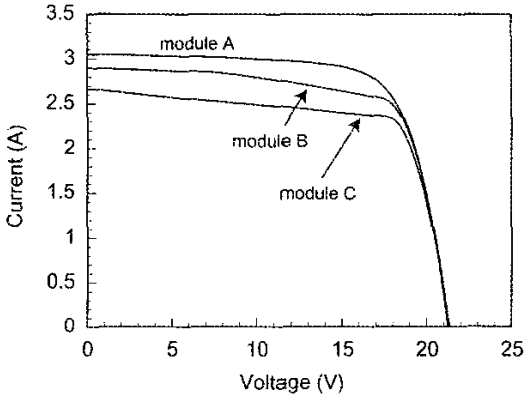

Fig. 8 I-V characteristics I_{out} (V) of c-Si modules with different degree of cloudy discoloration. A: After outdoor exposure. No appreciable discoloration. B: After outdoor exposure. 1/3 of the active area of a cell in the module shows discoloration. C: After outdoor exposure. 1/2 of the active area of a cell in the module shows discoloration. Step-like structures of the I_{out}(V) indicates that the module include solar cells whose I_{sc} is smaller than others.

3.3 Cloudy Discoloration Due to the Delamination at the Cell/EVA Interface

Visible discoloration of the module is a well known degradation mode. In this study, about 400 modules showed some degree of visible cloudy discoloration, although most of them was observed in a minor part of the module. The degree of the discoloration was very dependent on the individual module. Extreme example is shown in Fig. 7. This was the most significant visible change during the 10 years outdoor exposure of the present study. This kind of discoloration, however, was limited to two module types. Modules of other types did not show this kind of discoloration, which indicates that this is not an essential problem of the material. The area of the discoloration ranged from 0~10% of the module, and grew larger year by year. The discoloration usually occurred as a small visual spots around the grid electrode, which do not affect the I-V characteristics of the modules at an initial stage of degradation. However, when the discoloration became significant as shown in Fig. 4, it resulted in reduced I_{sc} of the module, which lead to the degradation in P_{max} (Fig. 8). Microscope and electron-probe microanalysis (EPMA) measurements indicate that the discoloration is due to the delamination of EVA from the c-Si solar cell. As the delamination enhances the optical reflectance and tends to splits the grid electrode from Si, insufficient collection of current probably resulted in reduced I_{sc}. Detailed indoor I-V measurements confirmed that the reduction in I_{sc} of the module is due to the reduction in I_{sc} of the cell where the discoloration is most significant. Although this can strongly affect the long term stability of the module, it will be possibly avoided by optimizing the lamination techniques.

3.4 Increase in R_s

Increase in the series resistance R_s is also a degradation mode which is reported by many field studies. Some modules showed decrease in FF of I_{out}(V), which is apparently due to the increase in the series resistance R_s without any appreciable visual change. Although this degradation mode was seen in limited module types, most of the ran-

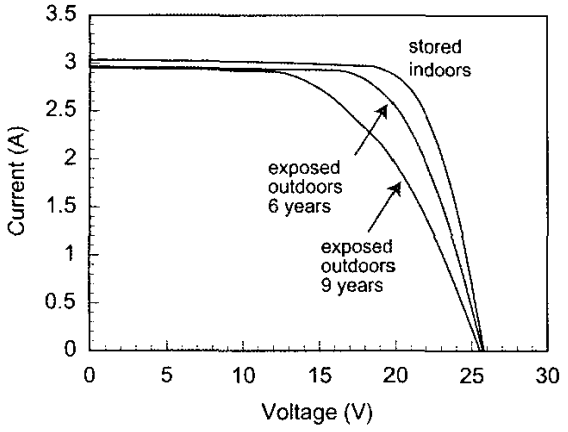

Fig. 9 I-V characteristics I_{out} (V) of c-Si modules which show drop in FF and P_{max} due to the increased series resistance R_s. These modules show no visual change.

domly selected modules of the type showed some degree of decrease in FF. Extreme examples are shown in Fig. 6. Estimated increase of the R_s due to the degradation of the module C in the figure is about 2 Ω. When the corrosion of the external connection of the was cleaned, the R_s decreased to 1.2 Ω. The R_s of a controlled module stored indoors was 0.5 Ω. Details based on updated experimental results are discussed in [11]. Microscope and thermo-viewer measurements suggest that the degradation in the soldering of electrodes such as microscopic crack is due to the increased R_s[11]. As this degradation mode seems to be accelerated by prolonged outdoor exposure, it can affect the long term reliability. Modification in the soldering processes will solve the problem.

3.5 Observed Other Degradation Modes

The tempered cover glass of the 14 out of the 2,400 modules broke during the 10 years. In addition, the following degradation modes were investigated in some modules. These were not so significant compared to the results of earlier modules, and do not appreciably affect the total output at the present stage.

(1) Delamination of back cover sheets such as tedlar.
(2) Rusty connection around the terminal box.
(3) Yellowish discoloration of EVA encapsulant.

4. CONCLUSION

Long-term stability of photovoltaic (PV) modules has been systematically investigated by indoor and outdoor measurements, with special attention to the initial drop in the I_{sc} of the modules. The study was based on about 2,400 field test PV modules manufactured in 1990's. No serious problems such as failed modules or modules which show more than 30% drop in the output power, were not observed, which demonstrates that the reliability of the modules in the present study is improved than that of the modules manufactured in 1980's or before. All the measured module showed initial loss in I_{sc}. Experimental results of the present study indicates that the primary origin of the drop in I_{sc} is the reduced transmittance of the glass in a wavelength range >600 nm. The present results also confirms that this degradation mode does not affect the long term reliability of the PV modules, as the I_{sc} become stable after the initial drop in the very fast stage (several hours) of light exposure.

Some of the modules showed reduced I_{sc} due to cloudy discoloration and increased R_s probably due to the degradation in electrode soldering. Although the overall system performance showed no distinct change within the 10 years of field test, the present results suggest that the above degradation features can affect the reliability of 20 - 30 years. Further study on the origin of the degradation features is useful for improving the stability of the PV modules.

ACKNOWLEDGEMENTS

This work was supported by NEDO under the Ministry of Economy, Trade and Industry.

REFERENCES

[1] A. L. Rosenthal, M. G. Thomas and S. J. Durand, Proc. 23rd IEEE Photovoltaic Specialists Conf. (1993) 1289

[2 G. H. Atmaram, G. G. Ventre et al., Proc. 25th IEEE Photovoltaic Specialists Conf. (1996) 1279

[3] I. J. Muirhead and B. K. Hawkins, Technical Digest of the International PVSEC-9, Miyazaki (1996) 1279

[4] L. N. Dumas and A. Shmka, Proc. 15th IEEE Photovoltaic Specialists Conf. (1981) 1279

[5] D. L. King et al., Prog. Photovolt. Res. Appl. 8 (2000) 241 (1996) 477

[6] K. Machida, T. Yamazaki and T. Hirasawa, Sol. Energy Mater. Sol. Cells 47 (1997) 149